SEISMIC RESPONSE OF DIAGONALLY REINFORCED COUPLING BEAMS WITH VARIED HOOP SPACINGS

by

Brian Howard
July 2017

Department of Civil Engineering and Applied Mechanics
McGill University
Montréal, Québec
Canada

A thesis submitted to the Faculty of Graduate Studies and Research
in partial fulfilment of the requirements of
the degree of Master of Engineering

ABSTRACT

Reinforced concrete shear walls are commonly used seismic force-resisting systems in high-rise structures. Shear walls with regular openings for elevators or staircases at floor levels act as a system of two shear walls linked by concrete beams located above and below the openings. These shear wall systems are referred to as coupled walls. Ductile coupling beams are important components of ductile coupled walls due to their inherent high energy dissipation properties and stable failure mechanisms. Coupling beams with low span to depth ratios typically include diagonal reinforcement to resist shear and flexural forces induced by wind or seismic loads. In order to achieve the necessary ductility, the current CSA Standard A23.3-14 (CSA, 2014) limits the spacing between the buckling prevention ties (hoops) which confine the diagonal reinforcing bars to the lesser of $24d_{hoop}$, $6d_b$ or 100 mm. These stringent requirements for ductile diagonally reinforced coupling beams are commonly applied to moderately ductile and conventional construction cases.

To simplify the construction of the coupling beams and provide realistic alternatives for the moderately ductile and conventional construction cases, the effect of an increased spacing of the buckling prevention ties in the coupling beams is investigated.

Reversed cyclic loading tests were carried out on fifteen reinforcing bar specimens as well as four full-scale coupled shear wall specimens.

The hysteretic response of the full-scale coupled wall specimens determined that an increased spacing of the buckling prevention ties performs adequately for the moderately ductile and conventional construction cases. Further research should be carried out to investigate the increase in resistance due to the longitudinal restraint of the coupling beams offered by the structure's floor slabs.

RÉSUMÉ

Les murs ductiles couplés sont des systèmes de contreventement fréquemment utilisés dans des structures gratte-ciels afin de résister aux charges latérales. Les poutres couplées sont des éléments importants dans le système de résistance latérale en raison de leur efficacité en dissipation d'énergie et leur méthode de défaillance prévisible. Les poutres couplées avec un rapport minime de portée à profondeur sont typiquement armées en diagonale. Afin d'atteindre un niveau de ductilité acceptable, les dispositions actuelles du Code CSA A23.3-14 limitent l'espacement entre les ligatures sismiques afin d'éviter le flambement des barres d'armature. Les provisions du code sont actuellement disponibles pour le cas ductile ($R_d = 4.0$) et sont typiquement appliquées aux poutres couplées modérément ductile ($R_d = 2.5$). Aucunes provisions n'existent pour le cas de construction conventionnelle ($R_d = 1.5$). Afin de simplifier la construction des poutres couplées ainsi que de fournir des alternatives réalistes pour les cas modérément ductile et de construction conventionnelle, l'effet d'un espacement augmenté des ligatures qui confinent les barres d'armature diagonales est investigué.

Des expérimentations cycliques inversées (reversed cyclic) ont été complétées sur quinze barres d'armature et quatre systèmes de murs couplés de pleine échelle.

Les comportements hystérétiques des spécimens nous permet de conclure que l'espacement des ligatures peut être augmenté pour les cas des murs modérément ductiles et de construction conventionnelle. De plus, l'effet de retenue de la dalle structurale sur les murs couplés devrait être investigué davantage.

ACKNOWLEDGEMENTS

TABLE OF CONTENTS

LIST OF FIGURES

LIST OF TABLES

LIST OF SYMBOLS

A_g	gross area
A_s	cross-sectional area of tensile reinforcement
C	compression
d	effective depth
d_b	nominal diameter of steel reinforcement bar
d_{tie}	nominal diameter of steel reinforcement tie
f'_c	compressive strength of concrete
f_u	ultimate strength of reinforcing steel
f_y	yield strength of reinforcing steel
FW	fixed wall
h_e	cross-sectional dimension of column core measured centre-to-centre of confining reinforcement
l_u	clear span
LW	loaded wall
m	slope
M_{cr}	moment to cause first cracking
R	force modification factor
s	centre-to-centre spacing of reinforcement
T	tension
V_y	shear force causing yield
V_u	ultimate shear force
α	angle of inclination of diagonal bar from the horizontal
Δ	deflection
Δ_y	deflection corresponding to general yielding
ε'_c	concrete strain at f'c
ε_{sh}	concrete strain at strain hardening
ε_u	ultimate concrete strain
ε_y	yield strain of reinforcing steel
ρ	ratio of area of reinforcement to area of concrete

CHAPTER 1

INTRODUCTION AND LITERATURE REVIEW

1.1. Coupled Shear Walls

Reinforced concrete shear walls are commonly used as lateral load resisting elements in low to high-rise structures. Shear walls are typically placed around elevator and staircase openings, along corridors or at exterior edges of the structure. In many of these locations, openings are made in the shear walls at each floor level for doors or windows, resulting in a system of two in-plane shear walls connected by beams at regular intervals. This type of lateral load resisting system, illustrated in Fig. 1.1, is commonly referred to as a coupled shear wall.
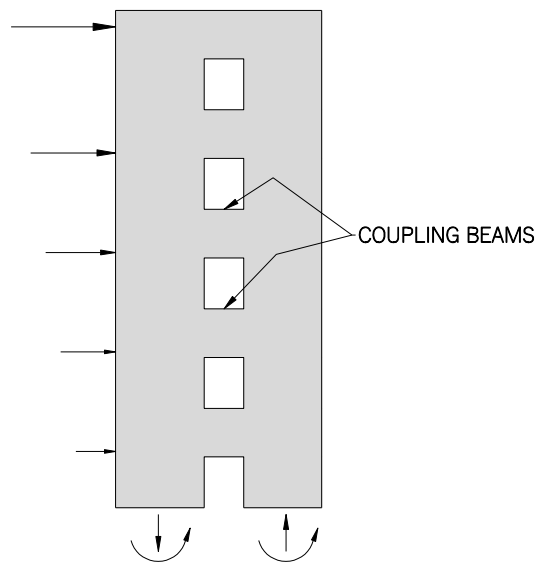
Figure 1.1 – Typical coupled shear wall

Coupled shear walls can be coupled by beams constructed using conventional longitudinal and transverse reinforcement or with a diagonal arrangement of the principal reinforcement, as shown in Fig. 1.4. A diagonal arrangement of the reinforcing steel is typically used in coupling beams with a small span-to-depth ratio or couplings beams which resist high shear forces and acts similar to structural steel cross-bracing, providing a more stable post-yield response than conventionally reinforced (with longitudinal steel and stirrups) concrete elements. The current experimental program investigates the behaviour of diagonally reinforced coupling beams having different ductility levels.

Coupling beams act as fixed-fixed beams since the concrete walls are generally much stiffer than the coupling beams. Under lateral load, the rotations of the beam at each extremity are approximately the same, thus coupling beams experience maximum moments at the beam-wall interface, zero moment at their midspan and a constant shear over the length of the beam (Paulay & Binney 1974). The internal forces of the coupling beams are illustrated in Fig. 1.2.
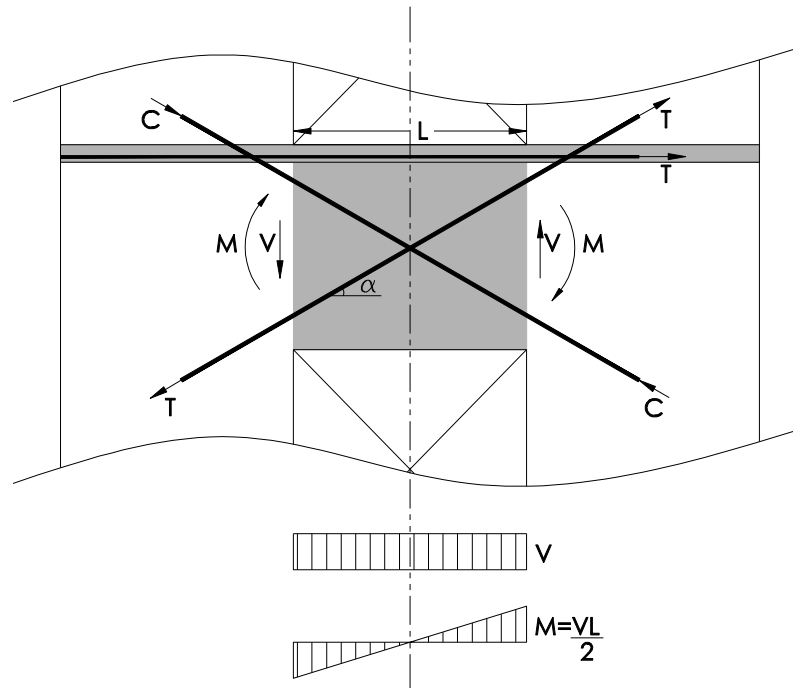
Figure 1.2 – Internal forces of a diagonally reinforced coupling beam (Paulay and Priestly, 1992)

2

Horizontal reinforcing placed in the connected floor slabs will interact with the coupling beams under lateral load. The interaction occurs because the lengthening of the reinforcing tension tie is greater than the shortening of the concrete strut in compression. Consequently all of the reinforcing steel in the coupling beam, including the contiguous floor slab, will be in tension (Paulay & Priestley, 1992).

If the coupling beams are very flexible they transmit only a limited amount of shear to the coupled walls. The system then acts similar to two independent cantilevered shear walls. If the coupling beams are very stiff and have very rigid connections the system acts similar to a single cantilevered shear wall without the openings. Typically, the behaviour of coupled shear walls lies between these two cases. Figure 1.3 illustrates the behaviour of coupled shear walls. Coupled shear walls must provide adequate lateral resistance, ductility, energy absorption and post-earthquake resistance in a stable, reliable and predictable manner.

(a) Pinned beam connections

(b) Fixed beam connections

(c) Actual beam connections
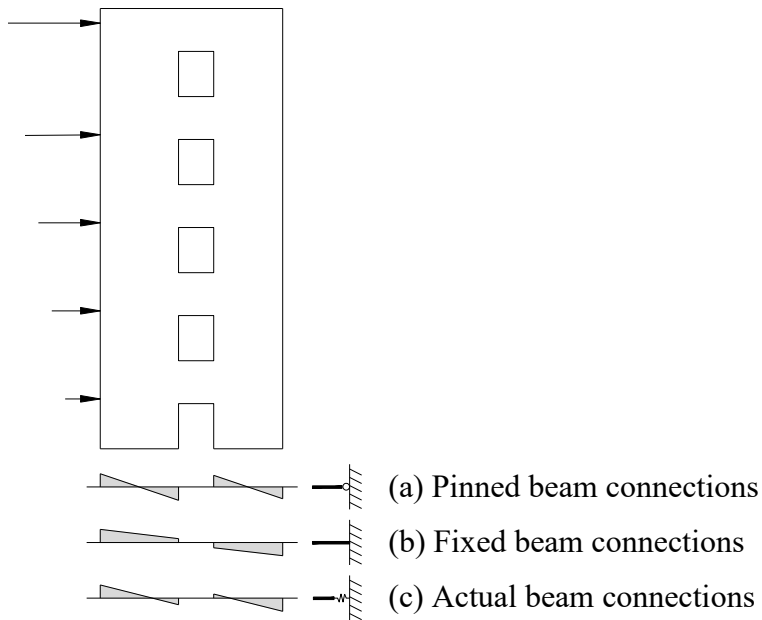
Figure 1.3 – Moments in coupled shear walls for different end conditions for the coupling beams (Harries, 1995)

In diagonally reinforced coupling beams, the concrete does not have a significant contribution in resisting the lateral load. The concrete is capable of resisting a minimal amount of tension at low load levels, however upon increasing the load and subjecting the beam to load reversals, the cracks in the concrete become large, the reinforcing bars elongate and the compressive and tensile loads are then completely resisted by the steel reinforcing bars. The reinforcing steel dissipates energy by tensile yielding and compressive buckling. The buckling of overstressed steel reinforcing bars under static loading is typically considered an undesirable brittle failure mode, one which does not provide many signs of distress prior to collapse. Under dynamic loading, however, bar buckling is associated with large deformations and can thus be considered ductile in nature, provided that rupture does not occur (Binney, 1972).

1.2. Concept of Diagonal Reinforcement

Previous research and current code provisions differentiate between conventionally reinforced and diagonally reinforced coupling beams, illustrated in Fig. 1.4.
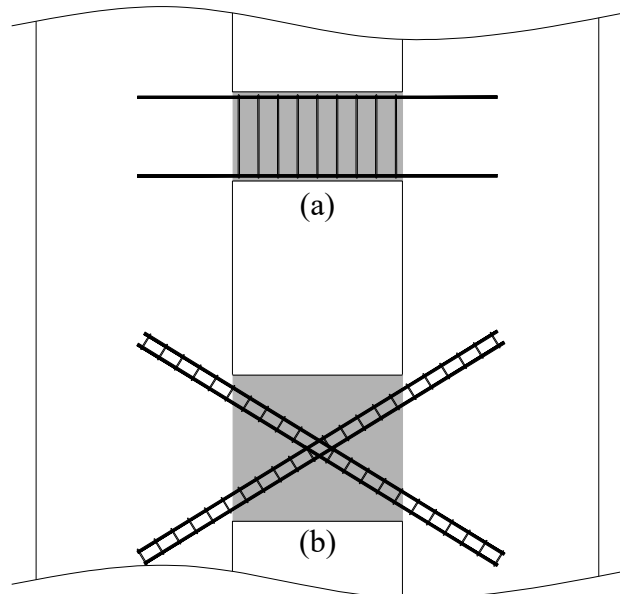
Figure 1.4 – (a) Conventionally reinforced and (b) diagonally reinforced coupling beams

Figures 1.5 – Characteristic failure of short coupling beams during the 1964 Alaskan Earthquake (Hansen et al., 1966 and Faison et al., 2004)

Following observations of the characteristic structural failures which occurred during the 1964 Alaskan earthquake, illustrated in Fig. 1.5, Paulay began to investigate methods to prevent shear failure of coupling beams with small span-to-depth ratios.

The early research of conventionally reinforced coupling beams with different span-to-depth ratios carried out by Paulay at the University of Canterbury also included an investigation of the effectiveness of a diagonal arrangement of the principal reinforcing steel in deep coupling beams (Paulay, 1969). Paulay found that all of the conventionally reinforced coupling beams constructed with a depth-to-span ratio of 1.29, and all of the conventionally reinforced deep coupling beams constructed with a depth-to-span ratio of 1.02, failed in diagonal tension or in sliding shear. The diagonal tension and sliding shear failure mechanisms are shown in Fig. 1.6.
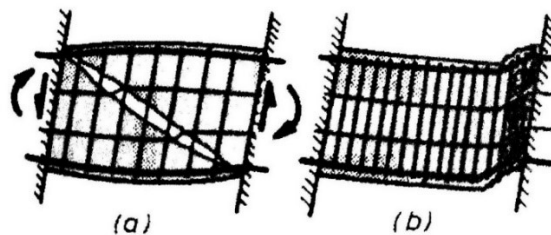
Figure 1.6 – (a) Diagonal cracking and (b) sliding shear failure mechanisms of coupling beams (Paulay & Priestley, 1992)

Further research on coupling beams was carried out by Binney (1972) at the University of Canterbury in order to investigate the response of diagonal reinforcing steel in deep coupling beams. Three coupling beam specimens were tested; the first being a conventionally reinforced coupling beam, the second a diagonally reinforced coupling beam without transverse buckling restraining hoops and the third a diagonally reinforced coupling beam with transverse buckling restraining hoops. The conventionally reinforced coupling beam failed in sliding shear. The diagonally reinforced coupling beam without transverse ties failed by the buckling of three of the four principal diagonal reinforcing steel bars adjacent to the connected wall, resulting in a large out of plane side-sway of the coupling beam. The diagonally reinforced coupling beam with transverse ties failed similarly to that without transverse ties. The research demonstrated that using a diagonal arrangement of the principal reinforcing steel would avoid the diagonal tension and sliding shear failure mechanisms. The testing also concluded that a high displacement ductility level could be reached in a stable manner with little reduction in strength. The transfer of the tensile forces in the concrete beam to the diagonal reinforcing steel results in an efficient energy-dissipating mechanism. The testing, however, was carried out on beams that were only six inches (6") in width. Binney (1972) recommended investigating similar detailing in thicker coupling beams with minimal transverse reinforcing spacing in order to eliminate or limit the observed buckling and unstable beam side-sway. Binney (1972) also recommended that basketting reinforcement be provided in order to limit the degree of spalling of the concrete.

1.3. Previous Research

Research carried out by Galano and Vignoli (2000) at the University of Florence investigated the effect of configuration of the reinforcing steel in coupling beams with span-to-depth ratios of 1.5. The responses of coupling beams reinforced with conventional, diagonal and rhombus configurations were investigated. The experimentation concluded that the diagonal configuration yielded the largest shear capacity while the rhombus layout provided the highest rotational ductility. Two diagonally reinforced coupling beam specimens were constructed. One specimen (P07)

had no transverse reinforcement to directly laterally brace the diagonal bars. The second specimen (P12) had transverse hoops in order to laterally brace the diagonal reinforcing bars. All of the specimens had basket reinforcement at the exterior faces of the coupling beam. Figure 1.7 illustrates the shear force versus rotation responses of the specimens.
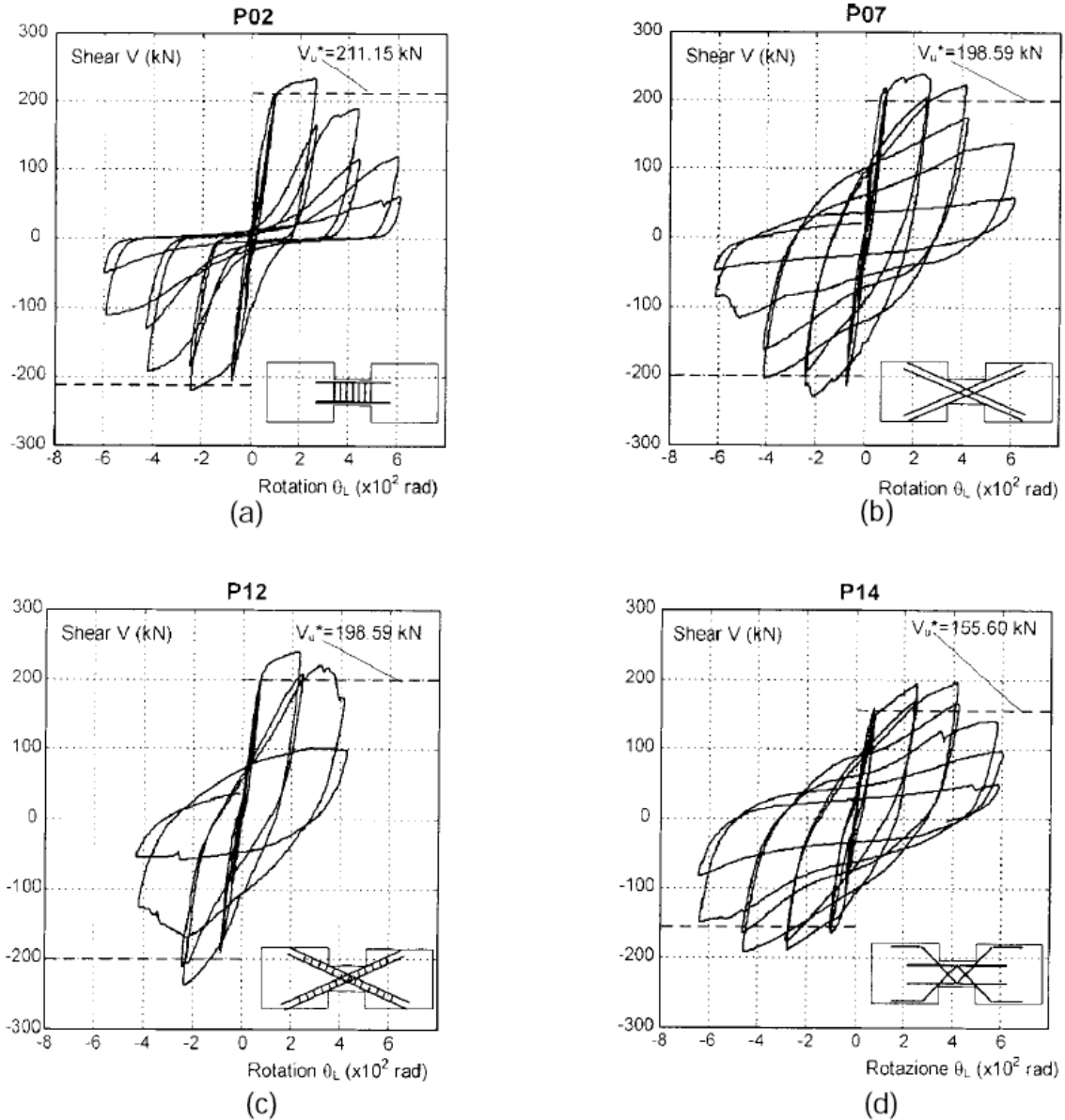
Figure 1.7 – **Hysteretic response of coupling beams with a (a) conventional layout, (b) diagonal layout without transverse hoops, (c) diagonal layout with transverse hoops and (d) rhombic layout of reinforcing bars (Galano & Vignoli 2000).**

7

The absence of transverse reinforcement to laterally brace the diagonal bars did not appear to adversely affect the ultimate shear resistance and rotational ductility of the coupling beams, however it is to be noted that the contribution of the higher compressive strength of the concrete in specimen P12 contributed to a higher shear resistance (f'_c of 48 MPa for P12 and 42.7 MPa for P09).

Research carried out by Dugas (2002) at McGill University investigated the effect of using headed bars to confine the diagonal reinforcing steel in deep coupling beams as a substitute to buckling prevention ties, in order to reduce congestion and simplify constructability. The research demonstrated that the headed bars provided adequate confinement to the diagonal reinforcing steel, resulting in coupled walls which performed as well or better than diagonally reinforced coupled walls and is thus a viable alternative. The use of headed bars provides a practical solution particularly for heavily reinforced coupling beams.

Research carried out by Lai (2002) at McGill University investigated the effect of using diagonal structural steel members in deep coupling beams as a substitute to conventional diagonal reinforcing bars in order to investigate the behaviour. The research demonstrated that the coupled walls with embedded structural steel members performed significantly better than conventional diagonally reinforced coupled walls and is thus a viable alternative.

Research carried out by Zhou (2003) at McGill University investigated the effect of using a diagonal orientation of the reinforcing steel in coupling beams with large span-to-depth ratios. The coupling beams had a span-to-depth ratio of 3.42. The diagonal bars did not have anti-buckling hoops by the beam was confined with hoops satisfying the requirements of hoops in ductile beams. The diagonal 25M reinforcing steel bars were placed at an angle of 14.6°. The research demonstrated that the diagonally reinforced slender coupling beams performed significantly better than conventionally reinforced slender coupling beams. One issue is the accurate placement of the inclined reinforcement during construction.

Research carried out by Naish et al. (2013) at the University of California investigated the impact of the longitudinal restraint provided by reinforced concrete floor

slabs on the response of coupled shear walls. Three types of coupling beams with a span-to-depth ratio of 2.4 were tested; the first with no restraining slab, the second with a conventionally reinforced slab and the third with a post-tensioned slab. The slabs framed into the top flange of the coupling beam.
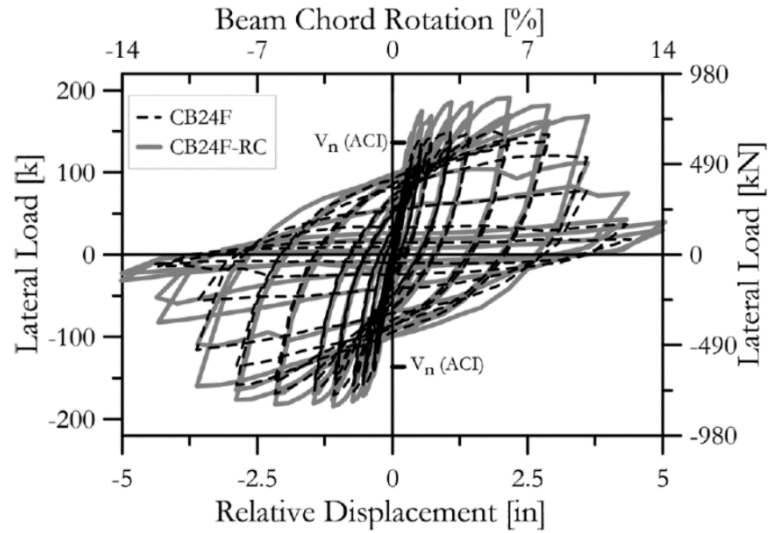
Figure 1.8 – Hysteretic response of specimens CB24F (without longitudinal restraint) and CB24F-RC (with longitudinal restraint) (Naish et al., 2013)

Figure 1.8 illustrates the hysteretic response of the coupled shears wall with (CB24F-RC) and without (CB24F) the restraint of a structural slab. The research demonstrated that the slab restrained the axial elongation and affected the stiffness, strength and deformation properties of the coupling beam. The presence of the slab increased the flexural capacity by approximately 20%. Figure 1.9 illustrates the effect of the slab on the axial elongation of the walls.

9
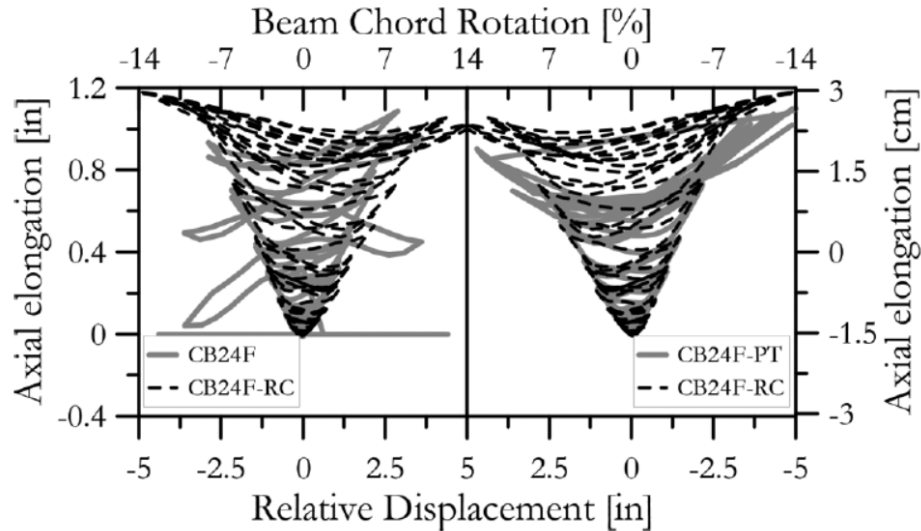
Figure 1.9 – **Axial elongation of specimens CB24F (without longitudinal restraint),
CB24F-RC (with conventionally reinforced longitudinal restraint) and
CB24F-PT (with post-tensioned longitudinal restraint) (Naish et al., 2013)**

1.4. CSA Standard A23.3-14 Seismic Design Criteria for Coupled Walls

Clause 21 of the Canadian Standards Association's (CSA) Standard A23.3-14, Design of Concrete Structures, (CSA, 2014) presents the provisions for the seismic design of reinforced concrete members. Clause 21.5.8 presents the additional requirements which apply to ductile and moderately ductile coupled shear walls. The diagonally reinforced coupling beam details are the same for the ductile and moderately ductile cases. There are no provisions for diagonally reinforced coupling beams in conventional construction. The code requirements for the detailing of coupled shear walls outside of the plastic hinge region are summarized in Table 1.1.

The CSA Standard A23.3-14 (CSA, 2014) distinguishes between coupled and partially coupled shear walls. The degree of coupling is defined as the amount of the overturning moment resistance provided by axial forces in the walls resulting from shear transferred from the coupling beams. If the degree of coupling is greater than or equal to 66% then the walls are classified as coupled walls, otherwise they are classified as partially coupled walls. The National Building Code of Canada (NBCC, 2015) prescribes ductility-related force modification factors (R_d) and overstrength-based force modification factors (R_o) to all seismic systems recognized in Canada. The R_d and R_o

10

factors for ductile and moderately ductile coupled and partially coupled shear wall systems are summarized in Table 1.2.

Coupling beams must be reinforced with two intersecting groups of diagonally placed bars unless the shear stress is less than $0.1 l_u / d \sqrt{f_c'}$ and the clear span of the beam is greater than $2 l_d$. Conventionally reinforced (with longitudinal steel and stirrups) coupling beams must be designed as ductile or moderately ductile moment frame members.

The maximum suggested shear stress resistance for diagonally reinforced coupling beams is $0.1 \sqrt{f_c'}$. The coupling beams must be centered on the coupled walls and the diagonal reinforcement in the coupling beam must be placed concentrically in the beam in order to avoid the associated out-of-plane moments. The diagonal reinforcing bars must be embedded into the coupled walls for a minimum distance of 1.5 l_d (straight bars) or 1.0 l_d (bars with standard hooks) and must be confined by hoops spaced not more than 100 mm.

Table 1.1 – Summary of the CSA Standard A23.3-14 (CSA, 2014) requirements for coupled shear walls

	Ductile (R$_d$=4.0)	Moderately Ductile (R$_d$=2.5)	Conventional Construction (R$_d$=1.5)
Limits on concrete compressive strength	80 MPa [cl. 21.2.6.1]	80 MPa [cl. 21.2.6.1]	80 MPa [cl. 21.2.6.1]
Type of reinforcement	Weldable [cl. 21.2.7.1.1]	No Requirement [cl. 21.2.7.1.1]	No Requirement [cl. 21.2.7.1.1]
Minimum Lap Splice Length	1.5 l$_d$ [cl. 21.5.4.1]	1.5 l$_d$ [cl. 21.5.4.1]	l$_{splice}$ [cl. 12.15]
Uniformly distributed reinforcement	ρ_{hor}, $\rho_{vert} \geq 0.0025$ [cl. 21.5.5.1]	ρ_{hor}, $\rho_{vert} \geq 0.0025$ [cl. 21.5.5.1]	$\rho_{hor} \geq 0.002$ $\rho_{vert} \geq 0.0015$ [cl. 14.1.8.5-6]
Concentrated reinforcement	0.001 b$_w$l$_w$ [cl. 21.5.6.1]	0.0005 b$_w$l$_w$ [cl. 21.5.6.1]	0.0005 b$_w$l$_w$ [cl. 21.5.6.1]
Concentrated reinforcement ties	$s \leq \begin{cases} 6\,d_{b,long} \\ 24\,d_{b,tie} \\ 1/2\,t_{wall} \end{cases}$ [cl. 21.5.8.3.1 & cl. 21.2.8.1]	$s \leq \begin{cases} 16\,d_{b,long} \\ 48\,d_{b,tie} \\ t_{wall} \\ 300\,mm \end{cases}$ [cl. 21.5.8.3.1 & cl. 7.6.5.2]	$s \leq \begin{cases} 16\,d_{b,long} \\ 48\,d_{b,tie} \\ t_{wall} \\ 300\,mm \end{cases}$ [cl. 21.5.8.3.1 & cl. 7.6.5.2]
Minimum shear force required for diagonal bars	0.1 (l$_u$/d)$\sqrt{f'c}$ b$_w$d [cl. 21.5.8.1.1]	Same as ductile	No Specification
Maximum span to depth ratio of coupled beams	h $\leq$ 2.0 l$_u$ [cl. 21.5.8.2.1]	Same as ductile	No Specification
Minimum # of diagonal bars	4 bars [cl. 21.5.8.2.2]	Same as ductile	No Specification
Spacing of hoops around diagonal bars	$s \leq \begin{cases} 6\,d_{b,\,long} \\ 24\,d_{b,\,tie} \\ 100\,mm \end{cases}$ [cl. 21.5.8.2.4]	Same as ductile	No Specification
Diagonal bars embedment length in surrounding wall	1.5 l$_{d,\,straight\,bar}$ 1.0 l$_{d,\,90\,hooked\,bar}$ Headed bar [cl. 21.5.8.2.5]	Same as ductile	No Specification

Table 1.2 – NBCC 2015 ductility-based force modification factors (R$_d$) and overstrength-based force reduction factors (R$_o$) (NRC, 2015).

Type of wall	R$_d$	R$_o$
Ductile coupled	4.0	1.7
Ductile partially-coupled	3.5	1.7
Moderately ductile coupled	2.5	1.4
Moderately ductile partially-coupled	2.0	1.4
Conventional Construction	1.5	1.3

1.5. ACI 318-11 Seismic Design Criteria for Coupled Walls

Clause 21 of the American Concrete Institution's 318-11 (ACI, 2011) standard also presents the provisions for the seismic design of reinforced concrete members. Clause 21.9.7 presents the additional requirements which apply to coupling beams. Similar to the NBCC, the American Society of Civil Engineers' 7 standard (ASCE, 2006) prescribes the response modification coefficients (R) and system overstrength factors (Ω_o) to all seismic systems recognized in the United States of America. Rather than referring to the seismic systems as ductile, moderately ductile and conventional construction, the ASCE distinguishes between special, intermediate and ordinary lateral load resisting systems. The R and Ω_o factors associated to special building frame reinforced concrete shear walls in the ASCE 7-16 standard, including special shear walls with coupling beams, are 6 and 2.5 respectively.

The ASCE 7-16 standard does not distinguish between coupled and partially coupled shear wall systems. The ACI 318-11 specifies that coupling beams with span-to-depth ratios greater than four shall be designed as special moment frame flexural members. Coupling beams with span-to-depth ratios less than two and with a shear stress exceeding $4\lambda\sqrt{f_c'}$ [psi] must be reinforced with two intersecting groups of diagonally placed bars. The maximum shear stress resistance for diagonally reinforced coupling beams is $10\sqrt{f_c'}$ [psi], equivalent to $0.083\sqrt{f_c'}$ [MPa]. No mention is made for whether coupling beams must be centered on the coupled walls. The diagonal reinforcement in the coupling beam need not be placed concentrically. The diagonal reinforcing bars must be

13

embedded into the coupled walls in order to develop 1.25 of the yield strength of the bar. Two confinement options are provided; the diagonal reinforcing bars must be confined by hoops spaced not more than 6 inches (150 mm) or by a heavily reinforced basket with hoops and crossties spaced not more than 6 inches in the longitudinal direction and 8 inches over the depth. Figure 1.10 illustrates the principal differences between the CSA and ACI code confinement requirements.
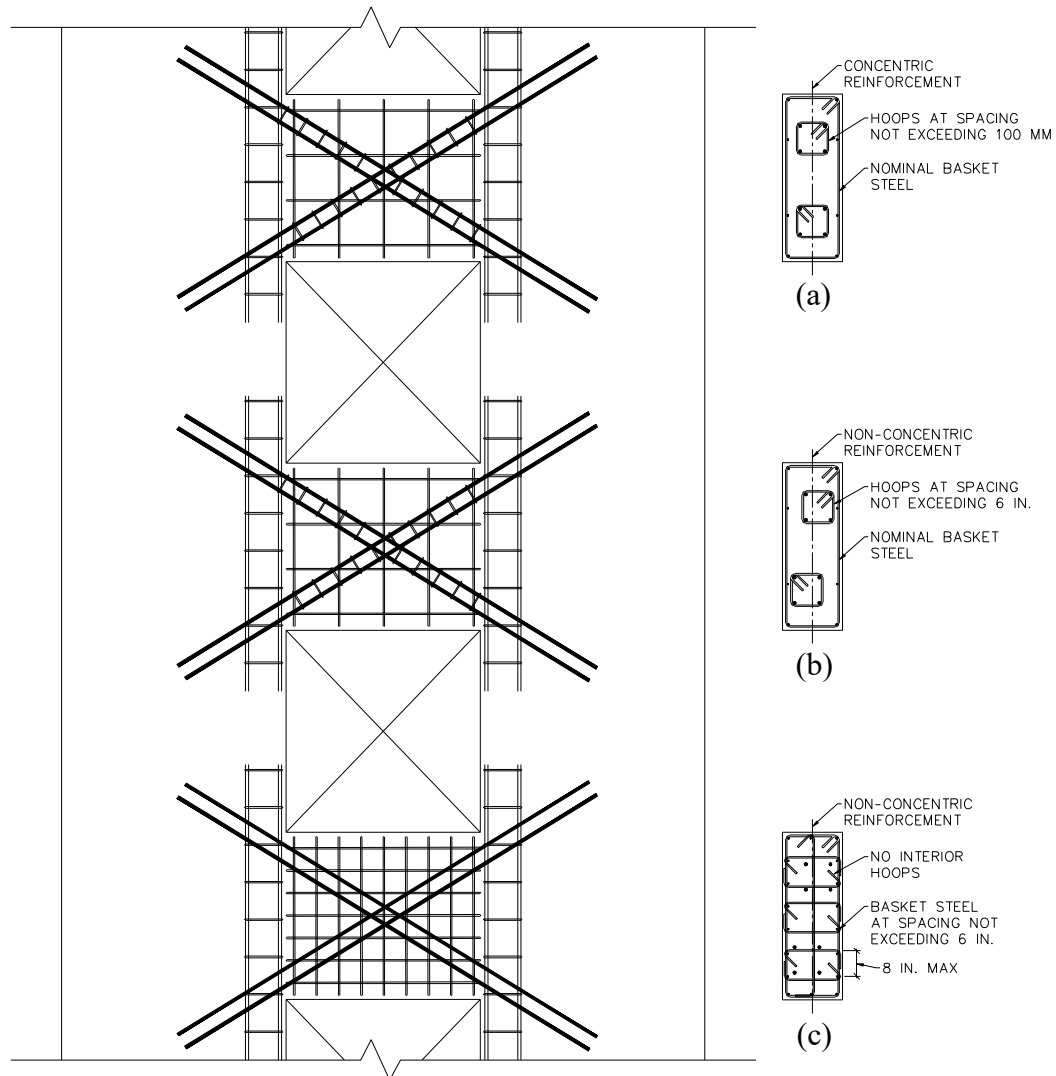
Figure 1.10 – (a) CSA Standard A23.3-14 and (b) and (c) ACI Standard 318-11 coupling beam confinement requirements

1.6. Purpose of the Research Program

The purpose of this research project is to evaluate alternative detailing requirements for diagonally reinforced coupling beams designed to satisfy the requirements of moderately ductile and conventional construction. This research is part of a larger program at McGill University investigating alternative detailing requirements for reinforced concrete coupling beams.

Currently, the CSA Standard A23.3-14 (CSA, 2014) detailing requirements for diagonally reinforced concrete coupled shear walls are the same for the ductile and moderately ductile cases. The ductile diagonally reinforced coupling beams require a high degree of confinement which is provided by closely spaced buckling prevention ties. The diagonal reinforcing steel system is enclosed by a cage of basketting steel, provided for crack control of the coupling beams. The small spacing of hoops combined with the crossing of the diagonal reinforcing bars inside the basket and the placement of the diagonal bars through the concentrated vertical wall steel result in problems with constructability and congestion of reinforcing steel in the coupling beams and at the coupling beam-shear wall interface.

In an attempt to simplify the constructability for the moderately ductile and conventional construction cases, it is proposed that the buckling prevention ties confining the coupling beams be spaced at a larger interval, requiring fewer ties over the length of the diagonal reinforcing.

1.7. Objectives of the Research Program

The objectives of the research program are:

- To compare the reversed cyclic loading response of full-scale coupling beam specimens with different reinforcing steel detailing.
- To investigate the effects of the spacing of the transverse hoops on the response of diagonally reinforced coupling beams subjected to reversed cyclic loading.
- To investigate the effect of the slab restraint on the response of diagonally reinforced coupling beams.
- To compare the constructability of diagonally reinforced coupling beams with different spacing of transverse hoops.
- To propose design guidelines for the detailing of moderately ductile and conventional construction diagonally reinforced coupling beams.

1.8. Methodology and Scope of Study

In order to obtain the required data to meet our research objectives, a research program was carried out as described in Chapters 2 and 3. The scope of the study is also detailed in Chapters 2 and 3.

CHAPTER 2

REVERSED CYCLIC LOADING RESPONSE OF STEEL REINFORCING BARS

2.1. Introduction

In the event of an earthquake, the main reinforcing bars in lateral force resisting members are subject to cyclic reversals of large compressive and tensile strains. In reinforced concrete members, the reinforcing steel resists the tensile stresses after cracking, while the reinforcing bars and the concrete the compressive stresses. After the concrete cracks in tension there is a loss of stiffness of the member. As the intensity of the tensile straining and the number of loading cycles increase, the cracks in the concrete become larger, the concrete cover begins to spall, the mechanical bond between the reinforcing steel and the concrete diminishes and thus the longitudinal reinforcing bars are no longer laterally braced by the surrounding concrete. After cracking and spalling of a diagonally reinforced coupling beam, hoops around the diagonal reinforcing bars serve as anti-buckling reinforcement. The spacing of the transverse hoops will affect the compressive resistance of the diagonal bars.

Reinforcing steel can sustain repeated inelastic tensile straining without a significant reduction in stress. When subjected to reversed cyclic loading, however, the stress-strain curve exhibits the Bauschinger effect for which the yield plateau is suppressed and nonlinear response occurs at a strain much lower than the yield strain (Paulay and Priestley, 1992).

The CSA Standard A23.3-14 (CSA, 2014) limits the spacing of the buckling prevention ties in diagonally reinforced coupling beams to the lesser of six times the diameter of the diagonal bars or to 100 mm. In this experimental program, 15M, 20M and 25M bars were tested under reversed cyclic loading at unbraced lengths of six, eight, ten, twelve and sixteen bar diameters ($6d_b$, $8d_b$, $10d_b$, $12d_b$, $16d_b$) in order to observe their response.

This chapter presents the experimental results from the fifteen reinforcing steel bar reversed cyclic tests. The results clearly demonstrate the effect of the unbraced length of reinforcing steel bars when subjected to reversed cyclic loading.

2.2. Test Setup

Fifteen reinforcing steel bar reversed cyclic tests were carried out. The target deflection levels established in the loading histories were based on the yield strains of the various reinforcing steel bars obtained from monotonic tensile tests. The load histories used in the reversed cyclic tests are illustrated in Fig. 2.1. Five tests were carried out on three reinforcing bars of different diameters; 15M, 20M and 25M. Each of the five tests was carried out at a different unbraced length of loading in order to simulate a corresponding reinforcing steel tie spacing, illustrated in Fig. 2.2. An illustration of the test setup is shown in Fig. 2.3.

The fifteen specimens are summarized in Table 2.1.

Table 2.1 – Summary of reversed cyclic loading specimens

Specimen	Unbraced length (mm)	Specimen #	Unbraced length (mm)	Specimen #	Unbraced length (mm)
15M-6d_b	90	20M-6d_b	120	25M-6d_b	150
15M-8d_b	120	20M-8d_b	160	25M-8d_b	200
15M-10d_b	150	20M-10d_b	200	25M-10d_b	250
15M-12d_b	180	20M-12d_b	240	25M-12d_b	300
15M-16d_b	240	20M-16d_b	320	25M-16d_b	400

The reinforcing steel bars were not machined prior to installation into the test setup. The loading mechanism of the MTS 793 testing machine is equipped with hydraulic grips are capable of adequately gripping the deformed reinforcing bars subjected to reversed cyclic loading. Preserving the deformations along the reinforcing steel bars was deemed necessary in order to accurately reflect the true behaviour of the deformed bars in a concrete member after spalling of the concrete has taken place (see Fig. 2.2).
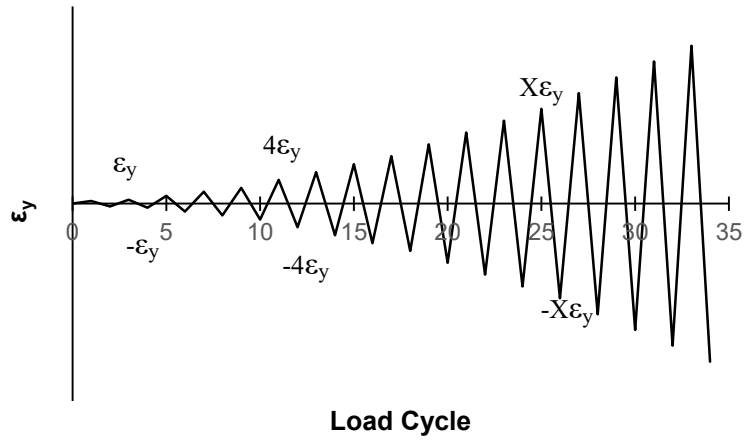
Figure 2.1 – Loading histories for the reinforcing bar reversed cyclic tests
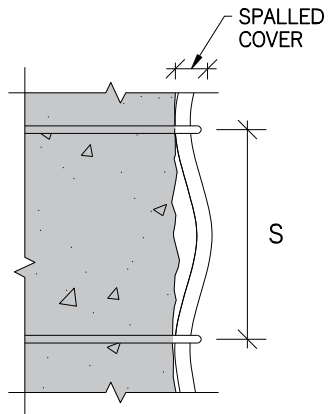
Figure 2.2 – Unbraced bar length between transverse hoops in reinforced concrete member after spalling of the concrete cover
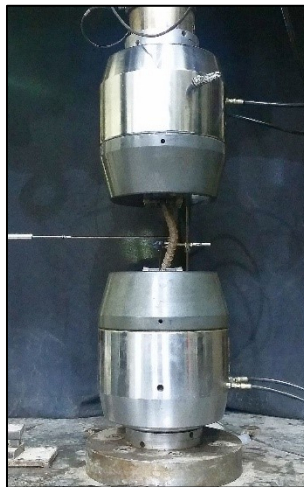
Figure 2.3 – Buckled reinforcing bar in the MTS 793 testing machine

19

2.3. Experimental Results

This section describes the response of the fifteen reinforcing steel bars tested under reversed cyclic loading. The stress versus strain hysteretic responses of the specimens are plotted in Fig. 2.6, Fig. 2.7 and Fig. 2.8. Also included in the figures are the typical monotonic stress-strain curve for each reinforcing bar size. More information related to the material properties is included in Chapter 3. The maximum stress and strain values for both the negative (compressive) and positive (tensile) loading recorded during the test are presented in Table 2.2. Table 2.3 presents the maximum positive and negative stresses and strains achieved prior to 20% of strength decay. The stresses and strains were calculated using the corresponding bar areas and the readings of the applied force and head displacement values from the MTS testing machine.

Table 2.2 – Maximum compression and tension stresses and strains

Bar Diameter	$16d_b$	$12d_b$	$10d_b$	$8d_b$	$6d_b$
15M	-462 MPa (-0.0573)	-467 MPa (-0.0478)	-467 MPa (-0.0477)	-471 MPa (-0.0571)	-516 MPa (-0.0666)
	462 MPa (0.0573)	496 MPa (0.0497)	504 MPa (0.0573)	525 MPa (0.0574)	550 MPa (0.0669)
20M	-435 MPa (-0.0575)	-474 MPa (-0.0575)	-473 MPa (-0.0515)	-477 MPa (-0.0574)	-481 MPa (-0.0671)
	461 MPa (0.0671)	477 MPa (0.0625)	491 MPa (0.0671)	514 MPa (0.0576)	526 MPa (0.0672)
25M	-472 MPa (-0.0411)	-486 MPa (-0.0411)	-492 MPa (-0.0411)	-533 MPa (-0.0412)	-599 MPa (-0.0514)
	592 MPa (0.0515)	592 MPa (0.0514)	617 MPa (0.0411)	636 MPa (0.0412)	672 MPa (0.0515)

Table 2.3 – Maximum compression and tension stresses and strains prior to 20% decay of the peak stress value

Bar Diameter	16d_b	12d_b	10d_b	8d_b	6d_b
15M	-462 MPa (-0.0063)	-467 MPa (-0.0096)	-467 MPa (-0.0191)	-471 MPa (-0.0316)	-516 MPa (-0.0570)
	462 MPa (0.0095)	489 MPa (0.0190)	504 MPa (0.0252)	525 MPa (0.0380)	550 MPa (0.0456)
20M	-435 MPa (-0.0032)	-474 MPa (-0.0096)	-473 MPa (-0.0127)	-477 MPa (-0.0254)	-481 MPa (-0.0478)
	461 MPa (0.0094)	477 MPa (0.0100)	491 MPa (0.0192)	514 MPa (0.0319)	526 MPa (0.0570)
25M	-472 MPa (-0.0068)	-486 MPa (-0.0102)	-492 MPa (-0.0270)	-533 MPa (-0.0412)	-599 MPa (-0.0514)
	592 MPa (0.0103)	592 MPa (0.0135)	617 MPa (0.0343)	636 MPa (0.0412)	672 MPa (0.0515)
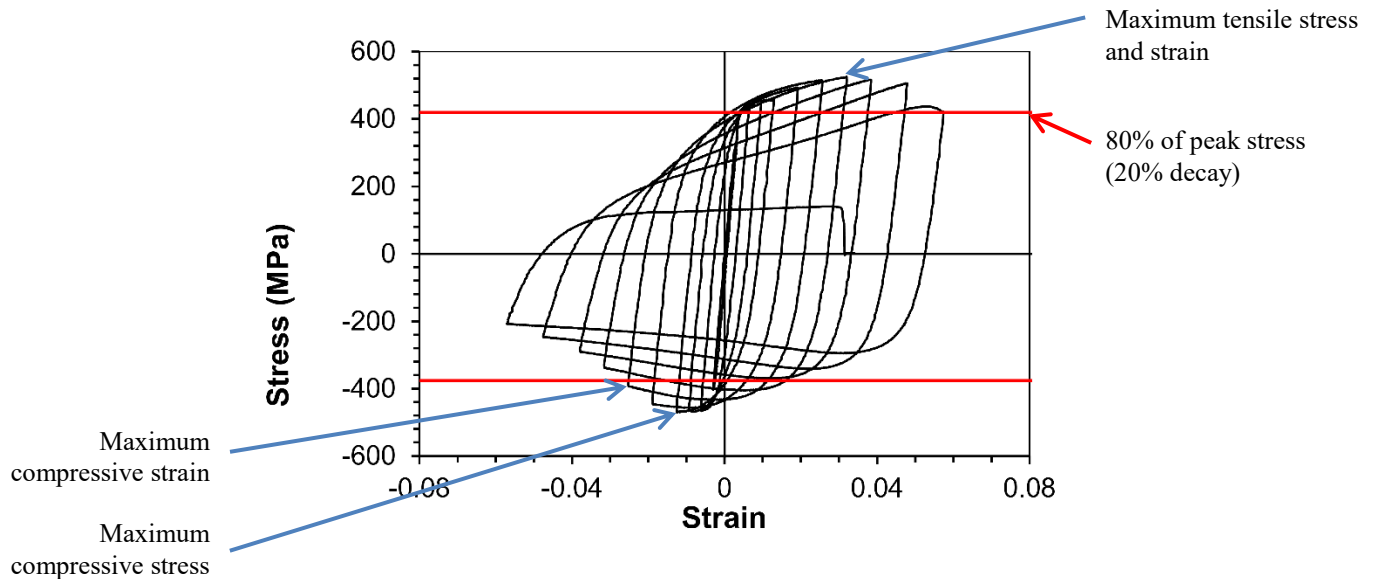
Figure 2.4 – Maximum stress and strain values prior to 20% decay of the peak stress value.
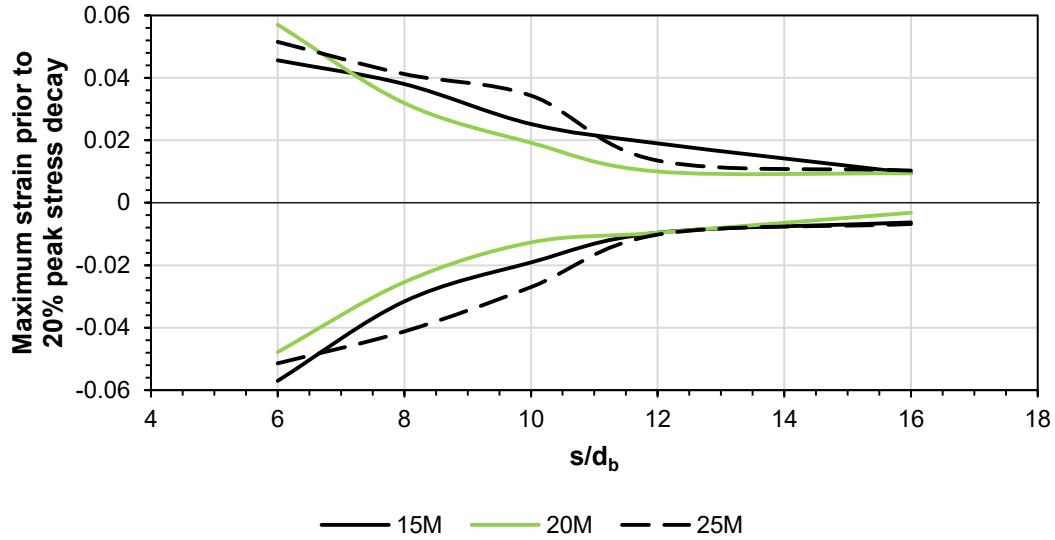
Figure 2.5 – Maximum and strain values prior to 20% decay of the peak stress value.

The influence of increasing the unbraced length on the early onset of buckling of the reinforcing steel occurred as expected. All of the specimens with the larger unbraced length showed early signs of buckling during the first elastic compressive load cycle, prior to attaining their yield strength in compression. A rapid loss in compressive strength was observed following the first elastic cycle. In all cases, reducing the unbraced length led to an increase in the performance of the reinforcing steel bars. The largest difference in behaviour appears to have occurred when the unbraced length was reduced from $8d_b$ to $6d_b$. The hysteretic responses of the specimens with the $6d_b$ unbraced length appear significantly superior to those having an unbraced length of $8d_b$, notably by the fuller hysteresis loops, significant strain hardening and a slow, gradual reduction in compressive strength. The specimens with the $6d_b$ unbraced length responses appear very stable.

In all cases smaller unbraced lengths led to more controlled, regular and higher energy-dissipating responses. The cumulative strain energy dissipation of the specimens are plotted in Fig. 2.7, Fig. 2.8 and Fig. 2.9. On average, the specimens with the $6d_b$ unbraced length absorbed 2.8 times as much energy as the corresponding specimens with $16d_b$ unbraced lengths.

22
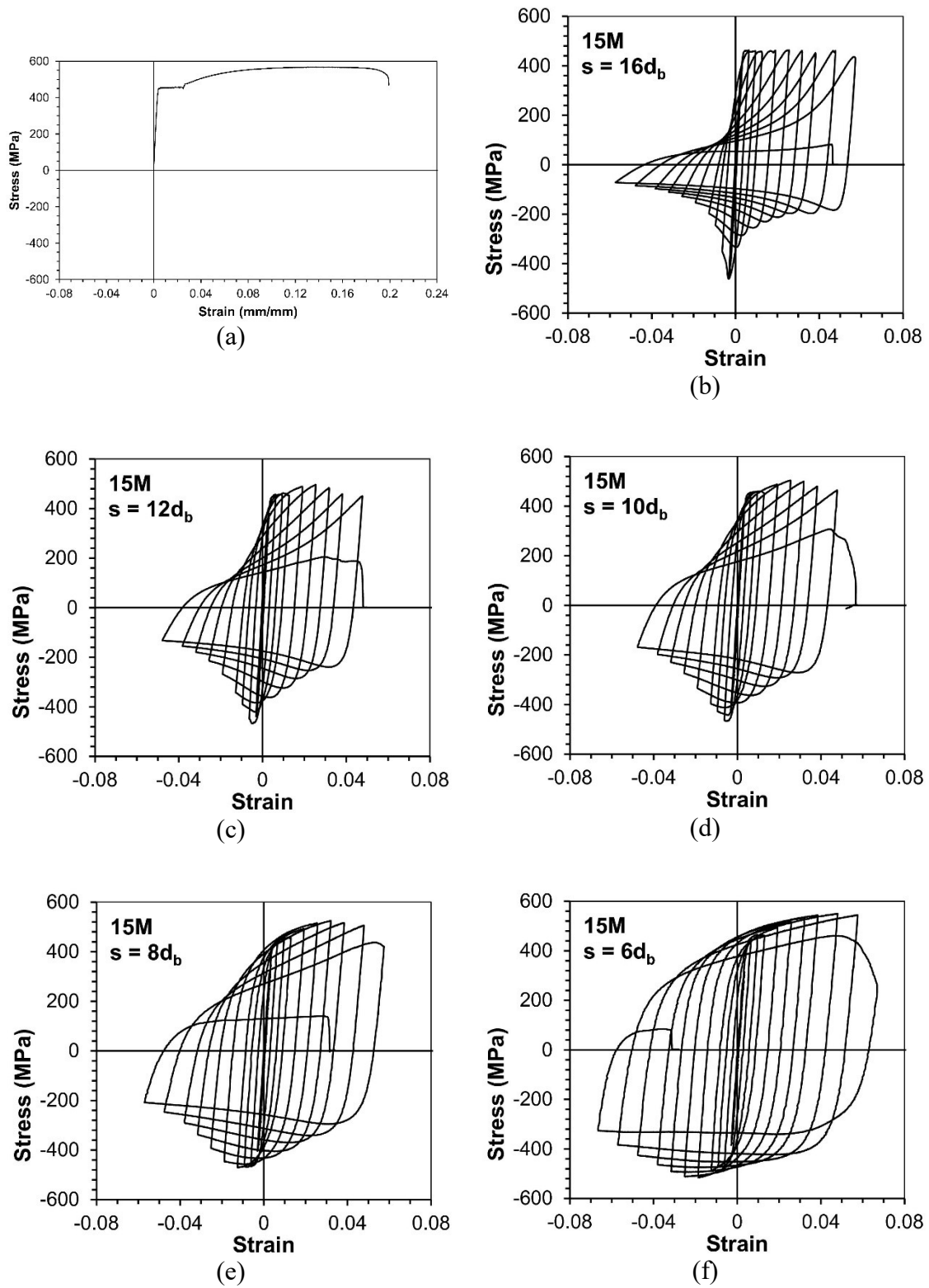
Figure 2.6 – Hysteretic response of 15M reinforcing bars subjected to reversed cyclic loading
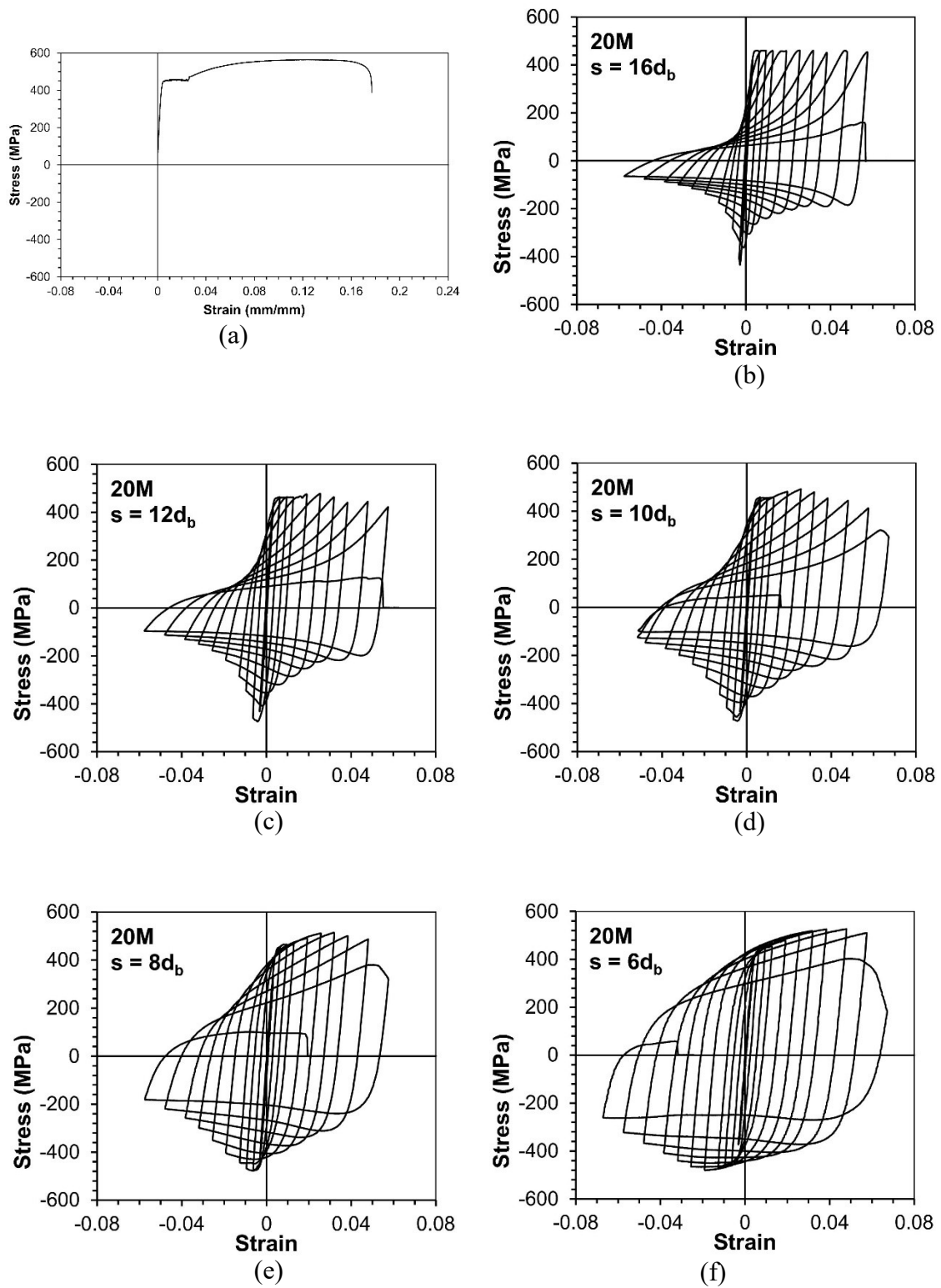
Figure 2.7 – Hysteretic response of 20M reinforcing bars subjected to reversed cyclic loading

24
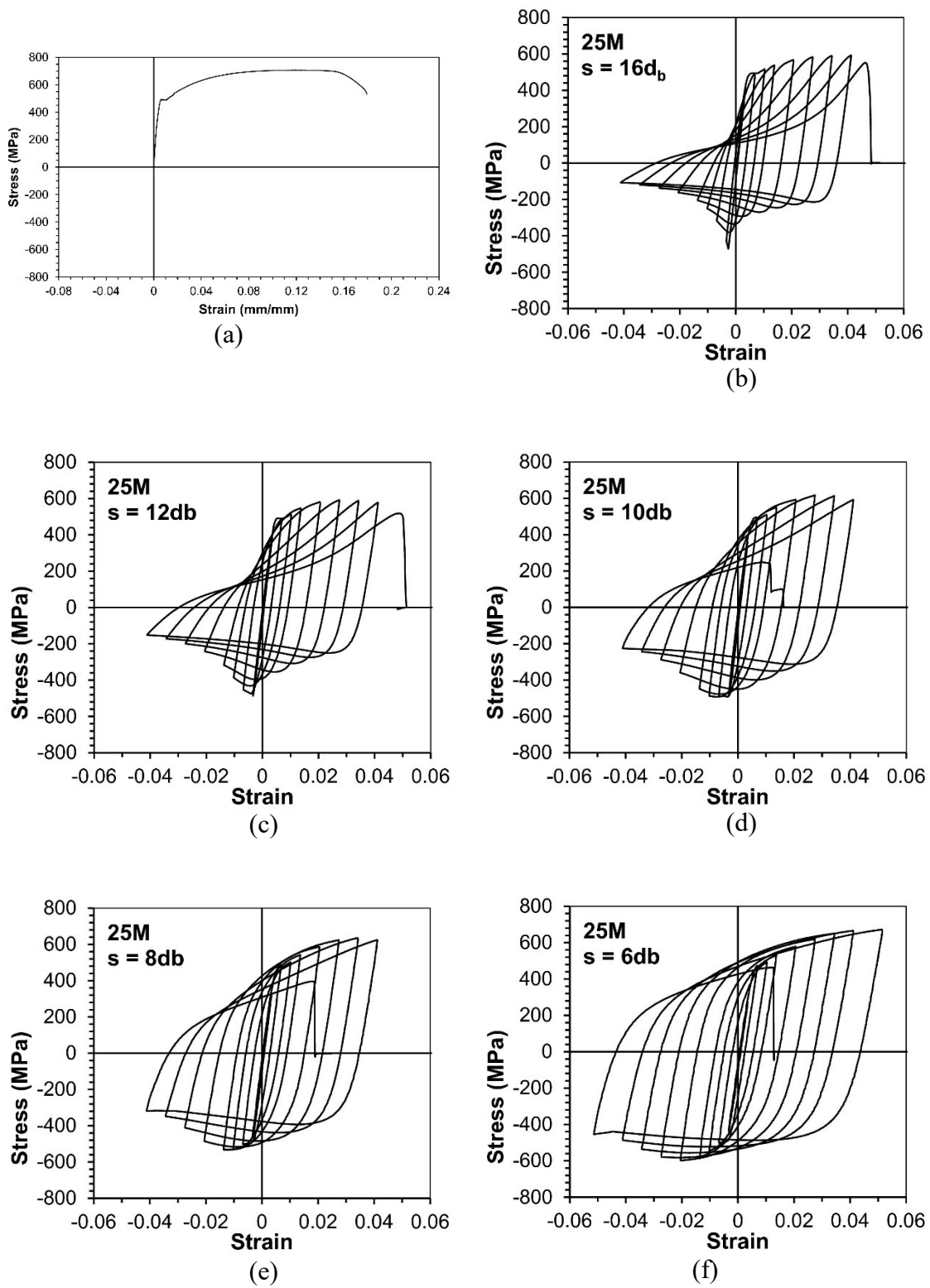
Figure 2.8 – Hysteretic response of 25M reinforcing bars subjected to reversed cyclic loading
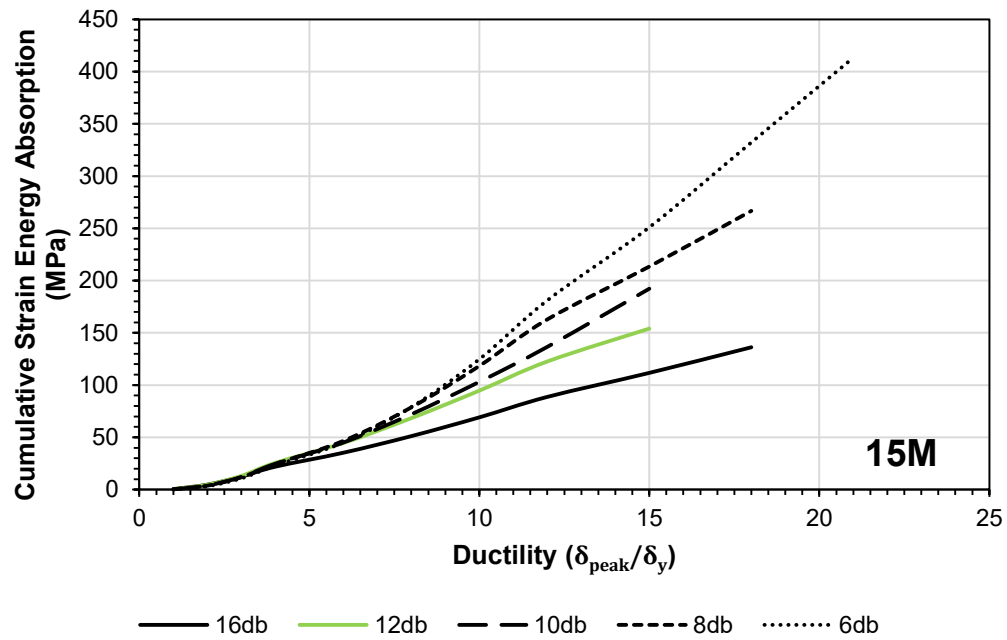
Figure 2.9 – Cumulative strain energy dissipation for 15M bars
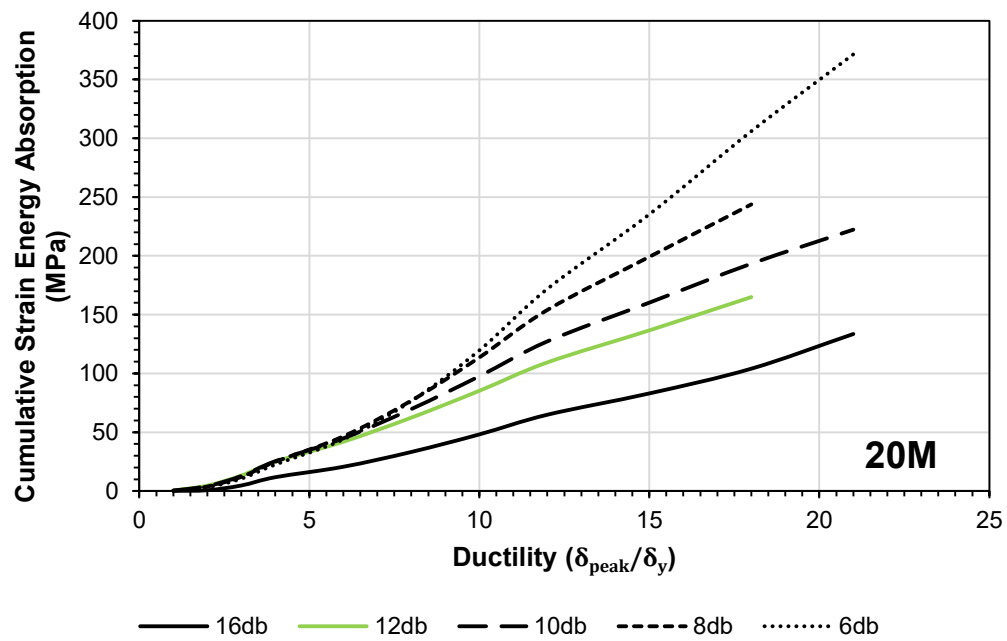
Figure 2.10 – Cumulative strain energy dissipation for 20M bars
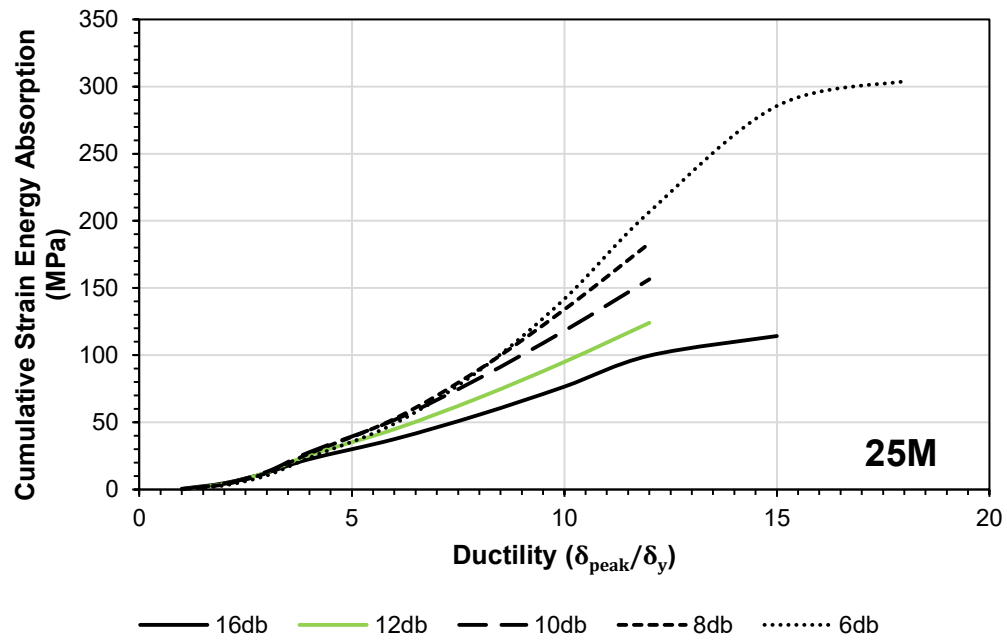
Figure 2.11 – Cumulative strain energy dissipation for 25M bars

CHAPTER 3

COUPLED WALLS EXPERIMENTAL PROGRAM

The coupled wall experimental program consisted of the construction and testing of four full-scale diagonally reinforced concrete coupling beams.

3.1. Diagonally Reinforced Concrete Coupled Walls Test Specimens

Four diagonally reinforced concrete coupling beams connected to walls were detailed and constructed. The four coupling beam-wall specimens were detailed for different levels of ductility in accordance with the CSA Standard A23.3-14 (CSA, 2014) as described in Table 3.1.

Table 3.1 – Summary of diagonally reinforced coupled shear wall specimens

Specimen	End Wall Detailing	# Diag. Bars in Each Direction	Diag. Bar Tie Spacing
CC-16d_b	Conventional Construction (cl. 14)	4-20M	16 d_b 320 mm
MD-10d_b	Moderately Ductile (cl. 21)	4-20M	10 d_b 200 mm
MD-8d_b	Moderately Ductile (cl. 21)	4-20M	8 d_b 160 mm
D-6d_b	Ductile (cl. 21)	4-20M	6 d_b 120 mm

The concrete dimensions of the coupled wall specimens were identical. Each end wall was 300 mm in width and measured 1500 mm in length by 1800 mm in height (1500 mm x 1800 mm x 300 mm). Each end wall had 4-20M concentrated vertical bars in the wall pier contiguous with the coupling beam and 2-20M vertical bars at the opposing end of the wall. The number and spacing of the column hoops and ties, vertical bars and horizontal bars in the walls were detailed based on the specified ductility.

Each coupling beam was 300 mm in width and measured 1000 mm in length by 880 mm in depth (1000 mm x 880 mm x 300 mm). The detailing of the confining hoops for the diagonal reinforcing bars of the coupling beams varied depending on the specified

ductility. Four 20M diagonal bars were provided in each direction in the coupling beams. The diagonal reinforcing bars were installed at an angle α of 30º. The "basket" reinforcing, used to prevent excessive spalling of the concrete, was identical in each of the specimens. In each basket four 10M vertical closed stirrups were provided at 300 mm spacing and four 10M horizontal reinforcing bars, which did not extend into the walls, were provided only to hold the basket stirrups in place.

A 20 mm concrete cover was provided for all of the exterior reinforcing bars.

3.1.1. Detailing of the Coupling Beams

All of the diagonally reinforced coupling beams had similar details. The only variance was the spacing the 10M buckling prevention ties which enclose the diagonal reinforcing steel bars. Figure 3.1 illustrates the detailing and cross-sectional details of a typical coupling beam.
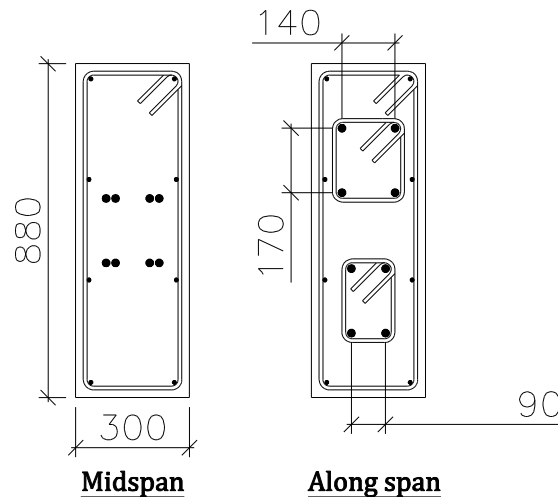
Figure 3.1 – Detailing of typical coupling beam

3.1.2. Detailing of Specimen CC-16d$_b$

The walls of specimen CC-16d$_b$ were detailed as "conventional construction" reinforced shear walls in accordance with Clause 14 of the CSA Standard A23.3-14 (CSA, 2014). The diagonal reinforced coupling beam was detailed as having four 20M diagonal bars with 10M ties spaced at 320 mm, equivalent to sixteen (16) times the diameter of the diagonal reinforcing bars. The embedment of the diagonal bars in the walls exceeded 1.5 times the development length in order to fully develop the bars at the coupling beam-end wall interface. Figure 3.2 illustrates the detailing of specimen CC-16d$_b$.
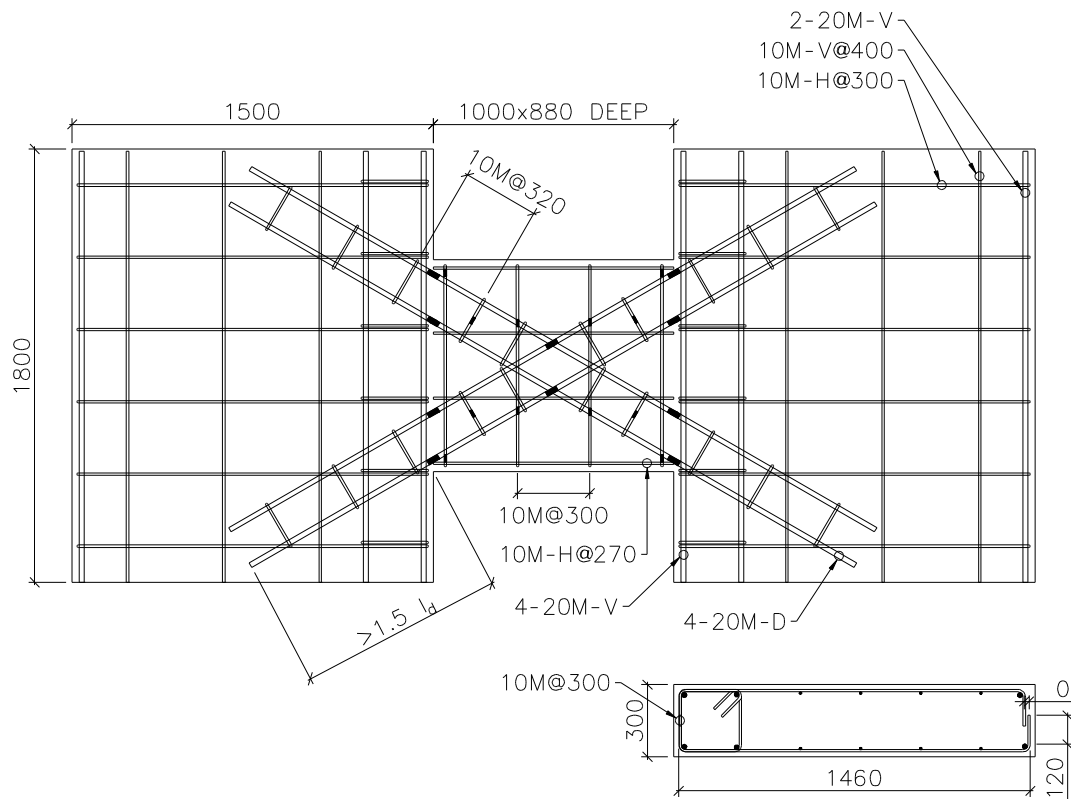
Figure 3.2 – Detailing of specimen CC-16d$_b$

3.1.3. Detailing of Specimen MD-10d$_b$

The end walls of specimen MD-10d$_b$ were detailed as moderately ductile shear walls in accordance with Clause 21 of the CSA Standard A23.3-14 (CSA, 2014). The diagonal reinforced coupling beam was detailed as having 4-20M diagonal bars with 10M ties spaced at 200 mm, equivalent to ten times the diameter of the diagonal reinforcing bars. The embedment of the diagonal bars in the walls exceeded 1.5 times the development length in order to fully develop the bars at the coupling beam-end wall interface. Figure 3.3 illustrates the detailing of specimen MD-10d$_b$.
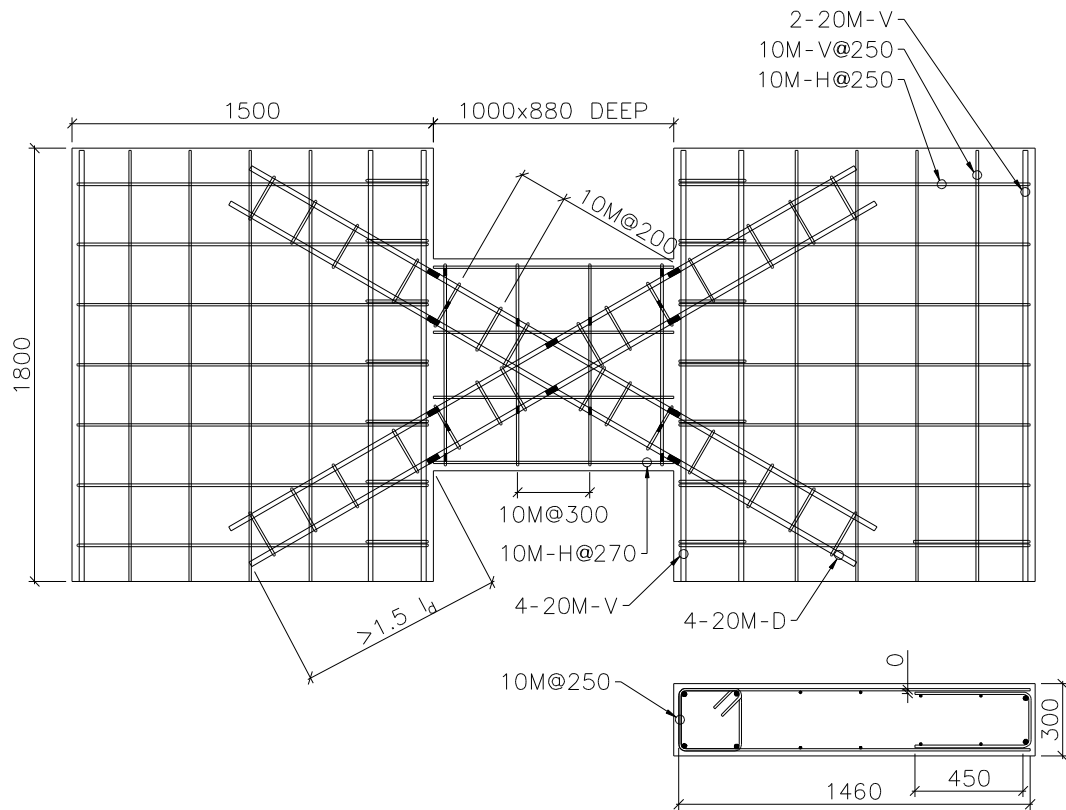
Figure 3.3 – Detailing of specimen MD-10d$_b$

31

3.1.4. Detailing of Specimen MD-8d$_b$

The end walls of specimen MD-8d$_b$ were detailed as moderately ductile shear walls in accordance with Clause 21 of the CSA Standard A23.3-14 (CSA, 2014). The diagonal reinforced coupling beam was detailed as having four 20M diagonal bars with 10M ties spaced at 160 mm, equivalent to eight times the diameter of the diagonal reinforcing bars. The embedment of the diagonal bars in the walls exceeded 1.5 times the development length in order to fully develop the bars at the coupling beam-end wall interface. Figure 3.4 illustrates the detailing of specimen MD-8d$_b$.
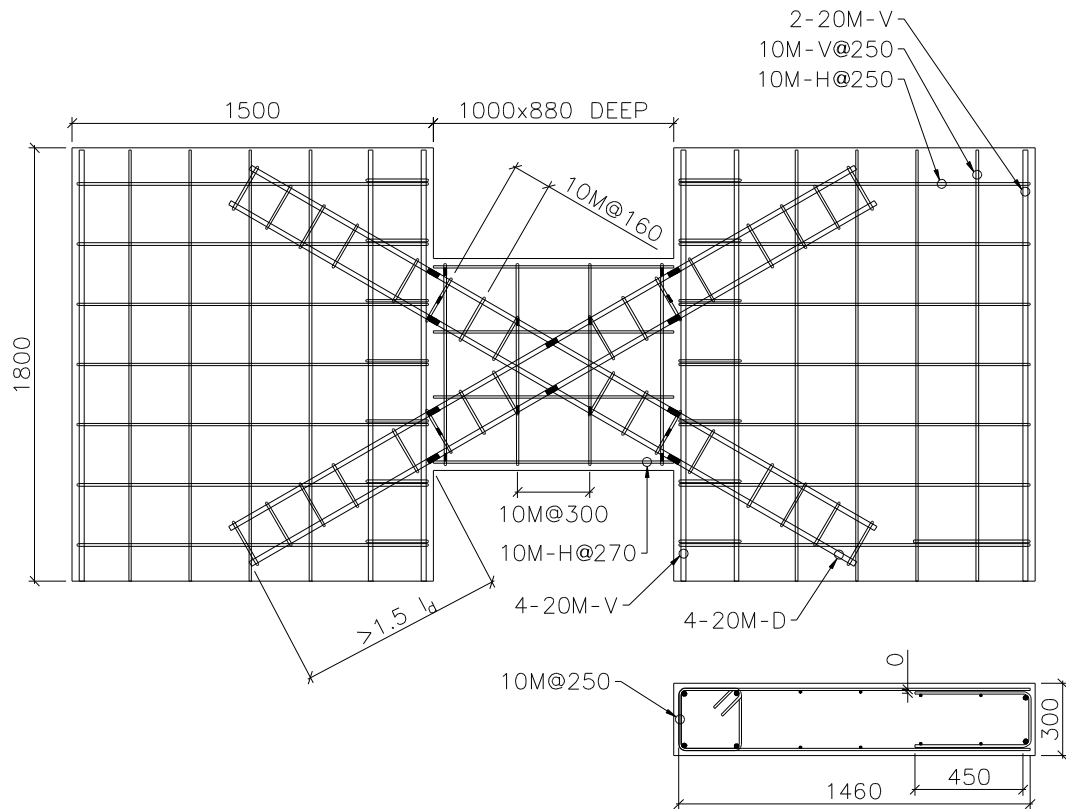
Figure 3.4 – Detailing of specimen MD-8d$_b$

3.1.5. Detailing of Specimen D-6d$_b$

The end walls of specimen D-6d$_b$ were detailed as ductile shear walls in accordance with Clause 21 of the CSA Standard A23.3-14 (CSA, 2014). The diagonal reinforced coupling beam was detailed as having four 20M diagonal bars with 10M ties spaced at 120 mm, equivalent to six times the diameter of the diagonal reinforcing bars. The embedment of the diagonal bars in the walls exceeded 1.5 times the development length in order to fully develop the bars at the coupling beam-end wall interface. Figure 3.5 illustrates the detailing of specimen D-6d$_b$.
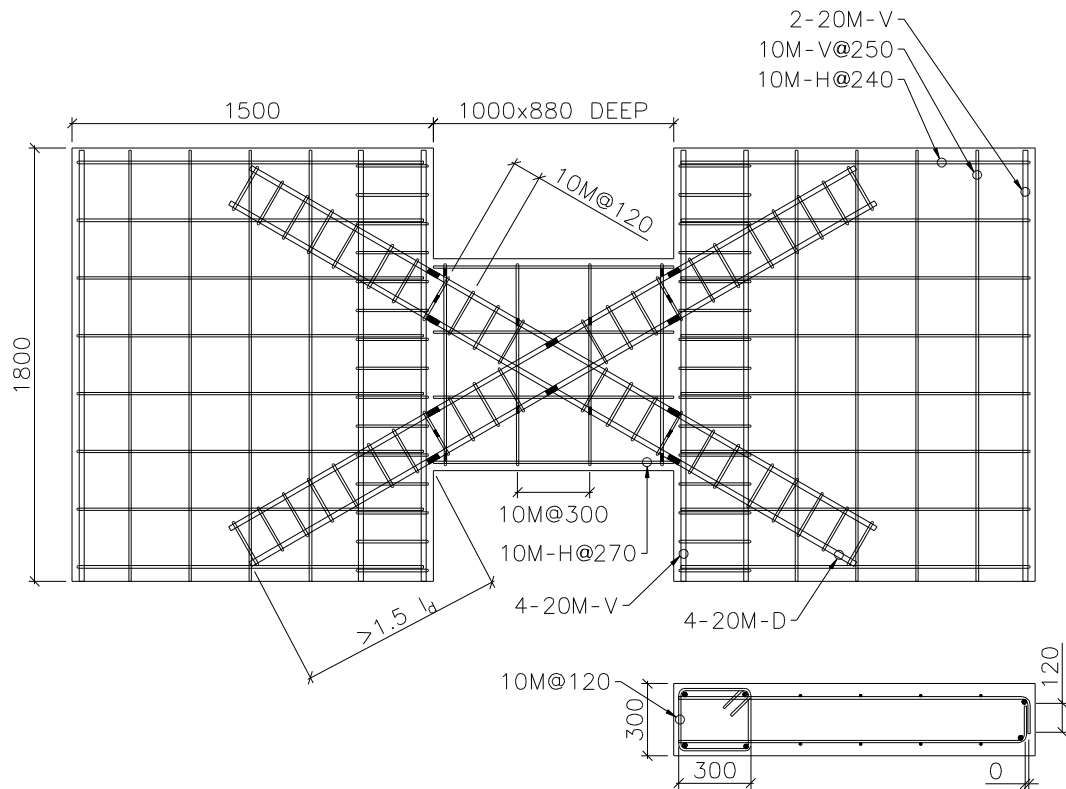
Figure 3.5 – Detailing of specimen D-6d$_b$

3.1.6. Comparison of the Constructed Specimens

Figure 3.6 illustrates the difference in the reinforcing steel layout for the four constructed coupling beams.
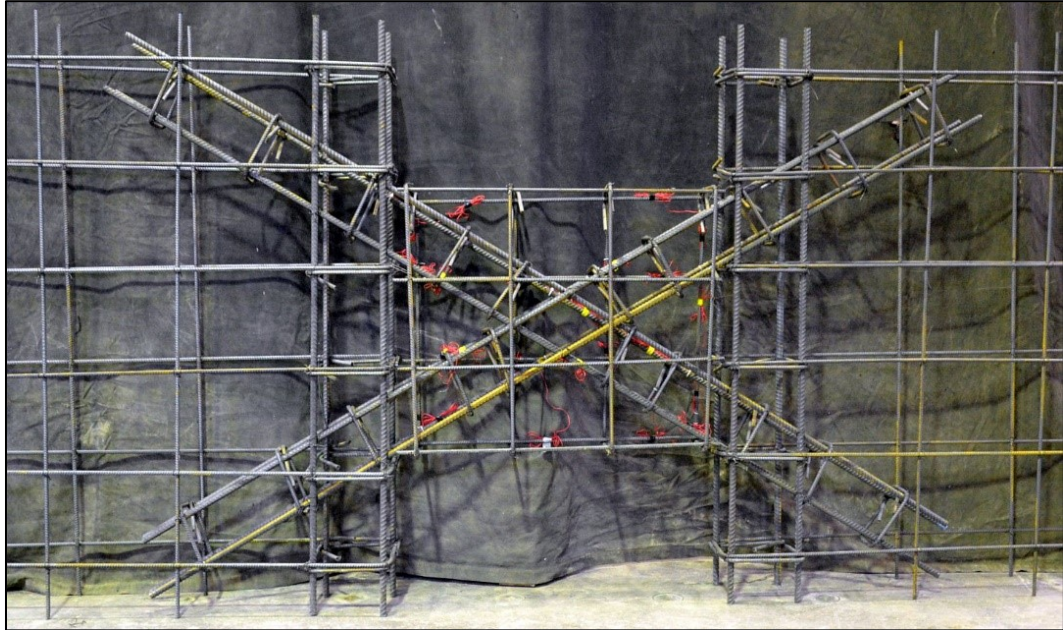
(a)
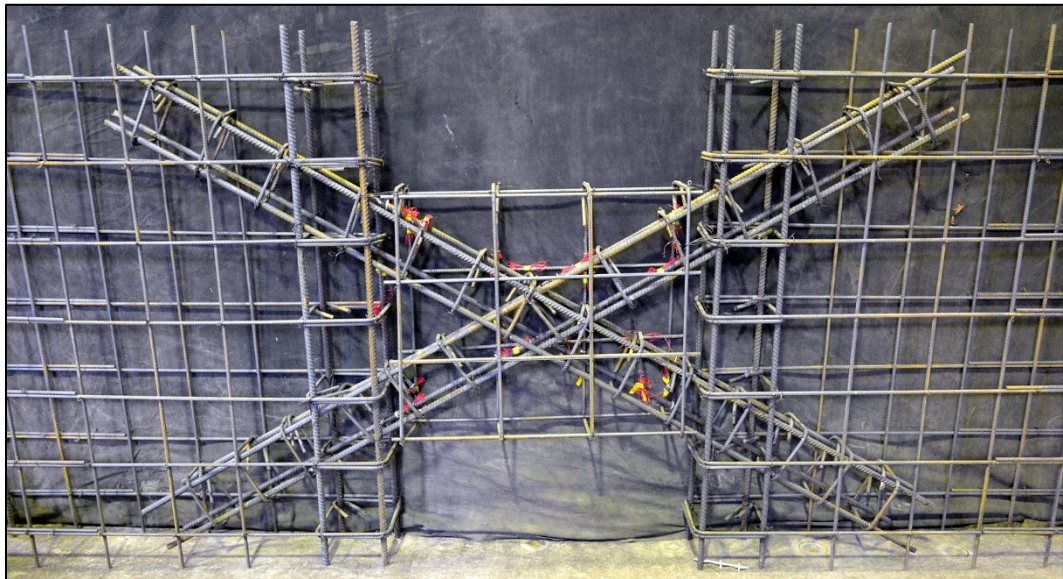
(b)

Figure 3.6 – Photographs of the reinforcement for the (a) CC-16d$_b$, (b) MD-10d$_b$, (c) MD-8d$_b$ and (d) D-6d$_b$ specimens
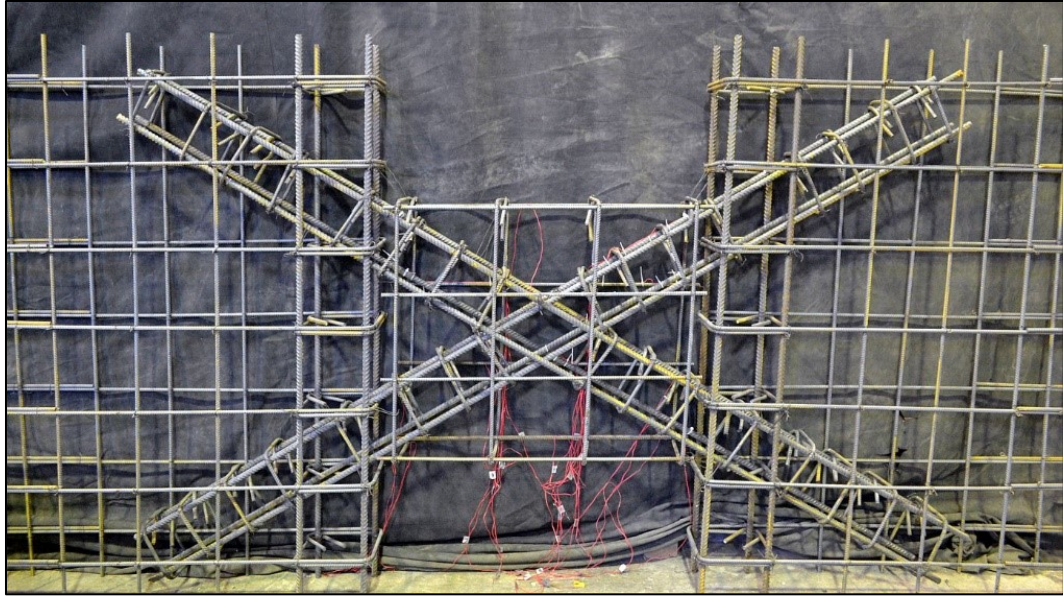
(c)
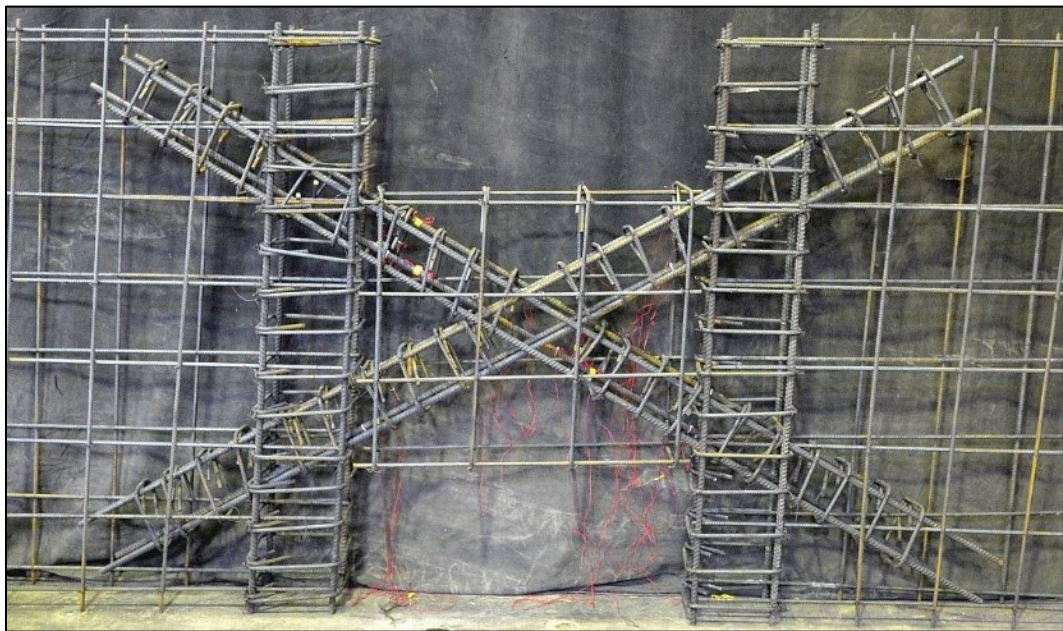
(d)

Figure 3.6 cont. – Photographs of the reinforcement for the (a) CC-16d$_b$, (b) MD-10d$_b$, (c) MD-8d$_b$ and (d) D-6d$_b$ specimens

3.2. Test Setup

The specimens were tested in the McGill University Jamieson Structures Laboratory using the McGill University Coupled Wall Testing Apparatus. The testing apparatus for specimens CC-16d_b, MD-10d_b and MD-8d_b is illustrated in Fig. 3.7 and Fig. 3.8. The testing apparatus for specimen D-6d_b, which included passive lateral restraint, is illustrated in Fig. 3.9 and Fig. 3.10.

Each specimen consisted of two shear walls connected by a coupling beam. The specimens were full-scale models of a typical floor level of a coupled wall system, including portions of the walls directly above and below the coupling beam. When a coupled shear wall structure is subject to lateral loading it is assumed that the centroidal axes of the coupled walls remain parallel at each floor level. This phenomenon is illustrated in Fig. 3.11. Fig. 3.12 illustrates how the McGill University Coupled Wall Testing Apparatus simulates the loading conditions.

The loading and reactions were applied to the walls through the loading beams located at the bases of each wall. At the loaded wall, the upward (positive) shear load was applied to the specimen at a location such that the line of action of the applied load passes through the midspan of the coupling beam. The upwards load was provided by three thirty-ton hydraulic jacks reacting against the topside of the strong floor. Similarly, the downward (negative) shear load was applied to specimen by two tension rods which were tensioned by three thirty-ton hydraulic jacks reacting against the underside of the strong floor. The maximum applicable shear force was thus ninety tons, equivalent to 800 kN. A single thirty-ton hydraulic jack placed at the far end of the loaded wall applied load in order to balance the dead load of the specimen and testing apparatus and in order to keep the two walls parallel throughout the reversed cyclic loading.

All externally applied loads were displayed in real time and recorded using load cells and a data acquisition system.

At the fixed wall, the fixed boundary conditions were achieved by clamping the reaction beam to the strong floor and then clamping the specimens to the reaction beam. At a location closest to the coupling, two tension rods were tensioned to 900 kN. At the far end of the loading beam, two tension rods were tensioned to 250 kN. The wall was

clamped to the loading and reaction beams using six pairs of tension rods, each pair tensioned to 300 kN.
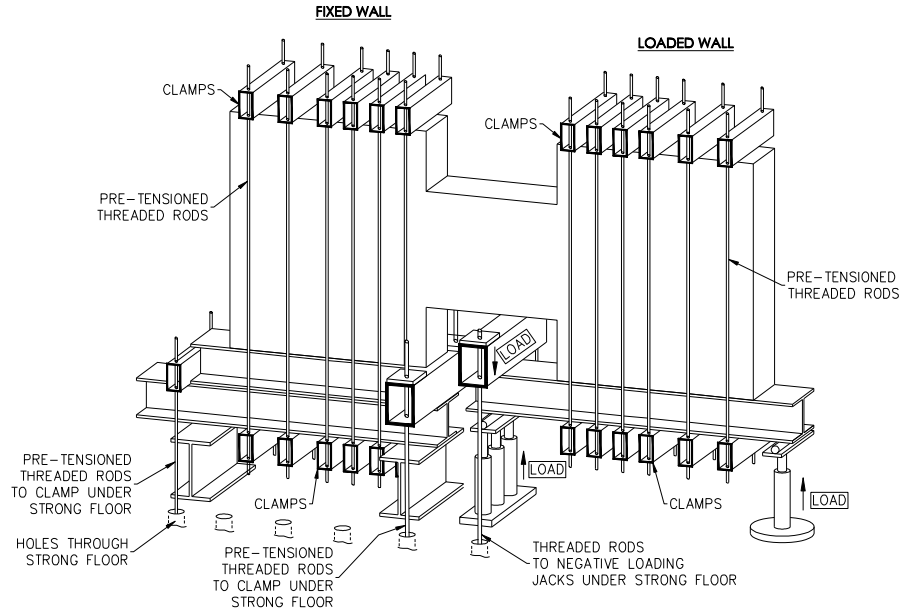
Figure 3.7 – Illustration of McGill University Coupled Wall Testing Apparatus for specimens CC-16d$_b$, MD-10d$_b$ and MD-8d$_b$

Figure 3.8 – Photograph of McGill University Coupled Wall Testing Apparatus for specimens CC-16d$_b$, MD-10d$_b$ and MD-8d$_b$

Longitudinal restraint was provided for a portion of the testing of specimen D-6d$_b$, in response to significant elongations observed during the previous specimen tests. The longitudinal clamping was provided by two pairs of tension rods spaced equally above and below the coupling beam's centroidal axis, avoiding load eccentricities. Each pair of tension rods were tensioned to 30 kN prior to the commencement of the testing procedure. This horizontal restraint corresponds to restraint provided by the reinforced concrete floor slab. The equivalent spring stiffness provided by two pairs of 25.4 mm diameter threaded rods was 76 kN/mm, calculated using Eq. 3.1.

$$k = \frac{nAE}{L} = \frac{4(0.75)(\pi)(25.4^2)(200000)}{4(4000)} = 76 \, {kN}/{mm} \tag{3.1}$$
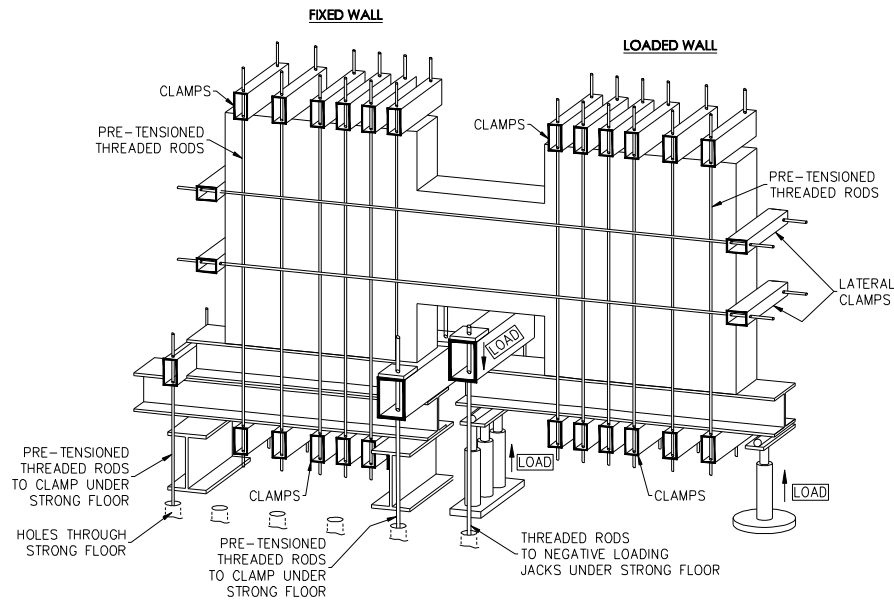
Figure 3.9 – Illustration of McGill University Coupled Wall Testing Apparatus for specimen D-6d$_b$

Figure 3.10 – Photograph of McGill University Coupled Wall Testing Apparatus for specimen D-6d$_b$
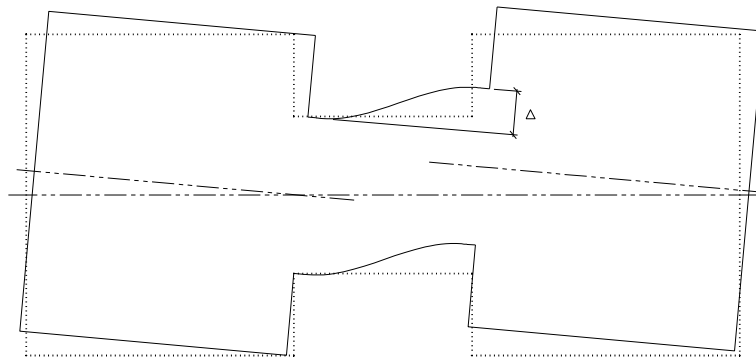
Figure 3.11 – Deformation of a coupled wall in an actual building
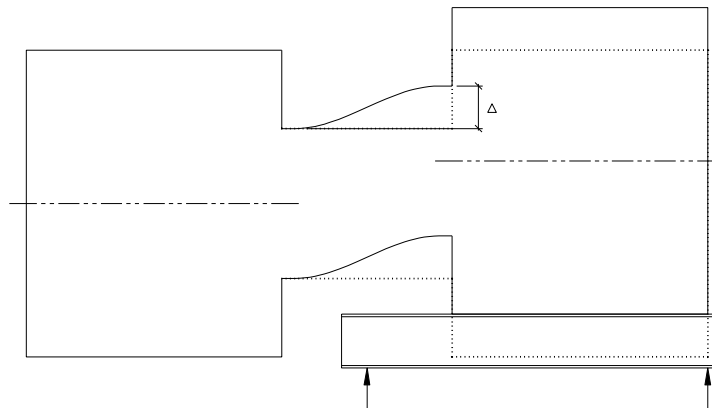
Figure 3.12 – Deformation of a coupled wall test specimen

3.3. Instrumentation

All of the instrumentation was connected to a computerized data acquisition system and displayed in real-time during the tests. The data acquisition system also recorded the data for post-processing analysis.

3.3.1. Load measurements

Figure 3.13 shows the locations of the load cells (LC) used to measure the loads applied to the coupled wall specimens. The load cells measured the applied load in real time. Three 75 kip (333 kN) capacity load cells, LC-1, LC-2 and LC-3, were installed above the strong floor to measure the external load applied through a line passing through the midspan of the coupling beam during the positive (upward) cycles. Two 100 kip (445 kN) capacity load cells, LC-4 and LC-5, were installed below the strong floor to measure the external load applied through a line passing through the midspan of the coupling beam during the negative (downward) cycles. One 75 kip (333 kN) capacity load cell, LC-6, was used to measure the external load applied by the leveling jack. For specimen D-6d_b, one 75 kip (333 kN) capacity load cell was installed at each pair of threaded rods (LC-7 and LC-8) in order to measure the passive external force applied by the clamps during the test.
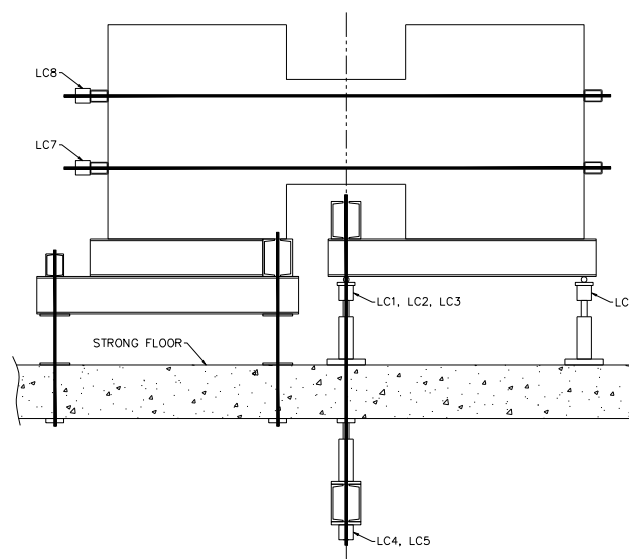
Figure 3.13– Load cell locations

3.3.2. Displacement measurements

Figure 3.14 shows the locations of the linear voltage displacement transformers (LVDTs) used for all four coupled wall specimens. Four LVDTs measured the vertical displacements at the locations indicated, allowing for the differential displacements and corresponding rotations to be determined in real time. Through the control of the displacements measured by the LVDTs and the applied loads, the vertical centroidal axes of the two connected walls were kept as parallel as possible during testing. The projected relative displacement (Δ) of the loaded wall was calculated using the translational displacement (Δ_T) and the rotational displacement (Δ_θ) given in Eq. 3.2 to Eq. 3.5. The rotational displacement component accounts for the differential rotations (i.e. slopes – m) of the loaded wall (LW) and fixed wall (FW). If the rotations of the walls are identical, the relative displacement is equivalent to the translational displacement.

$$\Delta_T = \left(\frac{\Delta_1 + \Delta_2}{2}\right) - \left(\frac{\Delta_3 + \Delta_4}{2}\right) \tag{3.2}$$

$$m_{LW} = \left(\frac{(\Delta_2 - \Delta_1)}{920}\right) \tag{3.3}$$

$$m_{FW} = \left(\frac{(\Delta_3 - \Delta_4)}{920}\right) \tag{3.4}$$

$$\Delta = \left(\Delta_2 + \frac{840}{920}(\Delta_2 - \Delta_1)\right) - \left(\Delta_3 + \frac{840}{920}(\Delta_3 - \Delta_4)\right) \tag{3.5}$$

where

$\Delta_1, \Delta_2, \Delta_3, \Delta_4$ = vertical displacements at the LVDT locations (see fig. 2.15)

Eight LVDTs were aligned with the diagonal reinforcing steel cages and placed at a known spacing in order to determine the average strains of the concrete.

Figure 3.15 illustrates the locations of the light emitting diodes (LEDs) used for the coupled wall specimens. An array of thirteen LEDs were installed at the front face of the specimens. The data acquisition system for the LEDs could not display the results in real-time and thus the displacement values were used in post-processing analysis only.

41
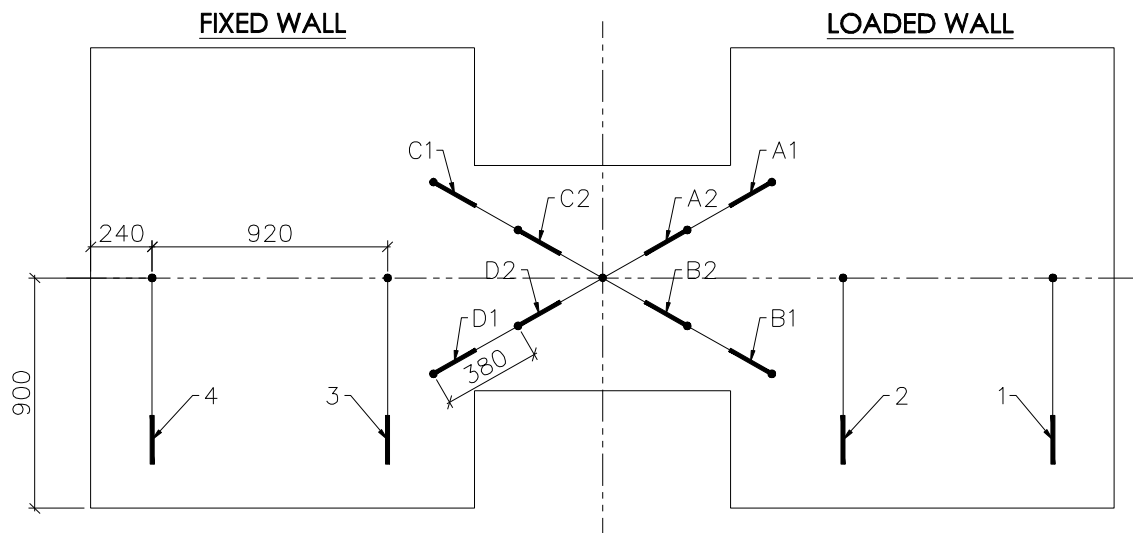
Figure 3.14 – Linear voltage displacement transformer (LVDT) locations
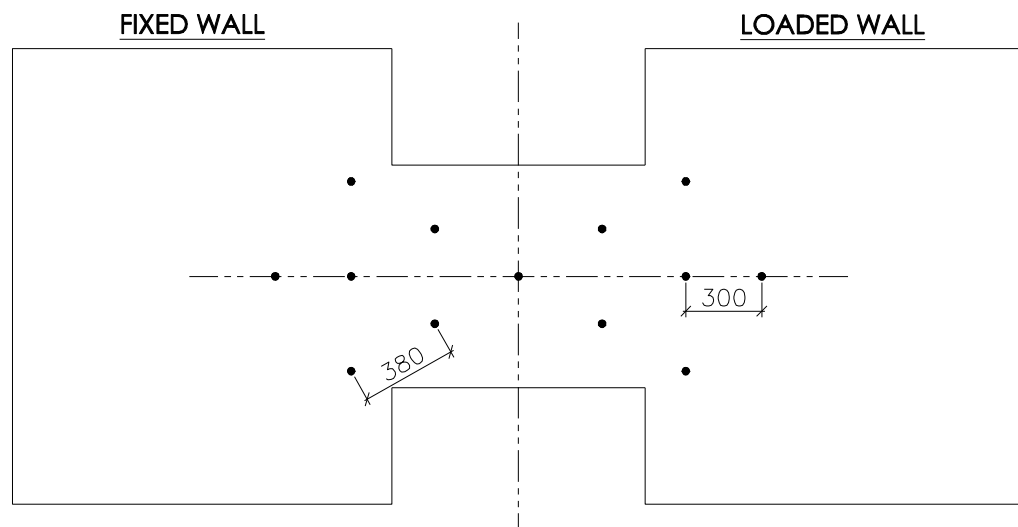
Figure 3.15– Light emitting diode (LED) locations

3.3.3. Strain measurements

Figure 3.16 shows the locations of the strain gauges installed on the reinforcing bars embedded in the concrete. The electrical resistance strain gauges installed on the 20M bars had a gauge length of 5 mm while the strain gauges installed on the 10M bars had a gauge length of 2 mm. Three strain gauges were installed on each of the four rear diagonal reinforcing steel bars. Two strain gauges were installed on each of the four basket steel stirrups. One strain gauge was installed on each of the buckling prevention ties in the coupling beam closest to the concentrated wall steel. The strain gauges installed on the diagonal reinforcing steel bars were closely monitored during the test in order to establish the first yielding of the diagonal reinforcing bars.
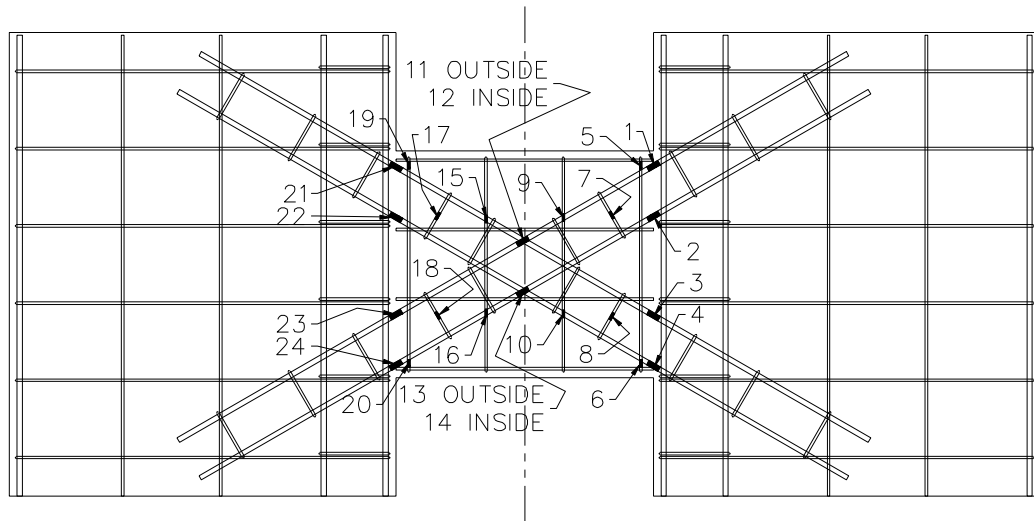
Figure 3.16 – Strain gauge locations

3.4. Loading Histories

The loading histories were based on Park's Quasi-Static Loading Test Procedure for Estabilishing a Ductility Factor for a Subassemblage (Park, 1989). The target load stages for each specimen are listed in Table 3.2 and illustrated in Fig. 3.17. At each load stage, three positive (upward) and three negative (downward) cycles were alternately applied to the specimens. Each cycle began and ended at zero applied load. At each load cycle, cracks widths were measured and the new cracks were marked using a black felt marker.

The load stages were separated into two types of loading; load controlled and deflection controlled. Each test began with several cycles in load control. The first cycle was an elastic load to ensure that all equipment was functioning correctly. The second cycle was the estimated load to cause flexural cracking at the coupling beam-wall interface. In all cases first cracking was observed at this load stage. The subsequent load control stages consisted of loads corresponding to

1. multiples of the cracking moment (1.33 or 2);
2. first yielding of a diagonal reinforcing bar, and;
3. general yielding of the coupling beam.

The displacement at which general yielding of the coupling beam was observed was established as the yield deformation (Δ_y) of the coupled walls. The load stages established after the general yield of the coupled walls were deflection controlled and were multiples of the specimen's Δ_y.

The target deflection controlled load cycles of the limited ductility specimen, CC-16d_b, were generally at half multiples of Δ_y, based on the inherent assumption that failure would occur at a lower deflection. The remaining specimens, MD-10d_b, MD-8d_b and D-6d_b increased by increments of 2Δ_y.

Table 3.2 – Load stages

	CC-16d$_b$	**MD-10d$_b$**	**MD-8d$_b$**	**D-6d$_b$**
Load Control	± 120 kN ± 150 kN ± 220 kN ± 265 kN ± 400 kN Bar Yield	- ± 150 kN ± 220 kN ± 265 kN ± 400 kN Bar Yield	- ± 150 kN ± 220 kN - ± 400 kN Bar Yield	- ± 150 kN ± 220 kN - ± 400 kN Bar Yield
Deflection Control	± General Yield ± 1.5 Δ_y ± 2.0 Δ_y ± 2.5 Δ_y ± 3.0 Δ_y ± 3.5 Δ_y ± 4.0 Δ_y ± 5.0 Δ_y ± 6.0 Δ_y ± 8.0 Δ_y ± 10.0 Δ_y	± General Yield ± 2.0 Δ_y ± 4.0 Δ_y ± 6.0 Δ_y ± 8.0 Δ_y ± 10.0 Δ_y	± General Yield ± 2.0 Δ_y ± 4.0 Δ_y ± 6.0 Δ_y ± 8.0 Δ_y -	± General Yield ± 2.0 Δ_y ± 4.0 Δ_y ± 6.0 Δ_y ± 8.0 Δ_y ± 10.0 Δ_y
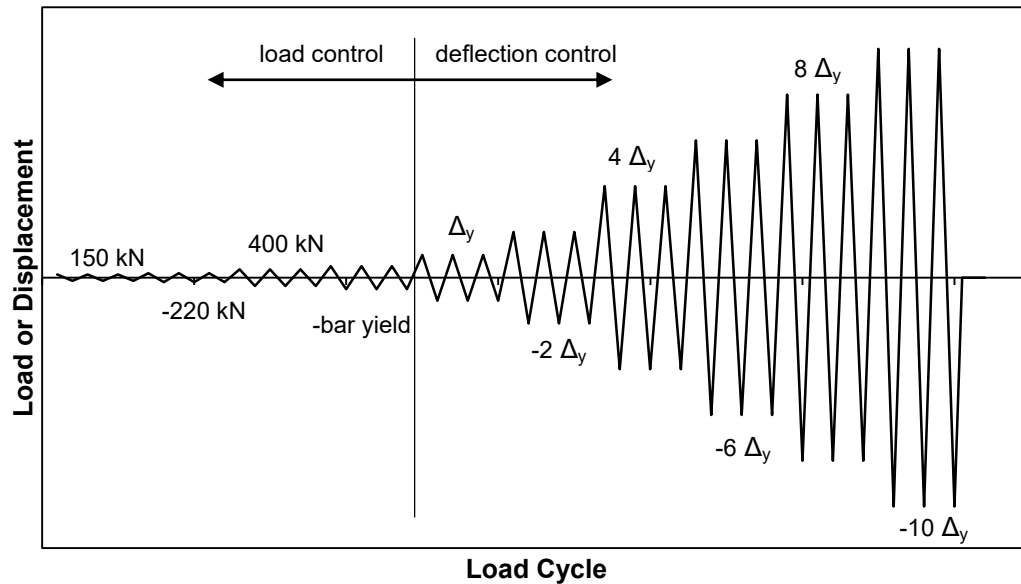
Figure 3.17 – Typical target load/deflection histories

3.5. Material Properties

3.5.1. Concrete

The coupled walls were cast in pairs. Each pair was cast using the same batch of ready-mix, normal density concrete. The concrete walls were moist-cured for four days in the formwork and then air cured until the testing began. The mix proportions of the ready-mix concrete used for both pairs of walls are listed in Table 3.3. The target ready-mix concrete properties are listed in Table 3.4.

Table 3.3 – Ready-mix concrete proportions

Component	Quantity
GU Cement (kg/m^3)	338
Sand (kg/m^3)	825
5-13 mm Aggregate (kg/m^3)	397
10-20 mm Aggregate (kg/m^3)	596
Water (kg/m^3)	160
Air Entrainement Agent (ml/100 kg)	25.76
Retarding Agent (ml/100 kg)	130

Table 3.4 – Expected ready-mix concrete properties

Property	Value
Concrete Strength (MPa)	30
Entrained Air (%)	5-8
Slump (mm)	80 ± 30
Water-Cement Ratio	0.48

Twelve cylinders and six flexural beam specimens were collected during each pour. The cylinders measured 100 mm in diameter and 200 mm in length. The flexural beams measured 100 mm by 100 mm by 350 mm in length (100 mm x 100 mm x 350 mm).

The following tests were carried out prior to testing each wall:

i. Three compression tests to determine the compressive strength, f_c', in accordance with the requirements of CSA Standard A23.3-9C (CSA, 2009).

ii. Three split-cylinder tests to determine the split cylinder tensile strength, f_{sp}, in accordance with the requirements of CSA Standard A23.3-13C (CSA, 2009).

iii. Three third-point flexural tests to determine the modulus of rupture, f_r, in accordance with the requirements of CSA Standard A23.2-8C (CSA, 2009).

The results of the testing are summarized in Table 3.5.

Table 3.5 – Summary of concrete sample testing

Specimen	average f'_c (MPa) (std. dev.)	average ε'_c (std. dev.)	average f_{sp} (MPa) (std. dev)	average f_r (MPa) (std. dev.)
CC-16d$_b$	38.4 (2.68)	0.00174	3.83 (0.14)	5.09 (0.17)
MD-10d$_b$	41.5 (1.55)	0.00181	4.46 (0.06)	5.63 (0.27)
MD-8d$_b$	43.0 (0.47)	0.00168	3.97 (0.20)	5.27 (0.14)
D-6d$_b$	44.8 (4.72)	0.00172	4.21 (0.18)	4.91 (0.56)

A typical stress-strain relationship for a uniaxial compression test from each cast is presented in Fig. 3.18.
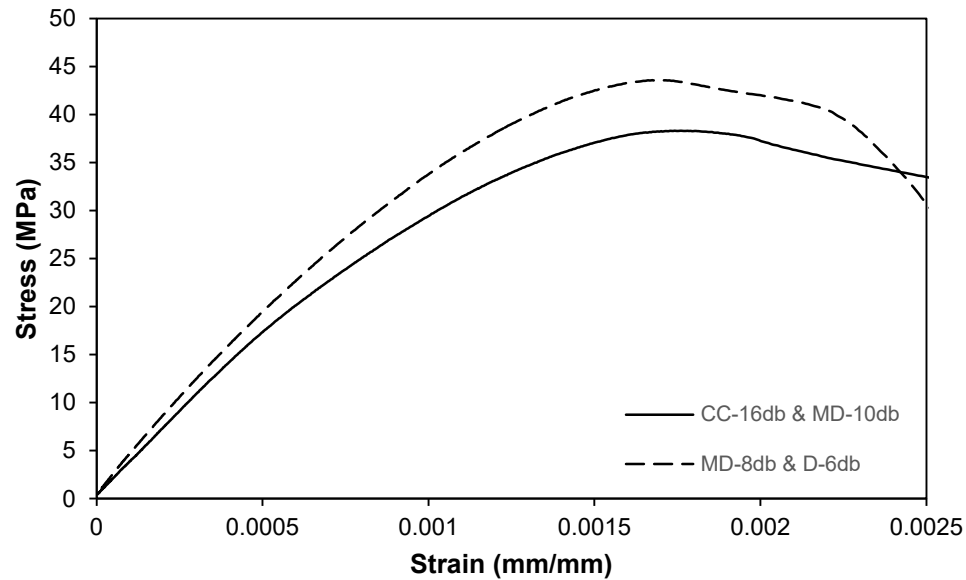
Figure 3.18 – Typical concrete stress-strain curve for uniaxial compression

3.5.2. Reinforcing Steel

The coupled wall specimens were constructed using reinforcing steel that were obtained from the same heat for each bar size. All of the bars conformed to CSA Standard G30.18-09 (CSA, 2009) and were 400W weldable grade. Three specimens of each bar diameter were tested in order to determine the mechanical properties. Samples of the different sizes of reinforcing bars were tested in accordance with the requirements of ASTM A615/615M-16 (ASTM, 2016). The strains were measured using a 200 mm extensometer. The average mechanical properties and the standard deviations for the reinforcing bars are listed in Table 3.6. The typical stress versus strain plots of the reinforcing bars are illustrated in Fig. 3.19.

Table 3.6 – Mechanical properties of reinforcing bars

Bar Diameter	average f_y (MPa) (std. dev.)	average f_{ult} (MPa) (std. dev.)	average ε_y (std. dev.)	average ε_{ult} (std. dev.)
10M	431 (3.34)	544 (9.70)	0.00268 (0.0005)	0.199 (0.0122)
15M	455 (1.45)	568 (2.03)	0.00248 (0.0001)	0.192 (0.0075)
20M	457 (2.50)	570 (6.44)	0.00220 (0.0001)	0.177 (0.0171)
25M	489 (2.92)	706 (0.44)	0.00339 (0.0010)	0.149 (0.0222)
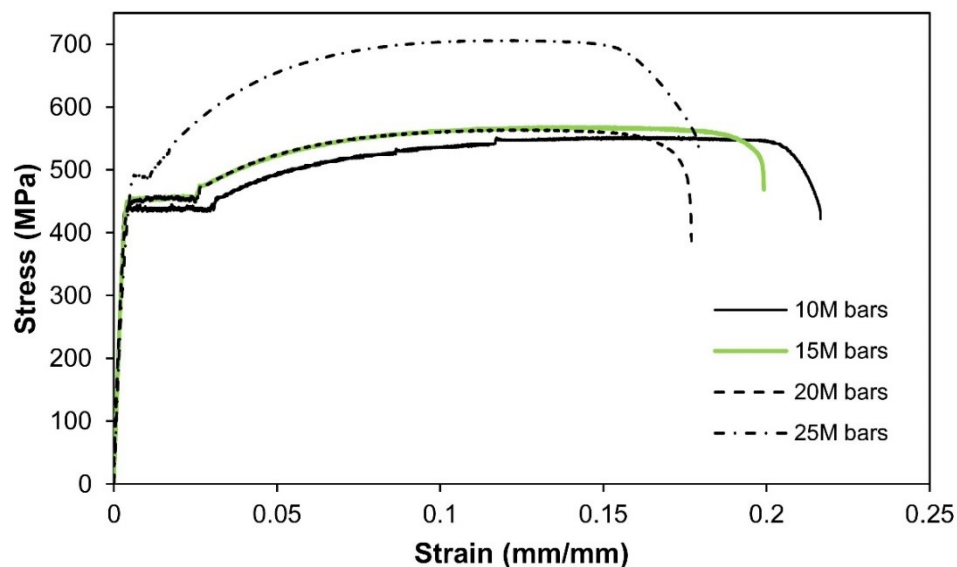
Figure 3.19 – Typical reinforcing steel stress-strain curves

CHAPTER 4

EXPERIMENTAL RESULTS

4.1. Introduction

This chapter presents the behaviour of the coupled shear wall specimens. The data presented was recorded during the specimen during testing by a computerized data acquisition system. Each specimen was subjected to reversed cyclic loading at pre-determined loading and deflection stages. Three cycles of reversed cyclic loading were carried out at each target load and deflection stage. The specimens were initially subjected to load-controlled cycles until general yielding of the coupling beam was reached. After general yielding the cycles were deflection-controlled. The deflection targets were multiples of the general yield deflection based on the expected ductility level of the specimen.

The applied shear force versus deflection hysteretic response of the coupled wall specimens are presented by plotting the applied load versus deflection results.

49

4.2. Response of Specimen CC-16d$_b$

Table 4.1 describes the key load stages for specimen CC-16d$_b$. Figure 4.1 illustrates the shear force versus deflection hysteretic response of specimen CC-16d$_b$. Because all four specimens contained the same diagonal reinforcement the average general yield displacement of 3.25 mm was used to determine the ductilities of the specimens. The predicted yield strength of the specimens was determined based on the yield strength of the reinforcing bars using the experimentally determined materials properties and using a phi factor of 1.0. The predicted capacities are explained in Section 5.3.

Table 4.1 – Target load stages for specimen CC-16d$_b$

Cycle	Target Description	Applied Shear (kN)	Deflection (mm)
1	Experimental Setup Verification Elastic Cycle	120.1 -120.1	0.073 -0.138
2		120.1 -120.5	0.085 -0.138
3		120.3 -120.9	0.078 -0.147
4	0.7 M$_{cr}$ Elastic Cycle	150.5 -150.7	0.183 -0.203
5		150.7 -150.8	0.149 -0.192
6		150.4 -150.4	0.145 -0.116
7	M$_{cr}$	220.2 -220.4	0.302 -0.255
8		221.7 -220.7	0.259 -0.349
9		222.8 -220.3	0.208 -0.351
10	1.2 M$_{cr}$	266.0 -265.3	0.329 -0.459
11		265.6 -265.7	0.395 -0.530
12		265.6 -265.7	0.456 -0.586

Table 4.1 cont. – Target load stages for specimen CC-16d_b

Cycle	Target Description	Applied Shear (kN)	Deflection (mm)
13	1.8 M_cr	401.5 / -400.4	1.09 / -1.35
14		401.5 / -400.6	1.14 / -1.33
15		401.8 / -400.9	1.32 / -1.37
16	Diagonal Bar First Yield	477.5 / -507.5	1.03 / -2.93
17		475.9 / -507.4	1.17 / -3.03
18		475.3 / -507.0	1.27 / -3.13
19	δ_y General Yield	586.5 / -581.0	2.92 / -3.33
20		580.0 / -558.2	3.19 / -3.29
21		569.4 / -562.5	3.23 / -3.33
22	1.48 δ_y	688.5 / -650.8	4.71 / -4.93
23		608.9 / -600.8	4.60 / -5.16
24		589.0 / -597.7	4.72 / -5.13
25	1.95 δ_y	641.6 / -618.5	6.21 / -6.48
26		591.7 / -587.4	6.17 / -6.56
27		576.9 / -578.9	6.24 / -6.62
28	2.43 δ_y	613.2 / -602.8	7.62 / -8.17
29		590.5 / -582.0	7.82 / -8.09
30		576.6 / -572.7	7.80 / -8.22
31	2.9 δ_y	601.2 / -593.0	9.19 / -9.67
32		592.1 / -566.4	9.16 / -9.65
33		583.4 / -553.4	9.19 / -9.84

Table 4.1 cont. – Target load stages for specimen CC-16d$_b$

Cycle	Target Description	Applied Shear (kN)	Deflection (mm)
34		594.9 -585.0	10.69 -11.20
35	3.37 δ_y	590.6 -562.1	10.71 -11.33
36		584.9 -557.8	11.03 -11.41
37		592.5 -574.9	11.84 -13.24
38	3.86 δ_y	582.3 -564.0	11.13 -12.85
39		582.0 -550.6	12.55 -13.02
40		609.0 -578.0	15.55 -15.83
41	4.83 δ_y	601.3 -566.2	15.81 -15.53
42		609.5 -556.4	15.74 -15.65
43		590.3 -581.7	18.43 -18.81
44	5.73 δ_y	577.2 -554.8	18.63 -19.97
45		577.9 -493.7	18.49 -19.72
46		555.2 -343.3	24.60 -25.94
47	7.93 δ_y	450.3 -294.1	24.70 -25.64
48		309.5 -150.3	24.75 -24.54
49	Final Loop 11.45 δ_y	433.1	37.20

Figure 4.1 – Hysteretic response of specimen CC-16d$_b$

First cracking of the specimen occurred at load cycle 8B, the second downward cycle at a load of -220.7 kN and a deflection of -0.349 mm. The first hairline crack initiated at the top left coupling beam–coupled wall interface. A second hairline crack initiated at the top right coupling beam–coupled wall interface at the following load cycle, 9A, at a load level of 222.8 kN and a deflection of 0.208 mm. Hairline cracks occurred at the bottom interfaces during the following 10A and 10B cycles at load levels of 266.0 kN and -265.3 kN respectively.

The first shear cracks occurred at load cycle 13B, the first downward cycle at a load of -400.4 kN and a deflection of -1.35 mm. Three shear cracks at approximately equal spacing formed at this load level and were perpendicular to the diagonal reinforcing steel bars that were acting in tension. The existing cracks extended and widened and new similar cracks initiated during the subsequent load cycles. A shear crack appeared in the orthogonal direction at load following cycle 14A, the second upward cycle at a load of 401.5 kN and a deflection of -1.14 mm The progression of the cracks is illustrated in Fig. 4.2.
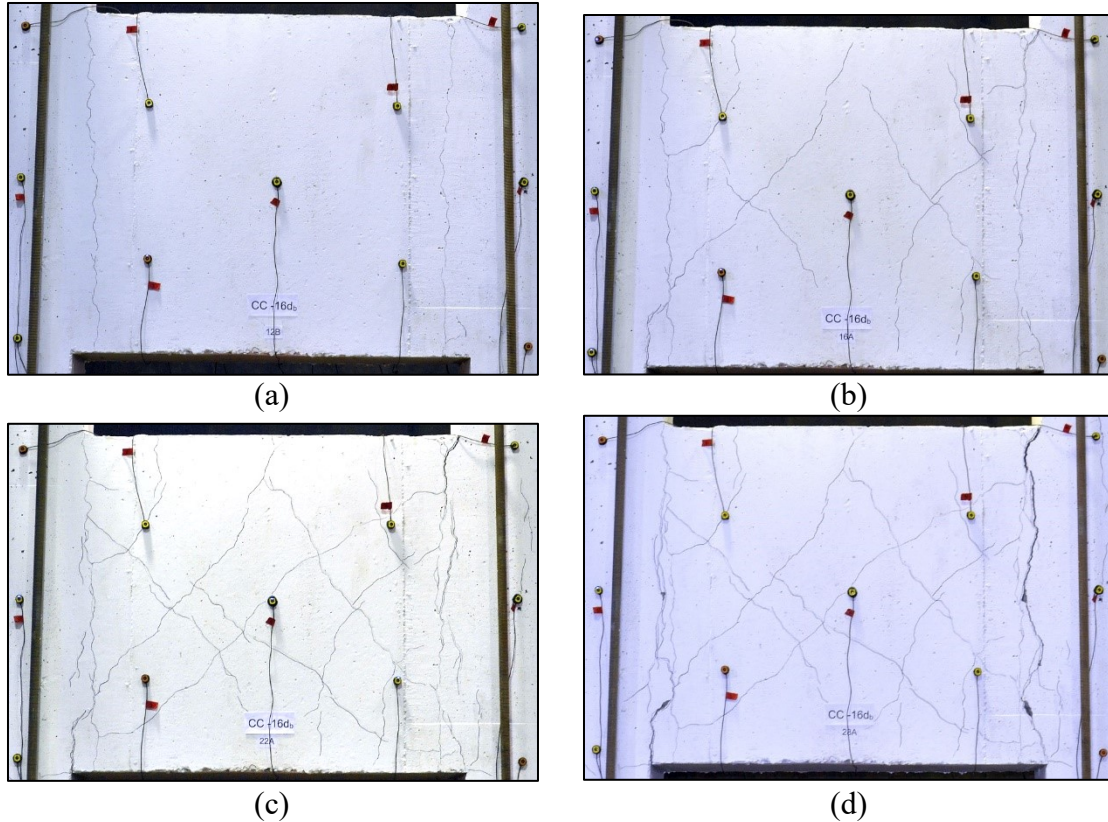
Figure 4.2 – Crack patterns of specimen CC-16d$_b$ at load stages (a) 12A, (b) 19A, (c) 22A and (d) 28A

First yield of the reinforcing steel bars occurred at load cycle 16A, the first upward cycle at a load of 477.5 kN and a deflection of 1.03 mm. Similar yielding occurred at the following load cycle 16B, the first downward cycle at a load of -507.5 kN and a deflection of -2.93 mm. First yielding was determined by monitoring the strain gauge readings on the diagonal reinforcing steel bars at the coupling beam–coupled wall interface.

General yield of the coupling beam occurred at load cycle 19A, the first upward cycle at a load of 586.5 kN and a deflection of 2.92 mm. Similar yielding occurred at the following load cycle 19B, the first downward cycle at a load of -581.0 kN and a deflection of -3.33 mm. General yielding was approximated during the test by monitoring the measured load vs deflection curve plotted by the data acquisition system and identifying the yield plateau. General yield was determined after the test to be ± 3.25 mm based on the bilinear approximation of the response (Park, 1989).

The largest positive resisted load occurred at load cycle 22A, the first upward cycle at a deflection of 1.48 δ_y, at a load of 688.5 kN and a deflection of 4.71 mm. Similarly, the largest negative resisted load occurred in load cycle 22B, the first downward cycle at a deflection of 1.48 δ_y, at a load of -650.8 kN and a deflection of -4.93 mm.

Significant spalling was observed at the right side coupling beam–coupled wall interface starting at load cycle 42A, the third upward cycle at a deflection of 4.83 δ_y.

Eighty percent of the maximum negative load was maintained up to load cycle 46B during which two diagonal reinforcing steel bars, located at the bottom-right front face of the specimen, ruptured. Cycle 46B was the first downward cycle at a deflection of 7.93 δ_y, reaching a load of -343.3 kN and deflection of -25.94 mm. The subsequent cycle, 47A, the second upward cycle at a deflection of 7.93 δ_y, failed to reach eighty percent of the maximum positive load, reaching a load of 450.3 kN and deflection of 24.7 mm. A second reinforcing steel bar, located at the bottom-right rear face of the specimen, ruptured during load cycle 48B. Cycle 48B was the third downward cycle at a deflection of 7.93 δ_y, reaching a load of -150.3 kN and deflection -24.54 mm.

The test was ended after the subsequent cycle 49A (see Fig. 4.3). The coupling beam experienced large out-of-plane movements measuring approximately 40 mm due to severe buckling of the diagonal reinforcing steel bars (see Fig. 4.4). Figure 4.5 captures the ruptured bars at the bottom right of the specimen.

Figure 4.3 – Final load cycle of specimen CC-16d$_b$ – 49A

Figure 4.4 – Severe diagonal bar buckling of specimen CC-16d$_b$

Figure 4.5 – Ruptured bars at bottom right of specimen CC-16d$_b$

The widths of the shear cracks remained relatively small (~0.30 mm) throughout the test despite the increase in load and deflection. The flexural cracks at the coupling beam–coupled wall interface widened significantly as the test was carried out. They no longer appeared to close after load cycle 30A, the third downward cycle at a deflection of 2.43 δ_y. The widening of these cracks was likely due to an overall elongation of the walls after yielding of the reinforcing steel bars in tension. The coupled walls experienced minor cracking during the test however these cracks appeared to have no effect on the response of the coupling beam.

Figure 4.6 illustrates the load versus reinforcing steel strain experienced by the diagonal reinforcing steel bars during the testing of specimen CC-16d$_b$.

It is evident from Fig. 4.6 (a) that the strain gauge on the diagonal reinforcing near the face of the wall (SG1) stopped functioning after yield and the damage in the concrete surrounding the gauge. The average strain obtained from the LVDT (A1) crossing the beam-wall interface clearly indicates that significantly high tensile strains were reached. The strain gauge on the diagonal reinforcement in the middle region of the beam showed tensile strains approaching the yield strain. LVDT A2 indicates

significantly less straining in the middle region of the beam than at the beam-wall interface.
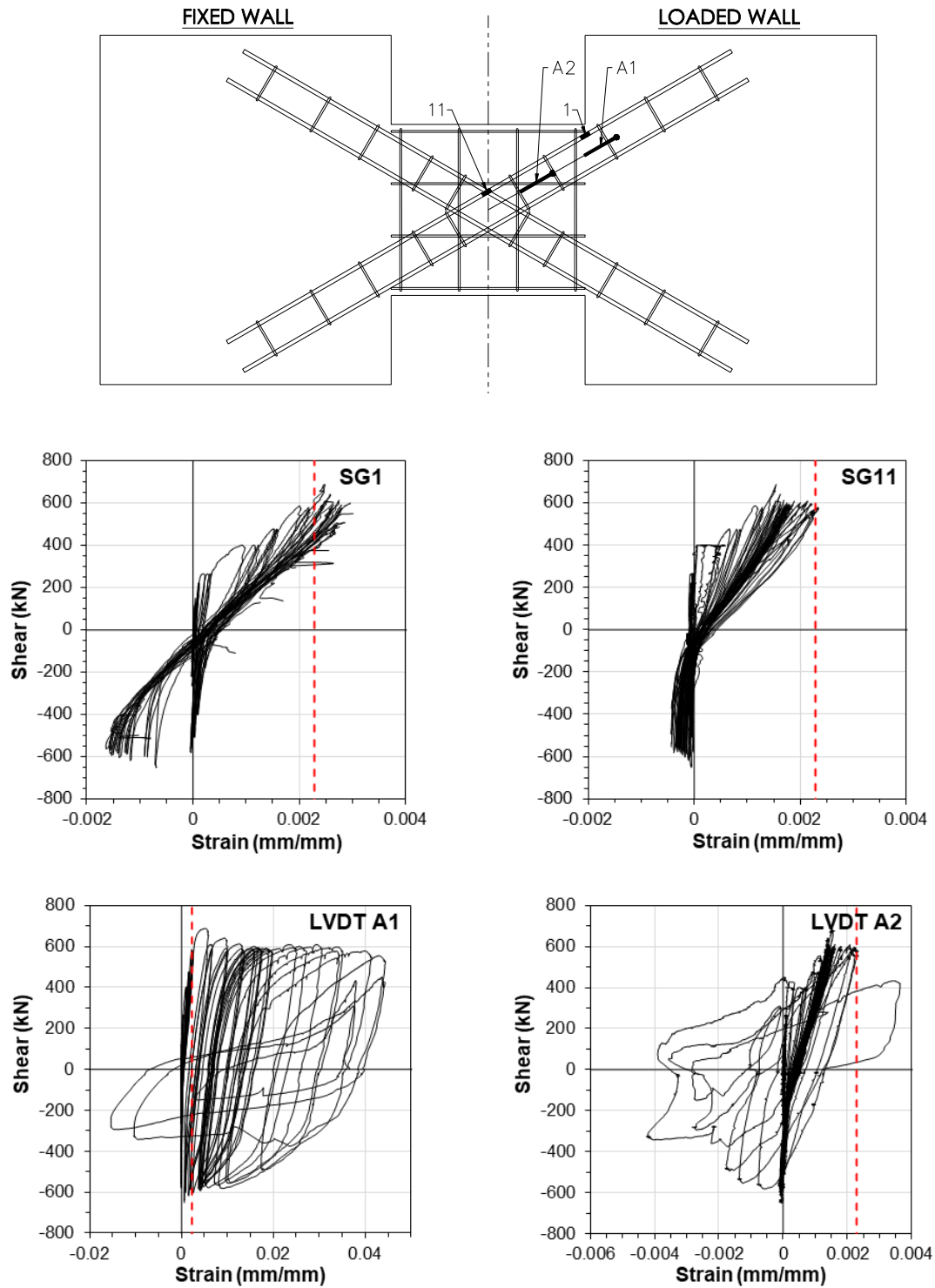
Figure 4.6 – Strain response of diagonal reinforcing steel of specimen CC-16d$_b$
------ = Bar yield

4.3. Response of Specimen MD-10d$_b$

Table 4.2 describes the key load stages for specimen MD-10d$_b$. Figure 4.2 illustrates the shear force versus deflection hysteretic response of specimen MD-10d$_b$.

Table 4.2 – Target load stages for specimen MD-10d$_b$

Cycle	Target Description	Applied Shear (kN)	Deflection (mm)
1		150.2 -150.3	0.17 -0.17
2	0.7 M$_{cr}$ Elastic Cycle	150.7 -150.5	0.27 -0.21
3		150.4 -151.0	0.29 -0.23
4		220.4 -220.6	0.29 -0.31
5	M$_{cr}$	221.0 -221.5	0.29 -0.45
6		220.9 -220.5	0.32 -0.43
7		265.6 -266.0	0.55 -0.58
8	1.2 M$_{cr}$	266.9 -266.0	0.61 -0.59
9		265.5 -265.7	0.60 -0.61
10		400.7 -400.4	1.24 -1.29
11	1.8 M$_{cr}$	400.9 -400.9	1.28 -1.39
12		400.5 -401.1	1.31 -1.43
13		498.9 -500.7	2.04 -2.17
14	Diagonal Bar First Yield	501.0 -501.0	2.16 -2.54
15		499.5 -499.5	2.33 -2.64
16		630.2 -601.7	3.15 -3.20
17	δ_y General Yield	605.0 -575.6	3.15 -3.25
18		573.2 -568.6	3.19 -3.24

Table 4.2 cont. – Target load stages for specimen MD-10d$_b$

Cycle	Target Description	Applied Shear (kN)	Deflection (mm)
19		749.7	6.45
		-642.3	-6.68
20	2.02 δ_y	635.3	6.78
		-585.5	-6.73
21		612.3	6.90
		-562.4	-6.72
22		773.8	13.92
		-631.5	-14.06
23	4.30 δ_y	657.9	13.68
		-593.4	-13.96
24		637.3	14.04
		-580.6	-14.04
25		701.4	20.92
		-612.3	-20.76
26	6.41 δ_y	635.5	19.53
		-589.5	-20.95
27		619.6	20.84
		-566.3	-20.88
28		621.6	27.95
		-563.2	-28.19
29	8.64 δ_y	587.5	27.50
		-499.6	-27.83
30		531.7	27.64
		-440.0	-27.61
31		458.6	34.94
		-456.1	-35.00
32	10.76 δ_y	174.2	35.37
		-405.3	-35.12
33		70.6	35.06
		-	-

Figure 4.7 – Hysteretic response of specimen MD-10d_b

First cracking of the specimen occurred at load cycle 4B, the first downward cycle at a load of -220.6 kN and a deflection of -0.310 mm. The first hairline crack initiated at the top left coupling beam–coupled wall interface. A second hairline crack initiated at the top right coupling beam–coupled wall interface at load cycle 7A, the first upward cycle at a load of 265.6 kN and a deflection of 0.550 mm. Hairline cracks occurred at the bottom left interface during the same 7A cycle. Cracking occurred at the bottom right coupling beam–coupled wall interface during the following load cycle, 7B, at load of -266.0 kN and a deflection of -0.530 mm.

The first shear cracks occurred at load cycle 11A, the second upward cycle at a load of 400.9 kN and a deflection of 1.28 mm. One shear crack formed at the upper right portion of the coupling beam, approximately perpendicular to the diagonal reinforcing steel bars that were acting in tension. The existing crack extended and widened and new similar cracks initiated during the subsequent load cycles. A shear crack appeared in the orthogonal direction at the following load cycle 11B, the first downward cycle at a load of -400.9 kN and a deflection of -1.39 mm The progression of the cracks is illustrated in Fig. 4.8.

61
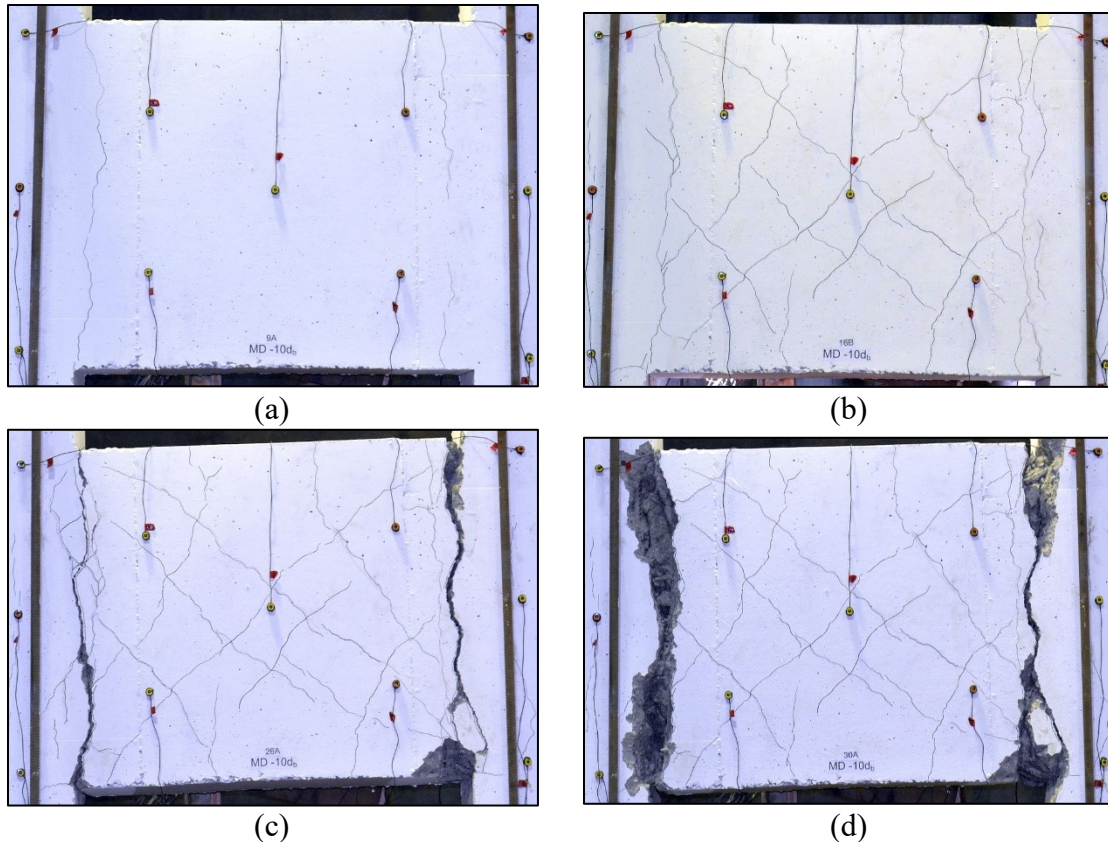
Figure 4.8 – Crack patterns of specimen MD-10d$_b$ at load stages (a) 9A, (b) 16B, (c) 26A and (d) 30A

First yield of the reinforcing steel bars occurred at load cycle 13A, the first upward cycle at a load of 498.9 kN and a deflection of 2.04 mm. Similar yielding occurred at the following load cycle 13B, the first downward cycle at a load of -500.7 kN and a deflection of -2.17 mm. First yielding was determined by monitoring the strain gauge readings on the diagonal reinforcing steel bars at the coupling beam–coupled wall interface.

General yield of the coupling beam occurred at load cycle 16A, the first upward cycle at a load of 630.2 kN and a deflection of 3.15 mm. Similar yielding occurred at the following load cycle 16B, the first downward cycle at a load of -601.7 kN and a deflection of -3.20 mm. General yielding was approximated during the test by monitoring the measured load vs deflection curve plotted by the data acquisition system and identifying the yield plateau. General yield was determined after the test to be ± 3.25 mm based on the bilinear approximation of the response (Park, 1989).

The largest positive resisted load occurred at load cycle 22A, the first upward cycle at a deflection of 4.30 δ_y, at a load of 773.8 kN and a deflection of 13.92 mm. In contrast, the largest negative resisted load occurred in load cycle 19B, the first downward cycle at a deflection of 2.02 δ_y, at a load of -642.3 kN and a deflection of -6.68 mm.

Significant spalling was observed at the bottom right side coupling beam–coupled wall interface starting at load cycle 26A, the second upward cycle at a deflection of 6.41 δ_y.

Eighty percent of the maximum positive load was maintained up to load cycle 29A during which a load of 587.5 kN (75.9% of the maximum) and deflection of 27.5 mm were reached. The subsequent cycle, 29B, failed to reach eighty percent of the maximum negative load, reaching a load of -499.6 kN (77.8% of the maximum) and deflection of -27.83 mm.

The first bar rupture occurred at load cycle 31A, during which one bar located at the bottom-left front face of the coupling beam ruptured. Cycle 31A was the first upward cycle at a deflection of 10.76 δ_y, reaching a maximum load of 458.6 kN (59.3% of the maximum) and deflection of 34.94 mm. A second bar rupture occurred during the subsequent upward cycle, 32A, where one bar, located at the bottom-left front face of the specimen, ruptured. Cycle 32A was the second upward cycle at a deflection of 10.76 δ_y, reaching a maximum load of 174.2 kN and deflection of 35.37 mm. A third bar rupture occurred during cycle 323, where one bar, located at the bottom-left back face of the specimen, ruptured. Cycle 33A was the third upward cycle at a deflection of 10.76 δ_y, reaching a maximum load of 70.6 kN and deflection of 35.06 mm.

The test was ended after cycle 33A (see Fig. 4.9). The coupling beam experienced large out-of-plane movements measuring approximately 40 mm (see Fig. 4.10) due to severe buckling of the diagonal reinforcing steel bars. Figure 4.11 captures the ruptured bars at the bottom left of the specimen.

Figure 4.9 – Final load cycle of specimen MD-10d$_b$ – 33A

Figure 4.10 – Severe twisting observed at the coupling beam

Figure 4.11 – Buckled bar at bottom right coupling beam–coupled wall interface

The widths of the shear cracks remained relatively small (~0.30 mm) throughout the test despite the increase in load and deflection. The flexural cracks at the coupling beam–coupled wall interface widened significantly as the test was carried out. They no longer appeared to close after load cycle 22B, the first downward cycle at a deflection of 4.30 δ_y. The widening of these cracks was likely due to an overall elongation of the walls after yielding of the reinforcing steel bars in tension. The coupled walls experienced minor cracking during the test however these cracks appeared to have no effect on the response of the coupling beam.

Figure 4.12 illustrates the load versus reinforcing steel strain experienced by the diagonal reinforcing steel bars during the testing of specimen CC-10d_b. It is evident from Fig. 4.12 (a) that the strain gauge on the diagonal reinforcing near the face of the wall (SG21) stopped functioning after yield and the damage in the concrete surrounding the gauge. The average strain obtained from the LVDT (C1) crossing the beam-wall interface clearly indicates that significantly high tensile strains were reached. The strain gauge on the diagonal reinforcement in the middle region of the beam showed tensile strains

approaching the yield strain. LVDT C2 indicates significantly less straining in the middle region of the beam than at the beam-wall interface.
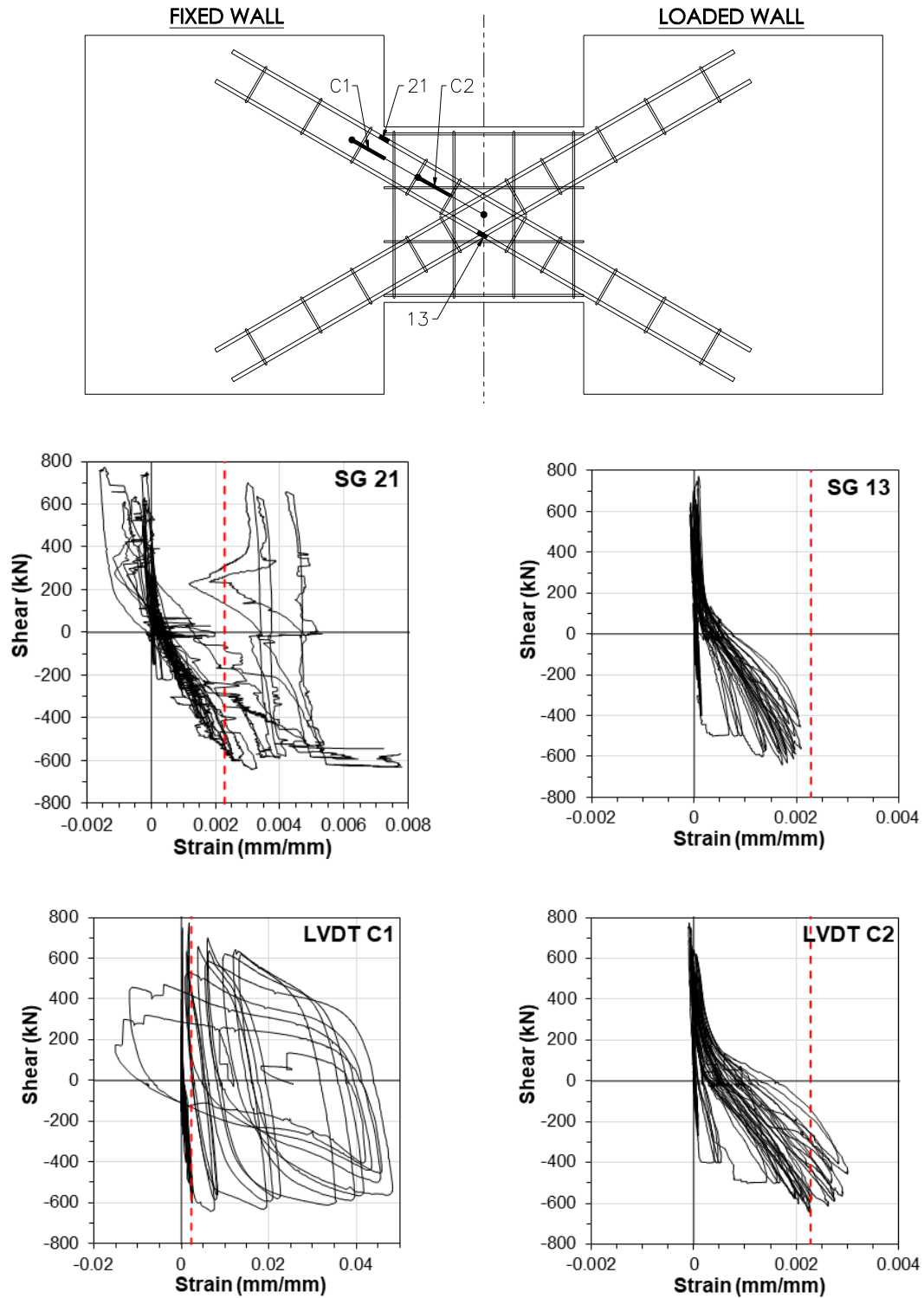
Figure 4.12 – Strain response of diagonal reinforcing steel of specimen MD-10d_b

66

4.4. Response of Specimen MD-8d$_b$

Table 4.3 describes the key load stages for specimen MD-8d$_b$. Figure 4.13 illustrates the shear force versus deflection hysteretic response of specimen MD-8d$_b$.

Table 4.3 – Target load stages for specimen MD-8d$_b$

Cycle	Target Description	Applied Shear (kN)	Deflection (mm)
1		151.4	0.15
		-150.8	-0.20
2	0.7 M$_{cr}$ Elastic Cycle	150.6	0.20
		-151.0	-0.20
3		150.7	0.28
		-150.5	-0.20
4		220.6	0.44
		-220.7	-0.47
5	M$_{cr}$	220.9	0.54
		-221.2	-0.51
6		219.8	0.57
		-221.9	-0.48
7		400.4	1.37
		-401.8	-1.63
8	1.8 M$_{cr}$	400.3	1.51
		-400.6	-1.83
9		400.6	1.59
		-400.8	-1.81
10		542.7	2.71
		-461.3	-2.30
11	Diagonal Bar First Yield	503.8	2.71
		-460.4	-2.55
12		496.8	2.72
		-450.3	-2.53
13		590.4	3.22
		-581.8	-3.27
14	δ_y General Yield	581.4	3.24
		-551.0	-3.23
15		557.2	3.28
		-540.4	-3.25
16		736.6	6.95
		-649.4	-7.18
17	2.17 δ_y	613.7	6.93
		-582.7	-6.95
18		590.2	6.98
		-576.9	-7.11

Table 4.3 cont. – Target load stages for specimen MD-8d_b

Cycle	Target Description	Applied Shear (kN)	Deflection (mm)
19		729.1 -651.3	13.94 -14.00
20	4.30 δ_y	624.4 -598.7	13.83 -13.92
21		607.6 -579.7	13.86 -14.04
22		659.5 -589.0	21.10 -20.82
23	6.45 δ_y	609.2 -547.5	20.77 -20.33
24		580.5 -547.0	20.85 -20.97
25		611.0 -284.0	27.84 -33.31
26	9.21 δ_y	556.9 -273.0	27.90 -27.66
27		458.4 -166.2	28.04 -28.11

Figure 4.13 – Hysteretic response of specimen MD-8d_b

First cracking of the specimen occurred at load cycle 4A, the first upward cycle at a load of 220.6 kN and a deflection of 0.44 mm. The first hairline crack initiated at the bottom left coupling beam–coupled wall interface. A second hairline crack initiated at the top left coupling beam–coupled wall interface at load cycle 4B, the first downward cycle at a load of -220.7 kN and a deflection of -0.47 mm. Cracking occurred at the top right and bottom right coupling beam–coupled wall interface during load cycles 5A and 5B respectively.

The first shear cracks occurred at load cycle 9A, the third upward cycle at a load of 400.6 kN and a deflection of 1.59 mm. Two relatively symmetrical shear cracks formed at the upper right and lower left portions of the coupling beam, approximately perpendicular to the diagonal reinforcing steel bars. The existing crack extended and widened and new similar cracks initiated during the subsequent load cycles. Shear cracks appeared in the orthogonal direction at load cycle 10B, the first downward cycle at a load of -461.3 kN and a deflection of -2.30 mm. The progression of the cracks is illustrated in Fig. 4.14.

(a)	(b)
(c)	(d)
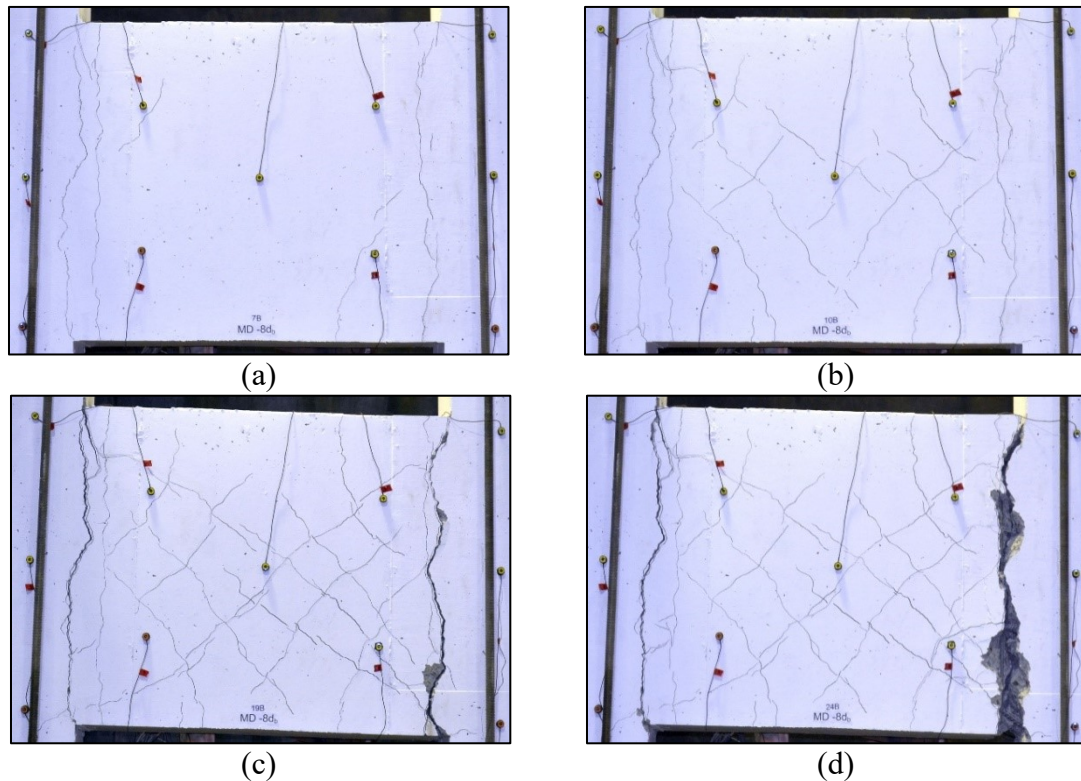
Figure 4.14 – Crack patterns of specimen MD-8d$_b$ at load stages (a) 7B, (b) 10B, (c) 19B and (d) 24B

First yield of the reinforcing steel bars occurred at load cycle 10A, the first upward cycle at a load of 542.7 kN and a deflection of 2.71 mm. Similar yielding occurred at the following load cycle 10B, the first downward cycle at a load of -461.3 kN and a deflection of -2.30 mm. First yielding was determined by monitoring the strain gauge readings on the diagonal reinforcing steel bars at the coupling beam–coupled wall interface.

General yield of the coupling beam occurred at load cycle 13A, the first upward cycle at a load of 590.4 kN and a deflection of 3.47 mm. Similar yielding occurred at the following load cycle 13B, the first downward cycle at a load of -581.8 kN and a deflection of -3.52 mm. General yielding was approximated during the test by monitoring the measured load vs deflection curve plotted by the data acquisition system and identifying the yield plateau. General yield was determined after the test to be ± 3.25 mm based on the bilinear approximation of the response (Park, 1989).

The largest positive resisted load occurred at load cycle 16A, the first upward cycle at a deflection of 2.17 δ_y, at a load of 736.6 kN and a deflection of 6.95 mm. In contrast, the largest negative resisted load occurred in load cycle 19B, the first downward cycle at a deflection of 4.30 δ_y, at a load of -651.3 kN and a deflection of -14.00 mm.

Significant spalling was observed at the bottom right side coupling beam–coupled wall interface starting at load cycle 23B, the second downward cycle at a deflection of 6.45 δ_y.

Eighty percent of the maximum positive load was maintained up to load cycle 24A during which a load of 580.5 kN (78.8% of the maximum) and deflection of 20.85 mm were reached. Cycle 25B also failed to reach eighty percent of the maximum negative load, reaching a maximum load of -284.0 kN (43.6% of the maximum) and deflection of -33.31 mm.

The first bar rupture occurred at load cycle 25B, during which two bars located at the bottom-right front face of the coupling beam ruptured. Cycle 25B was the first downward cycle at a deflection of 9.21 δ_y, reaching a maximum load of -284.0 kN (43.6% of the maximum negative load) and deflection of -33.31 mm. A third bar rupture occurred during load cycle, 27B, where one bar, located at the bottom-right rear face of

the specimen, ruptured. Cycle 27B was the third downward cycle at a deflection of 9.21 δ_y, reaching a maximum load of -166.2 kN and deflection of -28.11 mm.

The test was ended after cycle 27B (see Fig. 4.15). The coupling beam experienced large out-of-plane movements measuring approximately 40 mm due to severe buckling of the diagonal reinforcing steel bars (Fig. 4.16). Figure 4.17 captures the ruptured bars at the bottom right of the specimen.

Figure 4.15 – Final load cycle of specimen MD-8d$_b$ – 27B

Figure 4.16 – Severe twisting observed at the coupling beam

Figure 4.17 – Ruptured bar at bottom right of specimen MD-8d$_b$

The widths of the shear cracks remained relatively small (~0.30 mm) throughout the test despite the increase in load and deflection. The flexural cracks at the coupling beam–coupled wall interface widened significantly as the test was carried out. They no longer appeared to close after load cycle 20A, the second upward cycle at a deflection of 4.30 δ_y. The widening of these cracks was likely due to an overall elongation of the walls after yielding of the reinforcing steel bars in tension. The coupled walls experienced minor cracking during the test however these cracks appeared to have no effect on the response of the coupling beam.

Figure 4.18 illustrates the load versus reinforcing steel strain experienced by the diagonal reinforcing steel bars during the testing of specimen CC-8d$_b$.
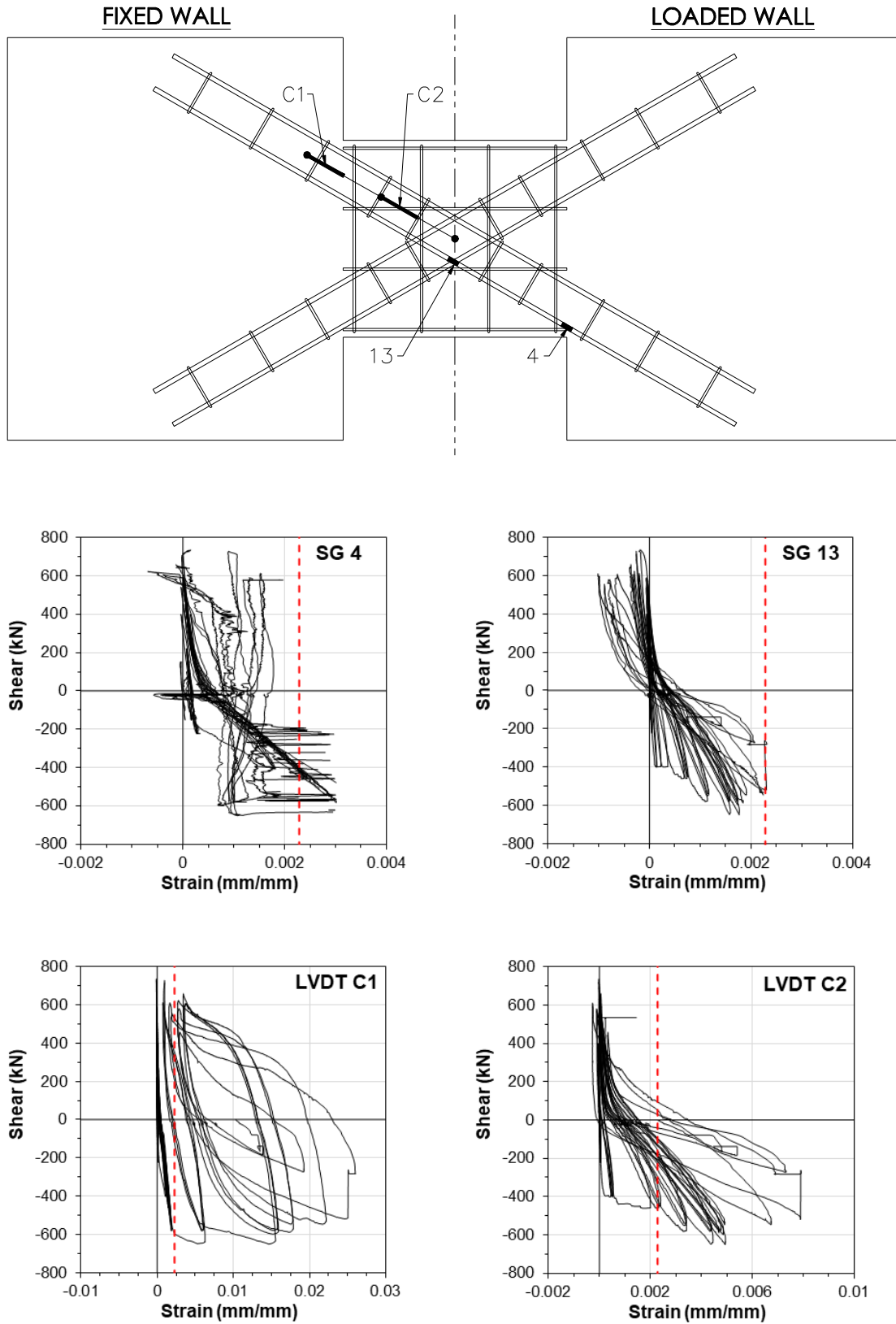
Figure 4.18 – Strain response of diagonal reinforcing steel of specimen MD-8d$_b$

4.5. Response of Specimen D-6d$_b$

Table 4.4 describes the key load stages for specimen D-6d$_b$. Figure 4.17 illustrates the shear force versus deflection hysteretic response of specimen D-6d$_b$. The predicted yield strength of the specimen was determined based on the yield strength of the reinforcing bars using the experimentally determined materials properties and using a phi factor of 1.0, however the longitudinal restraint was not accounted for. The predicted capacities are explained in Section 5.3.

Table 4.4 – Target load stages for specimen D-6d$_b$

Cycle	Target Description	Applied Shear (kN)	Deflection (mm)
1		150.6	0.10
		-150.3	-0.12
2	0.7 M$_{cr}$ Elastic Cycle	150.8	0.12
		-150.7	-0.10
3		150.3	0.10
		-150.7	-0.19
4		220.6	0.33
		-221.2	-0.27
5	M$_{cr}$	221.0	0.30
		-221.1	-0.38
6		220.4	0.27
		-221.5	-0.41
7		400.3	0.98
		-400.58	-1.00
8	1.8 M$_{cr}$	400.4	1.12
		-400.5	-1.19
9		400.4	1.12
		-400.9	-1.31
10		565.5	2.33
		-534.3	-2.33
11	Diagonal Bar First Yield	562.4	2.54
		-513.4	-2.52
12		556.2	2.59
		-502.4	-2.48
13		645.0	3.15
		-616.0	-3.37
14	δ$_y$ General Yield	695.1	3.40
		-608.7	-3.32
15		653.7	3.40
		-584.9	-3.29

Table 4.4 cont. – Target load stages for specimen D-6d$_b$

Cycle	Target Description	Applied Shear (kN)	Deflection (mm)
16		825.7 / -774.9	6.08 / -6.37
17	1.92 δ$_y$	817.8 / -732.1	6.62 / -6.56
18		814.9 / -696.6	6.53 / -6.47
19		998.8 / -810.1	12.51 / -13.76
20	3.44 δ$_y$	846.6 / -782.2	13.48 / -14.02
21		798.8 / -743.0	13.06 / -13.93
22		718.7 / -623.1	19.80 / -20.38
23	6.20 δ$_y$	642.8 / -581.0	19.42 / -20.40
24		616.8 / -560.4	19.60 / -20.41
25		631.0 / -568.6	25.72 / -26.98
26	8.09 δ$_y$	597.5 / -534.9	26.59 / -27.09
27		552.7 / -488.5	26.46 / -27.50
28		573.3 / -478.4	33.20 / -33.55
29	10.3 δ$_y$	364.3 / -	26.15 / -
30		-	-
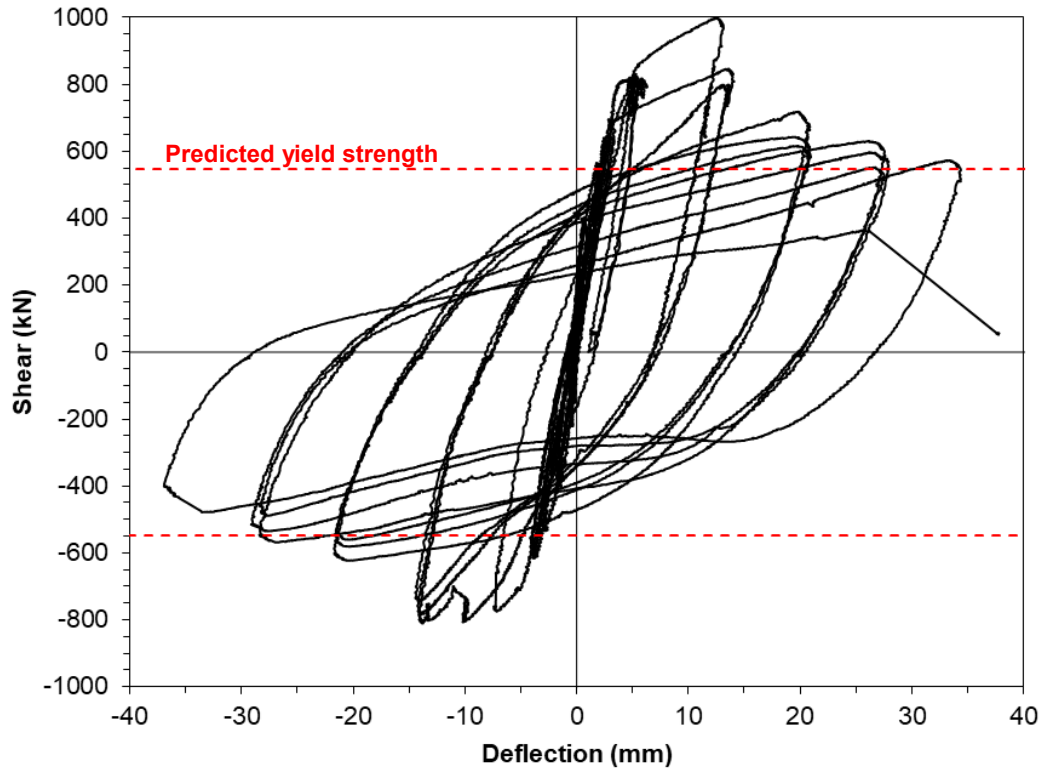
Figure 4.19 – Hysteretic response of specimen D-6d$_b$

Passive lateral restraint was provided at the beginning of the testing of specimen D-6d$_b$. The lateral restraint was added to simulate the effect of a structural slab which would restrict the axial elongation of the wall.

As expected, the lateral restraint increased the load carrying capacity of the coupled wall system. As the shear load was increased on the loaded coupled wall the load in the clamping rods also increased, leading to some compression in the coupling beam and thus increase the moment capacity. Since the clamping force increased considerably during the test, the nuts attaching the clamps were loosened during the experimentation in order to simulate cracking in the slab and a loss of stiffness. The clamping load vs. shear load is illustrated in Fig. 4.18. The lateral restraint lead to an increase of moment resistance by approximately twenty-nine percent 29%. Since the McGill University Coupled Wall Testing Apparatus was designed for a maximum applied shear load of 890 kN (200 kips), difficulties arose in applying and measuring the twenty percent (20%) increase in load. A fourth 30-ton hydraulic jack was added during the experimentation in

order to increase the applied load. The load contributed by the fourth hydraulic jack was estimated using a pressure gauge attached to the output of the manual hydraulic pump. The load values were combined with those obtained through the computerized data acquisition system in creating the hysteretic response of the specimen illustrated in Fig. 4.19.

Once the specimen reached the maximum applicable force, the clamps were removed completely for the remainder of the test.

First cracking of the specimen occurred at load cycle 4A, the first upward cycle at a load of 220.6 kN and a deflection of 0.33 mm. The first hairline crack initiated at the bottom left coupling beam–coupled wall interface. A second hairline crack initiated at the top left coupling beam–coupled wall interface at load cycle 4B, the first downward cycle at a load of -221.2 kN and a deflection of -0.38 mm. Cracking occurred at the top right and bottom right coupling beam–coupled wall interface during load cycles 7A and 7B respectively.

The first shear cracks occurred at load cycle 10A, the first upward cycle at a load of 565.6 kN and a deflection of 2.33 mm. Three shear cracks formed at the coupling beam, approximately perpendicular to the diagonal reinforcing steel bars. The existing crack extended and widened and new similar cracks initiated during the subsequent load cycles. Shear cracks appeared in the orthogonal direction at load cycle 10B, the first downward cycle at a load of -534.3 kN and a deflection of -2.33 mm. The progression of the cracks is illustrated in Fig. 4.20.
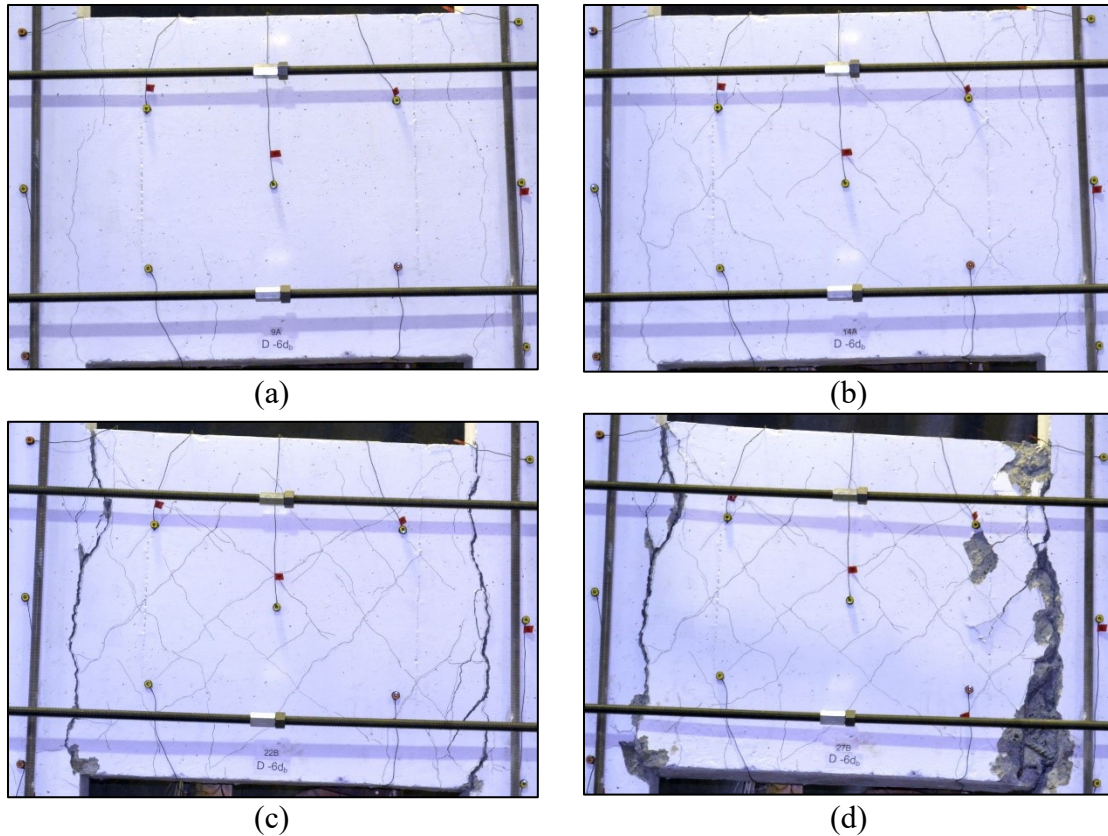
Figure 4.20 – Crack patterns of specimen D-6d$_b$ at load stages (a) 9A, (b) 14A, (c) 22B and (d) 27B

First yield of the reinforcing bars occurred at load cycle 10A, the first upward cycle at a load of 565.6 kN and a deflection of 2.33 mm. Similar yielding occurred at the following load cycle 10B, the first downward cycle at a load of -534.3 kN and a deflection of -2.33 mm. First yielding was determined by monitoring the strain gauge readings on the diagonal reinforcing steel bars at the coupling beam–coupled wall interface.

General yield of the coupling beam occurred at load cycle 13A, the first upward cycle at a load of 645.0 kN and a deflection of 3.15 mm. Similar yielding occurred at the following load cycle 13B, the first downward cycle at a load of -616.0 kN and a deflection of -3.37 mm. General yielding was approximated during the test by monitoring the measured load vs deflection curve plotted by the data acquisition system and identifying the yield plateau. General yield was determined after the test to be ± 3.25 mm based on the bilinear approximation of the response (Park, 1989).

The largest positive resisted load occurred at load cycle 19A, the first upward cycle at a deflection of 3.44 δ_y, at a load of 998.8 kN and a deflection of 12.51 mm. Similarly, the largest negative resisted load occurred in load cycle 19B, the first downward cycle at a deflection of 3.44 δ_y, at a load of -810.1 kN and a deflection of -13.76 mm.

The lateral restraint clamps were removed after load cycle 21B. For the purpose of estimating 80% of the maximum load, peak values for positive and negative maximum unrestrained shear loads of 760 kN and -650 kN respectively were used, based on the previous test specimens.

Severe spalling was observed at the bottom right side coupling beam–coupled wall interface starting at load cycle 26A, the second upward cycle at a deflection of 8.09 δ_y.

Eighty percent of the maximum estimated positive load was maintained up to load cycle 26A during which a load of 597.5 kN (78.6% of the estimated maximum) and deflection of 26.59 mm were reached. Cycle 27B failed to reach eighty percent of the maximum estimated negative load, reaching a maximum load of -488.5 kN (75.2% of the estimated maximum) and deflection of -27.50 mm.

The first bar rupture occurred at load cycle 28B, during which one bar located at the bottom-right front face of the coupling beam ruptured. Cycle 28B was the first downward cycle at a deflection of 10.3 δ_y, reaching a maximum load of -478.4 kN (73.6% of the estimated maximum negative load) and deflection of -33.55 mm. A second bar rupture event occurred during subsequent load cycle, 29A, where three bars, located at the top-right of the specimen, ruptured. Cycle 29A was the second upward cycle at a deflection of 10.3 δ_y, reaching a maximum load of 364.3 kN and deflection of 26.15 mm.

The test was ended after load cycle 29A (see Fig. 4.21). The coupling beam experienced large out-of-plane movements measuring approximately 70 mm due to severe buckling of the diagonal reinforcing steel bars. Figure 4.22 captures the ruptured bars at the bottom right of the specimen.
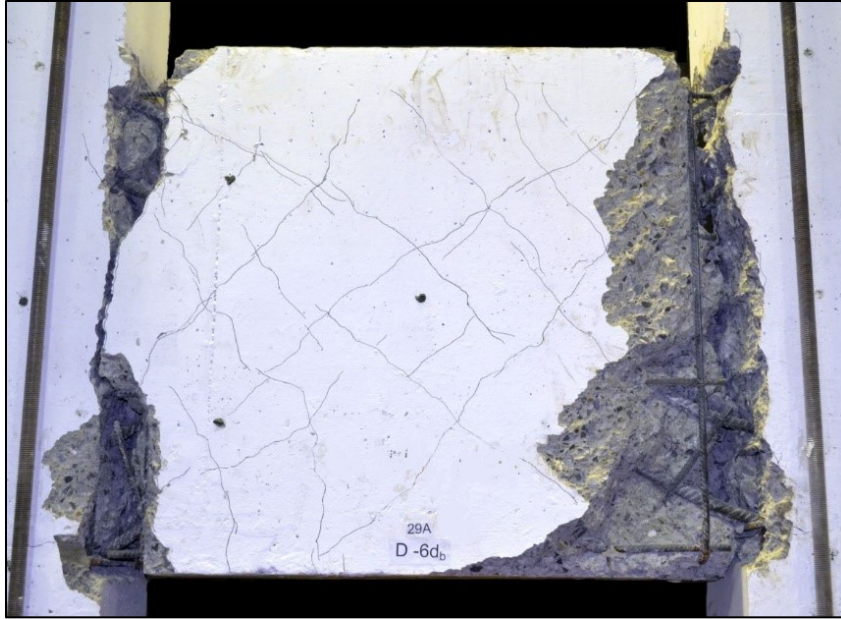
Figure 4.21 – Final load cycle of specimen D-6d$_b$ – 29A

Figure 4.22 – Ruptured bar at bottom right of specimen D-6d$_b$

The widths of the shear cracks remained relatively small (~0.30 mm) throughout the test despite the increase in load and deflection. The flexural cracks at the coupling beam–coupled wall interface widened significantly as the test was carried out. They no longer appeared to close after load cycle 22A, the first upward cycle at a deflection of 6.20 δ_y. The widening of these cracks was likely due to the removal of the lateral restraints, leading to an overall elongation of the walls after yielding of the reinforcing steel bars in tension. The coupled walls experienced minor cracking during the test however these cracks appeared to have no effect on the response of the coupling beam.

CHAPTER 5

COMPARISON OF RESULTS

5.1. Introduction

This chapter compares the responses and constructability of the four coupled wall specimens. The specimens are compared with respect to:

Constructability

Predicted capacity and maximum load achieved

Response to reversed cyclic loading:

- Influence of s/d_b ratio
- Hysteretic responses
- Displacement ductility
- Inelastic rotational capacity
- Cumulative energy absorption
- Stiffness degradation
- Load sustainability

5.2. Constructability
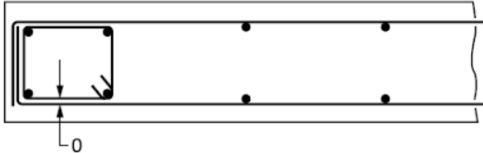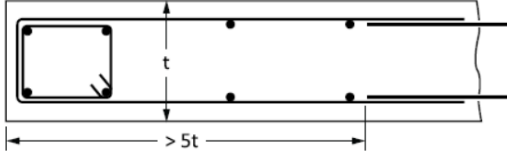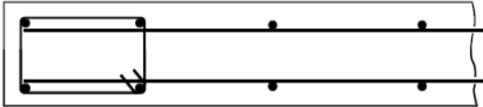
The four specimens were detailed based on their design ductility-related force modification factor, R_d. The coupled wall detailing was different for the conventional construction, moderately ductile and ductile specimens as described in Chapter 3. The coupling beams in each of the four specimens were identical with the exception of the spacing of the confining reinforcing. In general, as R_d increases the number of confinement reinforcement around the diagonal bars increases making it more difficult to construct the beam.

Construction of the Coupled Walls:

The primary differences between the construction of the three types of coupled walls with different corresponding R_d factors were:

- the confinement detailing of the horizontal reinforcing steel, shown in Fig. 5.1,
- the spacing of the horizontal and vertical wall reinforcing steel as described in Chapter 3, and
- the spacing of the concentrated reinforcing column ties, as described in Chapter 3.

CSA Standard A23.3-14 (CSA, 2014) provides requirements for the detailing of the anchorage of the horizontal wall reinforcing bars as shown in Fig. 5.1.

Type	Brief description	Figure
1	Standard 90° hook around vertical end bar	
2	U-bar around vertical end bars; staggered lap splices minimum five times wall thick from end of wall	
3	Anchored within tied vertical reinforcement	

For wall systems designed using:	Permitted Anchorage
R_d = 1.5	Type 1, 2, or 3
R_d = 2.0 or 2.5	Type 2 or 3
R_d = 3.5 or 4.0	Type 3

Figure 5.1 – Shear wall horizontal bar detailing excerpt from CSA Standard A23-3-14 cl. 21.5.5.3 (CSA, 2014).

Construction of the Coupling Beams:

The construction of the couplings beams was generally complicated, difficult and time consuming. The coupled walls and basketting steel were constructed first, then held in place temporarily at their approximate locations. The diagonal reinforcing bars were then placed within the basketting steel and boundary elements. In order to do so, the diagonal buckling prevention ties had to be placed during the manually insertion of the diagonal reinforcing steel bars through one end of the coupled walls. Once one direction of the diagonal reinforcing steel was installed, the orthogonal reinforcing steel bars were slid through the opposing end of the coupled shear walls. The most difficulty arose when the buckling prevention ties were located within the coupled wall concentrated reinforcing steel region. The diagonal reinforcing steel bars had to be intertwined with the coupled wall concentrated reinforcing steel ties, as illustrated in Fig. 5.2 and Fig. 5.3, all while being adequately confined by the diagonal buckling prevention ties.

Once the diagonal reinforcing steel cages were constructed, the entire assembly was tied solidly in place and then lifted into the formwork with a crane.
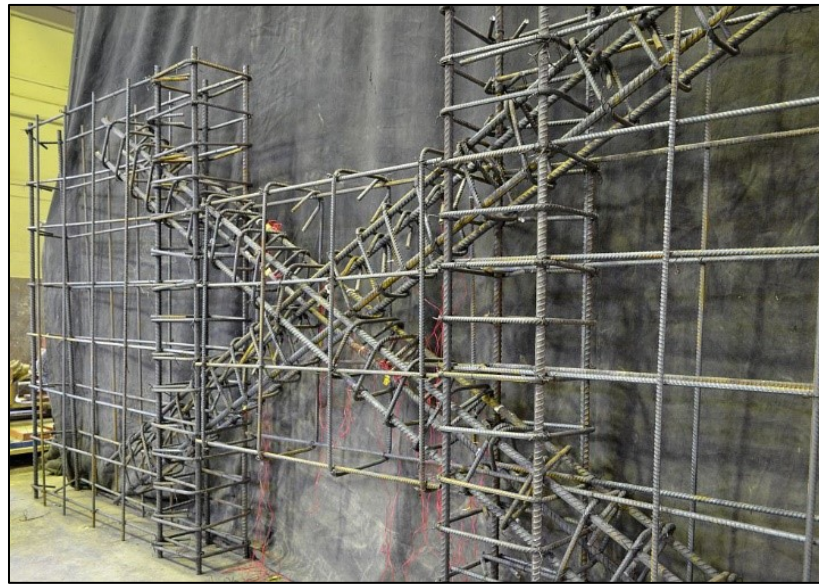
Figure 5.2 – D-6d_b specimen

Figure 5.3 –Intertwined concentrated and diagonal reinforcing steel of specimen D-6d$_b$

Concrete Placement:

The congestion of reinforcing steel in the MD-8d$_b$ and D-6d$_b$ specimens led to difficult concrete placement. Much care was needed in vibrating the concrete during placement in order to achieve proper consolidation. It was difficult to pass the vibrator through the coupling beam – coupled wall interface due to the intertwined concentrated reinforcement ties and diagonal buckling prevention ties.

5.3. Predicted Capacities

The predicted yield and ultimate capacities of the specimens were calculated using Eq. 5.1 and Eq. 5.2 which are derived from statics:

$$V_y = 2A_s f_y \sin(\alpha) \tag{5.1}$$

$$V_u = 2A_s f_u \sin(\alpha) \tag{5.2}$$

where

A_s = the area of diagonal reinforcing steel in one of the diagonal arms.

f_y = the experimentally determined yield stress of the diagonal reinforcing steel bars.

α = the angle of inclination of the diagonal reinforcing steel bars from the horizontal.

f_u = the experimentally determined ultimate stress of the diagonal reinforcing steel bars.

Based on the details of the diagonal reinforcement consisting of 4-20M bars (area of 1200 mm^2), a yield stress of 457 MPa, an ultimate stress of 570 MPa and an angle of inclination of 30 degrees, the predicted shear at yielding and ultimate were 548.4 kN and 684 kN respectively. Table 5.1 compares the shear resistance results of the specimens. The value of the equivalent f_u was determined from Eq. 5.2, from experimentally determined V_u.

Table 5.1 – Comparison of reversed-cyclic test results

Specimen	V_{test}	Equivalent f_u	V_y	V_u
CC-16d$_b$	688.5 kN	573.8 MPa		
MD-10d$_b$	773.8 kN	644.8 MPa		
MD-8d$_b$	736.6 kN	613.8 MPa	548.4 kN	684 kN
D-6d$_b$ (with restraint)	998.8 kN	832.3 MPa		
D-6d$_b$ (without restraint)	718.7 kN	598.9 MPa		

Based on the results it is clear that the concrete contributes significantly to the resistance of the coupled wall, illustrated by the difference in the equivalent f_u values in comparison to the measured ultimate strength of the reinforcing bars. In general, the higher degree of confinement lead to an increase in the ultimate obtained shear load. As is apparent from Table 5.1, the effect of restraint against lengthening increased the shear capacity of the coupling beam by approximately 29%. The CSA standard A23.3 (CSA, 2014) design equations do not take the lateral restraint contribution into consideration. The contribution of the lateral restraint provided by the structural slab should further investigated.

5.4. Comparisons of Responses to Reversed Cyclic Loading

5.4.1. Influence of s/d_b ratios

After studying the photographs of the reinforcing cages before casting the concrete it was determined that within the most critical region of the diagonal reinforcement, the region nearest the coupling beam – coupled wall connection, both specimens MD-10d_b and MD-8d_b had an effective hoop spacing corresponding to 8d_b. This is due to the angle of the hoops and the presence of the concentrated wall reinforcement, illustrated in Fig. 5.4. It was concluded that for the analysis of the results, specimen MD-10d_b had an effective s/d_b ratio of 8d_b.
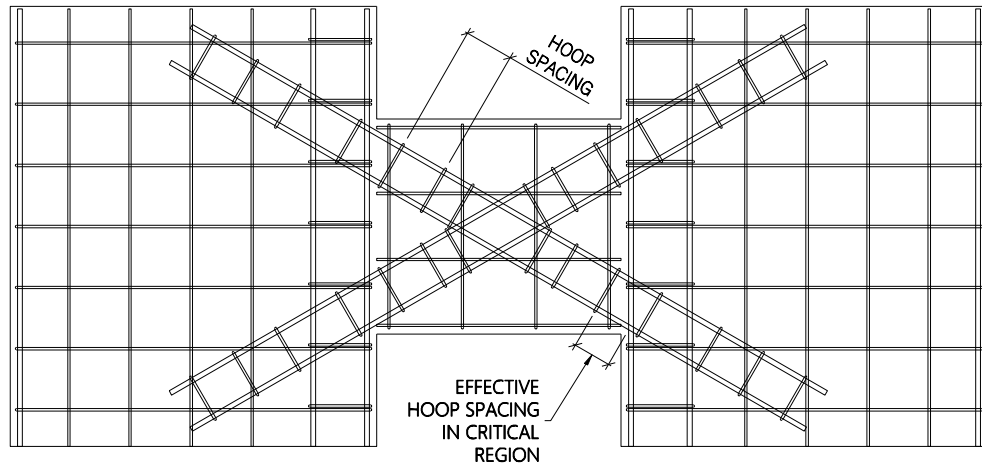
Figure 5.4 – Effective hoop spacing in critical reinforcing bar buckling region

5.4.2. Shear force versus deflection hysteretic responses

Figure 5.5 presents the shear force versus deflection hysteretic responses of the coupled wall specimens. Table 5.2 compares the load-deflection response values of the specimens at key load stages. The displacement ductility, energy absorption, stiffness degradation, load sustainability and reinforcing steel strains characteristics are compared in this section.

It is clear from Fig. 5.5 that specimen CC-16d_b did not attain the same maximum load level as the other three coupling beams. Specimens MD-10d_b and MD-8d_b had very similar responses. As noted above both of these specimens have an effective s/d_b of 8d_b near the wall interface. Specimen D-6d_b had a higher ductility and ultimate capacity than the moderately ductile specimens, strongly due to the longitudinal restraint provided. After the removal of the longitudinal restraint the coupling beam performed in a very similar manner to the moderately ductile specimens.

(a) CC-16d_b

(b) MD-10d_b

(c) MD-8d_b

(d) D-6d_b
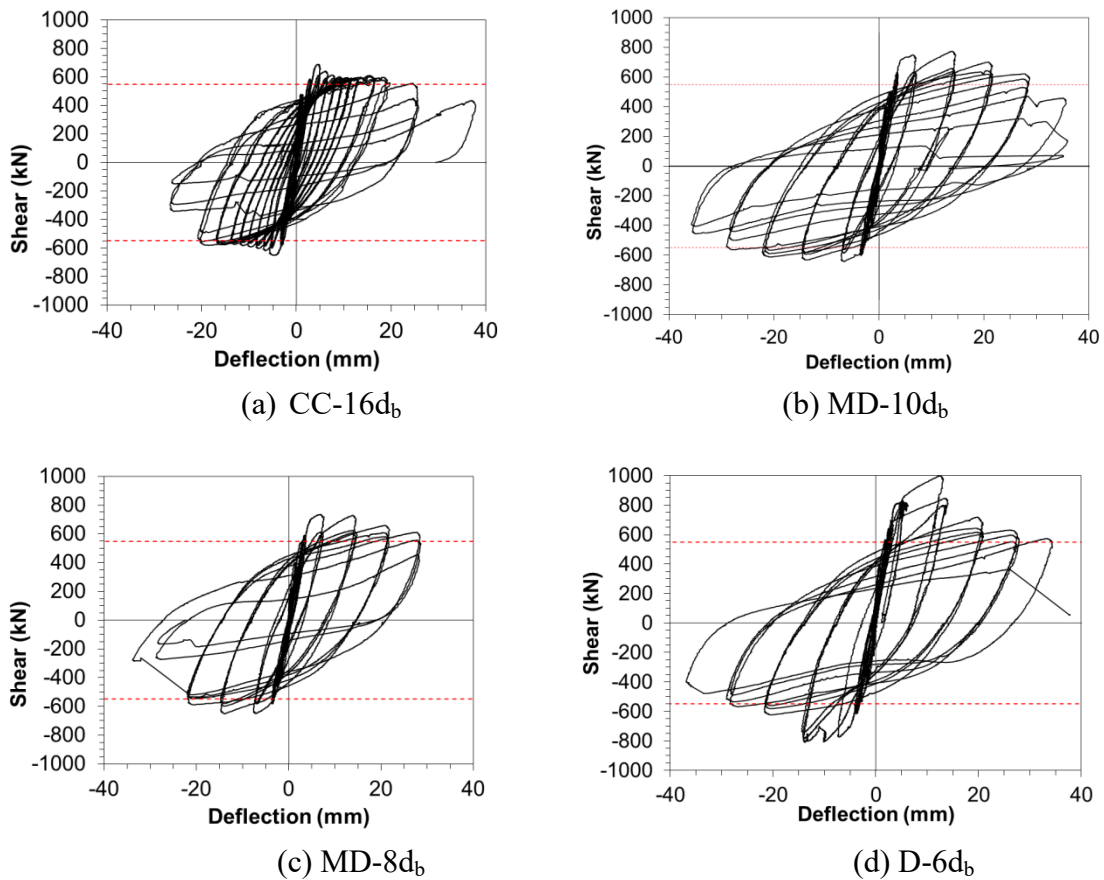
Figure 5.5 – Shear versus deflection response of the tested coupling beams

Table 5.2 – Comparison of key specimen response values

	CC-16d_b			MD-10d_b			MD-8d_b			D-6d_b		
	Cycle	Deflection (mm)	Load (kN)	Cycle	Deflection (mm)	Load (kN)	Cycle	Deflection (mm)	Load (kN)	Cycle	Deflection (mm)	Load (kN)
First Cracking	8B	-0.349	-220.7	4B	-0.31	-220.6	4A	0.44	220.6	4A	0.33	220.6
First Yield	16A 16B	1.03 -2.93	477.5 -507.5	13A 13B	2.04 -2.17	498.9 -500.7	10A 10B	2.71 -2.30	542.7 -461.3	10A 10B	2.33 -2.33	565.6 -543.3
Highest Load Capacity	22A 22B	4.71 -4.93	688.5 -650.8	22A 19B	13.92 -6.68	773.8 -642.3	16A 19B	6.95 -14.00	736.6 -651.3	19A 19B	12.51 -13.76	998.8 -810.1
Capacity at Failure	49A	37.2	433.1	33A	70.6	35.06	27B	-28.11	-166.2	29A	26.15	364.3
Ultimate Deflection	49A 46B	37.2 -25.94	433.1 -343.3	32A 32B	35.37 -35.12	174.2 -405.3	27A 25B	28.04 -33.31	458.4 -284.0	28A 28B	33.20 -33.55	573.3 -488.5

5.4.3. Displacement Ductility

The displacement ductility was determined by dividing the maximum displacement attained during three cycles without significant strength decay (>80% V_u) by the displacement at general yielding. The displacement ductility of the specimens were very similar, as shown in Table 5.3. Because all four specimens contained the same diagonal reinforcement the average general yield displacement of 3.25 mm was used to determine the ductilities of the specimens. It is apparent from Table 5.3 that the two specimens with an effective s/d_b ratio of 8 had greater ductilities than the specimen with an s/d_b ratio of 16. The ductility achieved in specimen D-6d_b was estimated assuming a response without longitudinal restraint. Coupling beam D-6d_b with an effective s/d_b ratio of 6 achieved the highest ductility.

Table 5.3 – Displacement ductility of the tested specimens

	CC-16d_b	MD-10d_b	MD-8d_b	D-6d_b
General Yield Deflection (mm)	3.25 -3.25	3.25 -3.25	3.25 -3.25	3.25 -3.25
Maximum Load (kN)	688.5 -650.8	773.8 -642.3	736.6 -651.3	998.8 -810.1
Maximum deflection sustained through three (3) cycles (mm)	18.63 -19.97	20.92 -20.95	21.10 -20.97	26.59 -27.50
Displacement Ductility	**5.73** **-6.14**	**6.44** **-6.45**	**6.45** **-6.49**	**8.18** **-8.46**

5.4.4. Inelastic Rotational Capacity

The inelastic rotational capacity was determined by dividing the average of the maximum positive and negative displacements divide by the coupling beam length of 1000 mm. From the experimental results the average inelastic rotational capacities were 0.025, 0.033 and 0.035 for effective s/d_b ratios of 16, 8 and 6, respectively. The CSA Standard A23.3-14 (CSA, 2014) limits the inelastic rotational capacity to 0.04 for diagonally reinforced coupling beams. The inelastic rotational capacity should be a function of the ductility used in design which is related to the s/d_b ratio. The values obtained in the experimental program are somewhat below the limit provided in the Standard.

5.4.5. Cumulative Energy Absorption

The cumulative energy absorption was determined by taking the cumulative area below the first loop of the hysteretic response at each target load/displacement level. Figure 5.6 illustrates the cumulative energy absorption for the specimens. As the effective s/d_b ratio decreases the cumulative energy absorption increases. Specimen MD-10d_b performed better than expected, exhibiting higher energy absorption than specimen MD-8d_b.
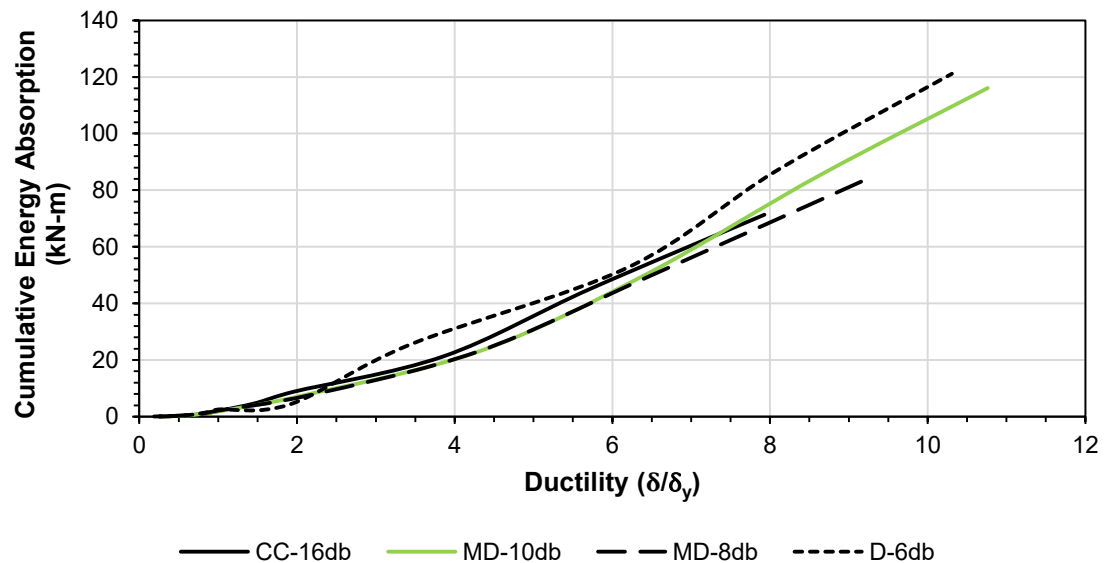
Figure 5.6 – Cumulative energy absorption versus ductility

5.4.6. Stiffness Degradation

The peak to peak stiffness is represented by the slope of a line which connects the positive and negative peaks of the first targeted load/displacement level. The peak to peak stiffness versus ductility of the four specimens is presented in Fig. 5.7.

The stiffness degradation was similar for all four specimens. Cracking of the specimens led to a significant decrease in stiffness, followed by smaller decreases in stiffness during subsequent load cycles.
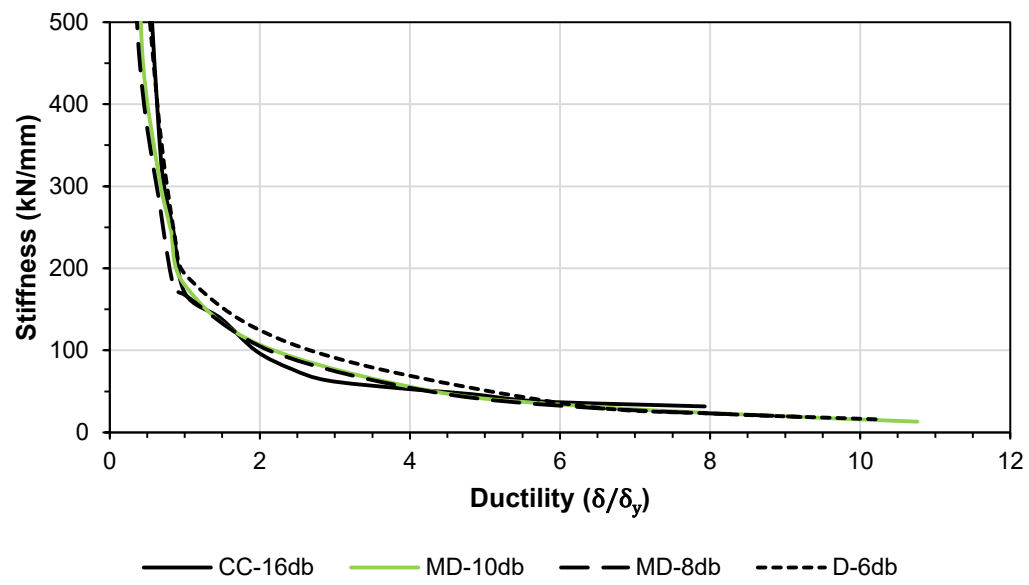
Figure 5.7 – Stiffness degradation versus ductility

5.4.7. Load Sustainability

Load sustainability is a measure of the specimens' ability to carry loads applied in the post-peak response. Load sustainability is an important indicator in the post-peak performance of the specimen. An increase in confinement of the diagonal reinforcing steel bars provided by closely spaced buckling prevention ties generally led to an increase in load sustainability. The presence and removal of the longitudinal restraint is apparent in the response of specimen D-6d$_b$.

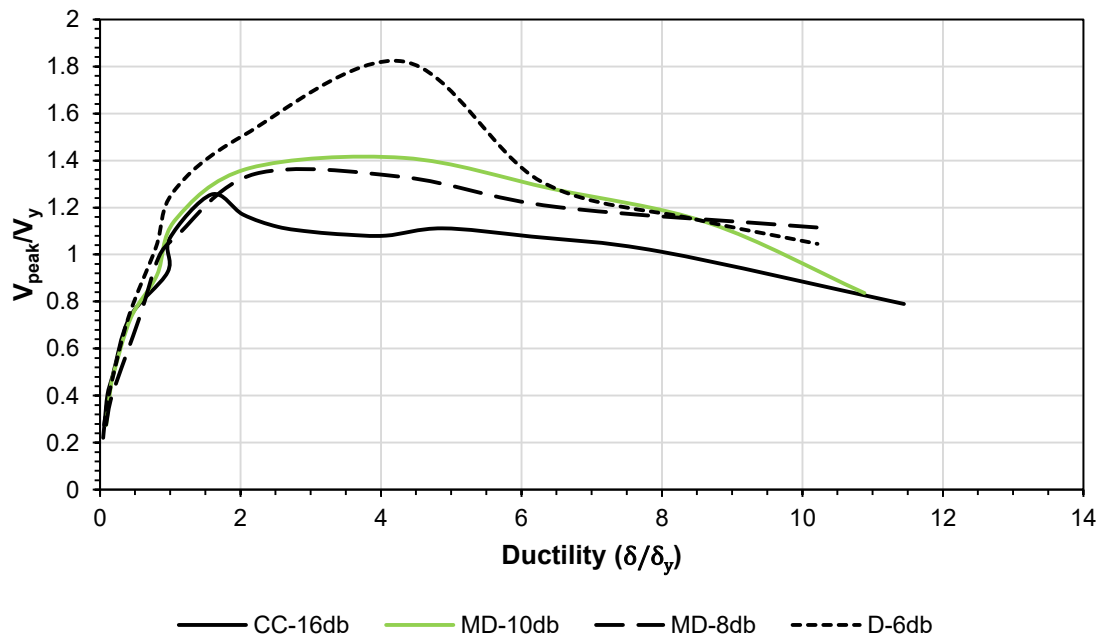Figure 5.8 presents the load sustainability of the four specimens.

Figure 5.8 – Load sustainability versus ductility

CHAPTER 6

CONCLUSIONS AND RECOMMENDATIONS

6.1. Conclusions and Recommendations

Four full-scale diagonally reinforced coupling beam specimens constructed in accordance with the CSA Standard A23.3-14 (CSA, 2014) provisions were tested under reversed cyclic loading. The specimens were detailed to represent different levels of ductility, namely conventional construction, moderately ductile and ductile coupling beams. In order to achieve these levels of ductility, the spacing of the buckling prevention ties confining the diagonal reinforcing steel was varied from 16 bar diameters (320 mm) to six bar diameters (120 mm). Longitudinal restraint, simulating the restraint effect of a structural slab surrounding the coupled wall system, was simulated in one of the test specimens.

Based on the specimen responses, the following conclusions and recommendations can be made:

1. Diagonally reinforced coupling beams provide an efficient, regular and reliable lateral load resisting system.

2. Basketting steel provided in diagonally reinforced coupling beams helps to maintain the integrity of the concrete surrounding the diagonal reinforcement.

3. Spalling of the diagonally reinforced coupling beam is typically limited to the coupling beam – coupled wall interface, which becomes the critical region for reinforcing bar buckling.

4. The influence of the spacing of the buckling prevention ties around the diagonal reinforcing steel becomes critical in the post-yielding response of the coupling beam, after extensive spalling of the concrete occurs at the coupling beam – coupled wall interface. It was found that the effective s/d_b ratio in this critical region controls the post-peak response.

5. The diagonal reinforcing steel generally ruptures due to low-cycle fatigue after spalling of the concrete and significant bar buckling occur at the coupling beam – coupled wall interface.

6. It was determined that hoop spacings of $6d_b$, $8d_b$ and $16d_b$ are appropriate for ductile, moderately ductile and conventional construction coupling beams, respectively.

7. The required spacing of anti-buckling reinforcement in the CSA Standard A23.3 can be increased for diagonally reinforced coupling beams classified as moderately ductile and of conventional construction.

8. Longitudinal restraint of coupling beams provided by reinforcement in the slab around the coupled wall system led to an increase in shear capacity of about twenty nine percent (29%). This increase in shear capacity should be investigated.

9. The maximum inelastic rotational capacity of coupling beams in the CSA Standard A23.3 should be re-examined and made a function of the ductility of the coupling beam.

References

American Concrete Institute. (2011). *Building Code Requirements for Structural Concrete ACI 318-11* . Farmington Hills: American Concrete Institute.

American Society of Civil Engineers. (2006). *Minimum Design Loads for Buildings and Other Structures ASCE 7-06.* American Society of Civil Engineers.

Binney, J. (1972). *Diagonally Reinforced Coupling Beams, M. Eng. Thesis, University of Canterbury.* Christchurch.

Canadian Standards Association. (2004). *CSA A23.1-04/A23.2-04, Concrete materials and methods of concrete construction / Methods of test and standard practices for concrete.* Mississauga: CSA.

Canadian Standards Association. (2009). *G30.18-09, Billet-Steel Bars for Concrete Reinforcement.* Rexdale, ON: Canadian Standards Association.

Canadian Standards Association. (2014). *CSA A23.3-14, Design of Concrete Structures.* Mississauga: CSA.

Dugas, D. (2002). *Seismic Response of Diagonally Reinforced Coupling Beams with Headed Reinforcement, M. Eng. Thesis, McGill University.* Montreal.

Faison, H., Comartin, C., & Elwood, K. (2004, September 14). Retrieved from World Housing Encyclopedia: http://www.world-housing.net/WHEReports/wh100108.pdf

Galano, L., & Vignoli, A. (2000, November/December). Seismic behavior of short coupling beams with different reinforcement layouts. *ACI Structural Journal*, pp. 876-885.

Hansen, W., Eckel, E., Schaem, W., Lyle, R., George, W., & Chance, G. (1966). *The Alaska Earthquake, March 27, 1964: Field Investigations and Reconstruction Effort.* Washington: United States Government Printing Office.

Harries, K. (1995). *Seismic Design and Retrofit of Coupled Walls Using Structural Steel, Ph.D. Thesis, McGill University.* Montreal.

Harries, K., Mitchell, D., Cook, W. D., & Redwood, R. (1993, December). Seismic Response of Steel Beams Coupling Concrete Walls. *Journal of Structural Engineering*.

Harries, K., Mitchell, D., Redwood, R., & Cook, W. D. (1997). Seismic design of coupled walls - a case for mixed construction. *Canadian Journal of Civil Engineering*, pp. 448-459.

Kent, D., & Park, R. (1973, July). Cyclic load behaviour of reinforcing steel. *Strain*, pp. 97-103.

Lai, K. (2002). *Use of Structural Steel Diagonal Reinforcement in Coupling Beams, M. Eng. Thesis, McGill University.* Montreal.

Mander, J. B., Panthaki, F. D., & Kasalanati, A. (1993, August). Low-Cycle Fatigue Behavior of Reinforcing Steel. *Journal of Materials in Civil Engineering*.

Naish, D. (2010). *Testing and Modeling of Reinforced Concrete Coupling Beams, Ph.D. Thesis, University of California.* Los Angeles.

Naish, D., Fry, A., Klemencic, R., & Wallace, J. (2013, November-December). Reinforced concrete coupling beams - Part 1: Testing. *ACI Structural Journal*, pp. 1057-1066.

National Research Council Canada. (2015). *National Building Code of Canada 2015.* Ottawa.

Park, R. (1989). Evaluation of Ductility of Structures and Structural Assemblages from Laboratory Testing. *Bulletin of the New Zealand National Society for Earthquake Engineering*, 155-166.

Paulay, T. (1969). *The Coupling of Shear Walls, Ph.D. Thesis, University of Canterbury.* Christchurch.

Paulay, T., & Binney, J. (1974). Diagonally Reinforced Coupling Beams of Shear Walls. In *Special Publication 42-26* (pp. 579-598). American Concrete Institute.

Paulay, T., & Priestley, M. (1992). *Seismic Design of Reinforced Concrete and Masonry Buildings.* United States of America: John Wiley & Sons.

Santhakumar, & R., A. (1974). *The ductility of coupled shear walls, Ph.D. Thesis, University of Canterbury.* Christchurch.

Zhou, J. (2003). *Effect of Inclined Reinforcement on the Seismic Response of Coupling Beams, M. Eng. Thesis, McGill University.* Montreal.